

MOBILE ATOMS IN A CAVITY FIELD: STATISTICAL AND QUANTUM ASPECTS

ANDRÁS VUKICS

supervisor:
PÉTER DOMOKOS

Dissertation submitted for the degree of
DOCTOR OF PHILOSOPHY
IN PHYSICS



INNSBRUCK – BUDAPEST – SZEGED

MMVI

KEDVES

ॐ

न वा अरे पत्युः कामाय पतिः प्रियो भवत्यात्मनस्तु कामाय पतिः प्रियो भवति ।
न वा अरे जायायै कामाय जाया प्रिया भवत्यात्मनस्तु कामाय जाया प्रिया भवति ।
न वा अरे पुत्राणां कामाय पुत्राः प्रिया भवत्यात्मनस्तु कामाय पुत्राः प्रिया भवन्ति ।
न वा अरे वित्तस्य कामाय वित्तं प्रियं भवत्यात्मनस्तु कामाय वित्तं प्रियं भवति ।
न वा अरे ब्रह्मणः कामाय ब्रह्म प्रियं भवत्यात्मनस्तु कामाय ब्रह्म प्रियं भवति ।
न वा अरे क्षत्रस्य कामाय क्षत्रं प्रियं भवत्यात्मनस्तु कामाय क्षत्रं प्रियं भवति ।
न वा अरे लोकानां कामाय लोकाः प्रिया भवत्यात्मनस्तु कामाय लोकाः प्रिया भवन्ति ।
न वा अरे देवानां कामाय देवाः प्रिया भवत्यात्मनस्तु कामाय देवाः प्रिया भवन्ति ।
न वा अरे भूतानां कामाय भूतानि प्रियाणि भवत्यात्मनस्तु कामाय भूतानि प्रियाणि भवन्ति ।
न वा अरे सर्वस्य कामाय सर्वं प्रियं भवत्यात्मनस्तु कामाय सर्वं प्रियं भवत्य्-
आत्मा वा अरे द्रष्टव्यः श्रोतव्यो मन्तव्यो निदिध्यासितव्यो ।
मैत्रेय्यात्मनो वा अरे दर्शनेन श्रवणेन मत्या विज्ञानेनेदः सर्वं विदितम् ॥

ब्रह्म तं परादादोऽन्यत्रात्मनो ब्रह्म वेद ।
क्षत्रं तं परादादोऽन्यत्रात्मनः क्षत्रं वेद ।
लोकास्तं परादुर्योऽन्यत्रात्मनो लोकान्वेद ।
देवास्तं परादुर्योऽन्यत्रात्मनो देवान्वेद ।
भूतानि तं परादुर्योऽन्यत्रात्मनो भूतानि वेद ।
सर्वं तं परादादोऽन्यत्रात्मनः सर्वं वेदेदं ब्रह्मेदं क्षत्रम् ।
इमे लोका इमे देवा इमानि भूतानीदः सर्वं यदयमात्मा ॥

Contents

1	Introduction	1
1.1	Optical Cavity Quantum Electrodynamics	1
1.2	Outline of the work	5
1.2.1	The system we consider	5
1.2.2	Theoretical models	6
1.2.3	The quantum simulation	8
1.2.4	Quantum regime of cavity cooling	9
1.2.5	Polariton cooling	11
1.2.6	The atom-cavity system as a quantum seesaw	11
1.2.7	Many-body aspects — Outlook	13
1.2.8	Appendices	13
I	Preliminaries	15
2	System	17
2.1	System parameters	17
2.2	Configurations	19
3	Models	20
3.1	Full model — Model 0	20
3.2	Semiclassical approach to Model 0 — Model 0sc	21
3.2.1	Langevin equation for the atomic motion	21
3.2.2	Heisenberg-Langevin equations	22
3.2.3	Bosonisation of the atomic dipole	23
3.2.4	Adding the recoil diffusion	24
3.2.5	Semiclassical field & polarisation	24
3.3	Eliminated model — Model 1	25
3.4	Semiclassical approach to Model 1 — Model 1sc	27

II	Achievements & Results	31
4	The quantum simulation	33
4.1	The MCWF method for the system	33
4.1.1	Discrete momentum basis	33
4.1.2	Jump operators	34
4.1.3	Some technical aspects	35
4.2	Statistical & quantum properties	37
4.2.1	Density operator	37
4.2.2	Characterising statistical properties in steady state	37
4.2.3	Characterising quantum properties	41
4.3	System parameters for the MCWFS	43
4.4	Relaxation & ergodicity	44
4.5	Thesis	46
5	Quantum regime of cavity cooling	47
5.1	Dynamical cavity cooling — mechanism	47
5.2	Role of the cavity	49
5.2.1	Scaling of parameters	49
5.2.2	Temperature, motional excitation quanta	50
5.2.3	Localisation	51
5.2.4	Quantum measures	54
5.2.5	Trapping & cooling times	56
5.3	The cavity FORT	59
5.3.1	Free-space FORT	59
5.3.2	Scaling of parameters	60
5.3.3	Temperature, localisation	61
5.3.4	Resonance in the trapping time	64
5.3.5	The $ \Delta_A \rightarrow \infty$ limit	65
5.4	Theses	65
6	Polariton cooling	67
6.1	Anomalous Doppler-effect	67
6.1.1	The effect as anticipated by Model 0sc	67
6.1.2	Microscopic picture	68
6.2	Cooling	69
6.3	The polariton	70
6.4	Remarks, Theses	73

7	The atom-cavity system as a quantum seesaw	75
7.1	The quantum-seesaw analogy	75
7.2	Role of entanglement and decoherence	76
7.3	Robustness of the final state	78
7.4	Remarks, Thesis	78
8	Many-body aspects — Outlook	81
8.1	The many-atom Hamiltonian	82
8.2	Toy many-body model	83
8.3	Mapping to a lattice model	85
A	The MCWF method made easy	89
B	Cavity sideband cooling	91
C	Self-organisation	93
C.1	Hydrodynamical approach	95
D	Összefoglalás — Summary	98
	Acknowledgements	105
	Bibliography	106
	List of publications	115

Introduction

1.1 Optical Cavity Quantum Electrodynamics

The past decade saw an amazing development in the field of optical resonators and that of cold atoms. Recently, by the fusion of these two fields, a new microscopic system has been created: a tiny optical resonator (cavity) embedding an atom, which is trapped for a long time and is strongly coupled to the electromagnetic field of the resonator. Here the light-matter coupling allows us to study the fundamental features of interacting systems in general. The atom-cavity interaction can be tuned very precisely, and the system eventually realizes a controllable coupled dissipative quantum dynamics on a quite generic level.

Previously, when dealing with *light-matter* interaction, one of the components could be utterly simplified to render it a parameter in the dynamics of the other component. On one hand there is optics, where *matter* is used to manipulate *light*: *matter* is put in parametric form (refractive index) into the Maxwell equations to describe the propagation of *light*. On the other hand, there is also a plethora of examples for the complementer case when *light* is used to manipulate atoms. When treating these phenomena, the amplitude of the *light* field is given as a prescribed function in the Newton or Schrödinger equation governing the behaviour of *matter*.

In a cavity, however, light-matter interaction is realized on a more general level since both the light and the matter components are dynamic. Cavity QED — CQED — [for reviews see 1, 2], though at first sight only a very special case in quantum optics, can therefore also be looked on as a generalisation of both optics, and matter manipulation by light, because of the introduction of a new dynamical element. These latter can in principle be obtained as certain limiting cases of CQED, cases when either the dynamics of the atom or that of the field can be omitted.

The origins of CQED can be traced back to the 1940s, when it was discovered [3] that the radiation properties of an atom are determined not only by its electronic struc-

ture, but also by the mode density of the surrounding electromagnetic field. This latter can be modified by boundary conditions, which allows us to manipulate the radiation properties of atoms. Indeed, in the 1980s it has been demonstrated experimentally that for excited atoms traversing a cavity the excited state's lifetime differs from the one measured in free-space [4, 5, 6, 7].

In these experiments the cavity was present as a passive element merely to tailor the mode density of the electromagnetic field surrounding the atom. The dynamics of the cavity field was irrelevant. It must be accounted for only in the regime of strong atom-field coupling. The parameter describing the atom-cavity coupling is the single-photon Rabi frequency: This is the frequency of the oscillation between atomic and cavity excitation (Rabi oscillation) when there is only one excitation quantum (atomic excitation or photon — hence the name “single-photon” Rabi frequency) in the system. Let us overview the characteristic frequencies of the system:

- single-photon Rabi frequency g ,
- spontaneous emission rate γ ,
- cavity decay rate κ ,
- inverse of the atom-cavity interaction time (atomic flight time through the cavity).

Strong coupling is achieved when the first one dominates all the rest. This clearly means that the atom and the cavity exchange the excitation several times before it is dissipated into the environment via either dissipation channels (cavity decay or spontaneous emission) or the atom leaves the cavity. In a sense, the identities of atom and field are lost and we are left with a single new object.

Strong coupling was first achieved in the micro-wave regime in the 1990s. With this system a series of very fundamental quantum mechanical experiments were performed such as the direct proof of field quantisation [8] and decoherence of quantum superpositions [9]. Reaching strong coupling in the optical domain is a much more challenging task, since due to the short wavelength very short cavity length ($10\mu\text{m}$ – $100\mu\text{m}$) is needed. Since the cavity length is short, photons are reflected more often, therefore to obtain small κ extremely good mirrors are needed (with transmission coefficient $\lesssim 10^{-5}$).

Hence, strong coupling can be interpreted as one single photon making several round trips in the cavity, each time impinging on the atom. An interesting consequence is that the optical resolution, which in free space equals the half of the wavelength is improved by a factor of the square root of the number of round trips. This has lead to the creation of the so called atom microscope: the trajectory of atoms in a cavity can be

reconstructed from the time-resolved analysis of the light intensity escaping the cavity [10, 11, 12].

Entering the optical domain yields a substantial difference as compared to the microwave regime since the momentum of optical photons is big enough to significantly act on the atomic centre-of-mass, making it a part of the dynamics. In an optical resonator even a very weak field, in fact, a single photon agitates the atom considerably, which was first experimentally demonstrated by Hood et al. [13]. Hence, in optical CQED we have three degrees of freedom: the atomic internal one (electronic configuration), the atomic CM motion, and the state of the cavity-field.

When an optical field impinges on a fixed atom, two types of forces emerge [14]:

Dipole force originates from photon absorption from the field followed by *stimulated* emission into the populated laser mode.

Radiation pressure arises from photon absorption from the field followed by *spontaneous* emission into a vacuum mode.

Their duality on the microscopic level clearly corresponds to the duality of the real part (phase shift) and imaginary part (absorption) of a macroscopic dielectric's complex refraction index. The dipole force is conservative and can be rendered by an optical potential. The radiation pressure is dissipative: the stochasticity of the emitted photon's direction yields momentum diffusion via atomic recoil (recoil diffusion).

When the atom moves, light forces depend not only on its position, but also on its velocity. In the simplest case this dependence is via the Doppler effect. Suppose a counter-propagating pair of laser beams red-detuned from the atomic resonance impinge on the atom. In this case a moving atom is more likely to absorb a photon with momentum opposite to its direction of motion since the counter-propagating mode is Doppler shifted nearer to resonance. The spontaneous re-emission of the photon, on the other hand, is isotropic and yields no momentum transfer on average. The momentum of the atom is therefore damped on average, which means cooling for an ensemble of atoms. This simplest method of laser cooling is called Doppler cooling [15, 16]. When applied in three dimensions, it resembles the atom moving in a viscous medium, hence the field of three pairwise orthogonal counter-propagating pair of red-detuned laser beams is often called "optical molasses". Similarly to classical Brownian motion, the final temperature is determined by the contest of the above described friction and recoil-induced diffusion, the lowest achievable temperature scaling with the spontaneous emission rate.

More elaborate laser cooling schemes include polarisation-gradient cooling, where the limiting temperature is determined by the stochasticity of the last spontaneously

emitted photon, so that it scales with the recoil frequency [17]. For certain atomic transitions even this recoil limit can be penetrated eg by velocity-selective coherent population trapping [18]. Here the temperature is already in the nano-Kelvin regime. Preparation of ultra-cold atoms and molecules has allowed for the study of many phenomena stemming from the quantum nature of matter (just think of eg atomic Bose-Einstein condensates [19, 20]), and has already yielded many applications such as atomic clocks, atomic interferometers, and lithography. Quantum objects absent from thermal noise and prepared in their ground state are vital for quantum information processing. Eg with laser-cooled ions in ion traps, quantum teleportation and multi-bit quantum operations have been performed [21].

In the above cooling schemes spontaneous emission is of paramount importance. At first sight it may seem that it merely heats the atoms via the recoil noise, and it may not be as transparent that this alone is responsible for cooling. Indeed: cooling is irreversible damping of the kinetic energy, and a dissipative channel must be inherent. In the laser-based cooling schemes the only irreversible process is light scattering from the laser into surrounding vacuum modes, that is, spontaneous emission.

Recognition of the central role of spontaneous emission calls the Purcell effect into our mind, that is, the possibility of modifying spontaneous emission by a cavity. This must have some impact on laser cooling properties. Based on the prohibition or increase of spontaneous emission on certain frequencies many cooling methods have indeed been developed [22, 23, 24, 25]. In a general form it has been pointed out by Vuletić et al. [26] that in inelastic scattering processes — that is, when the scattered photon's frequency differs from the incoming one due to atomic recoil — the resonator as a spectral filter prefers converting the photon frequency upwards. The necessary energy must be taken from the atomic kinetic energy. Let us emphasise again that in this approach the resonator is a passive element to tailor the mode density of the surrounding vacuum field.

Laser cooling methods based on spontaneous emission have a very serious common barrier: Since a single spontaneously emitted photon carries away only very little energy, a closed optical cycle is necessary to be able to repeat the scattering process. Now in general an excited atom can end up in many different final states after spontaneous emission. For a special class of atoms by applying repumping lasers for the incidental dark states it can be achieved that the atoms remain in a closed subspace. However, there is no mean to develop a general method to cool arbitrary atoms or molecules. For the latter, the situation is even more complicated because the rotational and vibrational states are so abundant that they form an almost continuous band in which the population is spread after a few scattering cycles. In fact, cooling of molecules by optical means is an unsolved problem.

Partly there lies the significance of dynamical cavity cooling. It was first proposed by Horak et al. [27] and studied theoretically in detail in Refs. [28, 29, 30]. Experimentally it was first observed by Maunz et al. [31]. The effect is an important motivation for the present work as well, the basic mechanism we shall overview in Sec. 5.1. The name “dynamical” refers to that here the role of the cavity is more than the passive role it plays in the Purcell effect. It introduces a new dynamical element to the system and with it a new dissipation channel — the cavity field and the cavity loss channel. In the strong coupling regime, the subsystems share all the available dissipation channels: The atomic kinetic energy can transform into the cavity field’s energy and leak into the environment via cavity loss. As a result it can be achieved that the limiting temperature scale with the cavity decay rate, instead of the spontaneous emission rate as in Doppler cooling. The former can be much lower than the latter for a good cavity.

Ultimately, spontaneous emission is not even necessary, all the cooling relies on the cavity loss channel, which makes that the mechanism is free from the limitations mentioned above for the spontaneous-emission based methods. Indeed, the method is in principle applicable to general polarisable particles, ie even to molecules. Note that dynamical cavity cooling outlines a very general cooling concept: to the object to be cooled we couple another object and a new dissipation channel via this one.

1.2 Outline of the work

The following Subsections correspond to further Chapters of the work giving its outline and the motivation for each Chapter. Most of the material to be presented in the work is published in different journals, the references to the corresponding articles are given here just after the title of each Subsection.

Part I of the work presents some preliminary material, most of which is *not* our own work. The material of Part II is, on the contrary, mostly the result of our own work performed during our PhD years since 2003.

1.2.1 The system we consider

Throughout but in the last Chapter we consider a prototype optical CQED system which consists of a single mobile atom interacting with the field of an open (Fabry-Perot like) optical resonator consisting of two opposing mirrors. When the atomic internal structure is considered at all, we assume the simplest: A two-level atom, where the upper level (excited state) can decay towards the lower (ground state), but the lower has no spontaneous decay. We also assume that incidental degeneracies in the cavity’s mode structure are fully resolved so that the atom is coupled only to one single mode

of the cavity field.

In Chap. 8 we consider many atoms interacting with the very same cavity mode. Though direct (dipole-dipole) interaction between the atoms is neglected, the problem is inherently a many-body problem because of the cavity-mediated interaction. The strength of this interaction does not even depend on the distance of the atoms, only the distance modulo the cavity wavelength is important. The interaction has been thoroughly studied in the simplest case of two atoms by Asbóth et al. [32].

1.2.2 Theoretical models

In Chap. 3 we describe four models that are used throughout the work depending on the parameter regime under consideration. To facilitate further reference we assign shorthand names for the different models

Model 0 is the standard quantum optical model for the atom-cavity system. It is a fairly straightforward model consisting of two Jaynes-Cummings like terms which describe the interaction of the atom with the cavity field and a driving laser field (atomic pump). The cavity driving is a simple coherent one. Note that in the Jaynes-Cummings approach some nontrivial approximations are already inherent:

Dipole approximation assumes that the atom interacts with the electromagnetic field only via its dipole moment.

Rotating-wave approximation consists of dropping very rapidly oscillating terms which is justified as long as one is interested in much slower processes.

Dissipative processes are accounted for by the Lindblad approach with the Markov approximation inherent. Note that Model 0 gives full account of an optical CQED system's three degrees of freedom: the atomic internal and motional ones and the state of the cavity field. Model 0 is *not* used for actual calculations in the work, it is presented because it is the origin of all the further models

Model 0sc [30, 33, 34] consists of the elimination of the atomic internal dynamics and the cavity field leaving us with only one degree of freedom: the atomic CM motion. Even this is utterly simplified since we consider the atom as a classical point-like particle. The elimination of the other two degrees of freedom is certainly *not* adiabatic but in first order of the atomic velocity. This makes that their dissipative dynamics is fully transferred to the atomic motion, which therefore resembles a classical Brownian motion and must be described by a Langevin equation. The noise stems directly from the quantum noise of the eliminated degrees of freedom, which explains the fact that this model is usually termed as “semiclassical”

in the literature, although the equations we actually solve are fully classical. A great conceptual advantage of the model is that it yields closed expressions for the coefficients of the Langevin equation, which allows for many analytic calculations.

Model 1 [30] consists of the *adiabatic* elimination of the atomic internal degree of freedom. With this we certainly lose eg the possibility of Doppler type cooling since this relies on the non-adiabaticity of the internal degree of freedom. The atomic dipole now becomes proportional to the electric field at the atom's position. This is just equivalent to a linearly polarisable particle, so that all results we derive from Model 1 are not specific to a two-level atom but valid for general linearly polarisable but possibly quantum mechanical particles, such as molecules or microscopic silicon balls. This model is valid in the regime where the driving is far detuned from the atomic resonance since in this case the atomic excitation is small, and the atomic internal structure is hardly perceived at all. In the present work we mostly consider this regime because this is most interesting from the point of view of cavity cooling: In this regime the conventional laser cooling methods fail, but the cavity cooling effect survives. Since the atomic excitation is small, spontaneous emission is suppressed, and the relevant dissipation channel is the cavity decay. It is with Model 1 that we demonstrate cavity cooling and trapping therefore this method indeed should be applicable to cool molecules, which is a major motivation for our work. In Sec. 3.3 we fully exhibit the correspondence between a two-level atom in the far-detuned regime and a general linearly polarisable particle, and we also show how the parameters of one transform into that of the other and vice versa.

Model 1sc [29, 30] is such a restriction of Model 1 in which both the atomic motion and the cavity field are described classically, but just as in Model 0sc, the correlated noise in their coupled dissipative dynamics is of fully quantum mechanical origin. A significant difference as compared to Model 0sc is that here the cavity field's dynamics is not eliminated, although in Sec. 5.3.3 we quite marginally use such a version of this model in which we make the elimination similarly to Model 0sc. The coupled dissipative dynamics of atomic CM and cavity field is described by a set of classical Langevin equations. Model 1sc is just about the simplest model that has any chance for seizing the basic physics of optical CQED with moving atoms. It is simple enough to be applicable to many atoms (even of the order of thousands) and was indeed successfully applied in the discovery of collective effects in many-atom optical CQED [35]. As shown in Sec. 3.4, a dimensionless version of the Model 1sc equations reveals us the real parameters

of the system. For one atom moving in one dimension we have to deal with six parameters while in the very far detuned regime five parameters remain.

1.2.3 The quantum simulation

[36] In Chap. 4 we consider a possible approximative but fully quantum mechanical solution of Model 1, based on the Monte Carlo Wave-Function (MCWF) method [first proposed in 37, but worked out later in 38, 39, 40]. Our motivation is to explore the quantum effects in the atom-cavity interaction, especially in such parameter regimes which are available with current experimental techniques, but where Model 1sc is supposed to be not reliable any more. At the same time we certainly outline the regimes where the latter model may be effective.

There are basically two regimes which cannot be accessed by the semiclassical approach Model 1sc:

- The regime where the mean photon number is very low. This is the quantum field limit, and as it will become transparent in Chap. 5, it manifests most of the effects related to the strong-coupling regime of cavity QED.
- The regime where the kinetic energy of atoms is damped down to so low temperatures that the quantisation of the atomic motion becomes necessary. This is especially true in such experiments where a Bose-Einstein condensate (BEC) or an atomic laser is made to interact with the cavity [as done mainly by 41]. In this regime both degrees of freedom has to be quantised to give account of eventual quantum correlations between the coupled degrees of freedom. Indeed, there arises a number of questions concerning the overall quantum state of the system. For example, quantum correlations pertain to any proposed scheme using the strongly coupled interaction of cold atoms and the cavity as a single-photon source [42, 43] or for quantum information processing [44].

Modelling an open quantum system with nonlinear dynamics as defined by Model 1 is a highly nontrivial task. *Ab initio* solution, ie a direct numerical integration of the Master equation was tried, but is hopeless because of the large dimension of the Hilbert space. The MCWF method reduces the problem of dimensionality with the help of a proper sampling of the density operator by random wave functions.

While in the original proposition of this method the idea was to evolve *several trajectories* to sample the density operator, here we find that to decipher certain measurable physical quantities, it is enough to evolve *one single trajectory* for longer times. This is of course the ergodic hypothesis, which we show to be practically applicable to the given system. This allows us to further reduce the computational requirements.

A significant novelty of our simulation is that using the peculiar form of the Model 1 Hamiltonian, everything is calculated in momentum space, so that during the actual simulation no numerical Fourier transformation is needed. This is a huge gain in both computational time and accuracy as compared to conventional methods for solving partial differential equations.

We note that Model 0 was simulated in [27, 45], and indeed, *a priori*, keeping the atomic internal degree of freedom is an increment by just a small factor in the dimension of the Hilbert space. In the physically significant far detuned regime, however, the simulation of Model 0 breaks down, due to the big frequency. Here with the effective dynamics of Model 1 gaining immensely on computational time, one can go much deeper into the physics of the problem.

In our approach there is no peculiar geometrical restriction for the atomic CM motion, though a cutoff in momentum space is of course necessary, which translates to a certain limitation for the fine structure of the wave function in real space. In a sense, we consider more “real” atomic motion than in several proposals where the atoms move quantum mechanically in a fixed external harmonic trap and interacts with a cavity [46, 47] or the potential generated by the cavity field is so strong that it can be considered harmonic [48, 49, 50]. In these proposals the atomic motional state is expanded in the eigenbasis of the corresponding harmonic oscillator and a cutoff is introduced in the number of oscillator excitations. The problem there is how to take into account the dynamical nature of the cavity-generated potential, which in their language translates to a varying oscillator frequency and therefore varying basis states. As we shall see in Chap. 8, a very similar problem arises when one tries to apply lattice models to the atom-cavity system in the many-atom case.

In the future our simulation can be also used to describe a BEC interacting with the cavity field. In the Gross-Pitaevski approximation this necessitates simply the addition of a nonlinear term to the Schrödinger equation while in a first approach spontaneous emission can be omitted, which is fairly justified in the far-enough detuned regime.

1.2.4 Quantum regime of cavity cooling

[36, 51] In Chap. 5 we enter such regimes of the atom-cavity interaction which cannot be described by the semiclassical approach Model 1sc for each of the two reasons mentioned above.

In Sec. 5.2 our main motivation is the work presented by Domokos et al. [29]. There the authors studied the properties of cavity cooling as a function of the linewidth of the relevant dissipation channel, that is, cavity decay. They used Model 1sc. It was proved that the limiting temperature indeed scales with the cavity decay rate. Now

armed with our quantum simulation we justify their results in a regime where both approaches are expected to work. We extend their work in two directions: we show that even when there is on average only one photon in the cavity, it still fully exhibits the cavity cooling effect. On the other hand, by decreasing the cavity decay rate we reach so low temperatures where the number of excitation quanta in the atomic motion is about 3. This is no semiclassical motion any more.

The authors of the above Reference also studied trapping time of the atom. This we also try to check, but find a substantial deviation. We conclude that the difference originates not solely from the quantum nature of the atomic motion since tunnelling is negligible with our parameters. A possible explanation, rather, lies in the quantum nature of the trapping cavity field. The potential it creates is not a classical one, but is proportional to the photon number *operator*. In particular, the 0th Fock state creates no potential. In a sense, the atom can escape via this 0th photon component. The effect can be significant as a proof for the “graininess” of the field. For this it is important to note that unlike in free space, in the atom-cavity system the average photon number and the potential depth are independently controllable, since the latter depends also on the atom-cavity coupling.

Sec. 5.3 is maybe the most significant part of the work. Here the role of the cavity is studied from another point of view: We vary the coupling constant, but in such a way that the Rabi frequency is kept constant. As we show this can be considered as transforming from a free-space far-off-resonance dipole trap (FORT) to the dynamical cavity cooling regime. In the strongly coupled regime very few photons yield the same Rabi frequency, so that at the same time we also enter the quantum field regime. We use Model 1sc and the MCWF solution of Model 1 in a complementary way.

We show that the dynamical cavity cooling mechanism unlike Doppler cooling does not vanish in the very-far detuned regime. This regime when the spontaneous photon scattering rate is kept constant is associated with deep optical traps. This, together with cavity cooling allows for trapping *in steady state*, which was not possible in the free-space FORT scheme. There, long time trapping is due to the fact that the atoms are heated very slowly, but in steady state they are not trapped.

By studying trapping times we show that trapping (embedding cooling) is most effective when the detuning between the cavity resonance and the driving approximately equals the cavity decay rate. This means a marked deviation from the previously proposed cavity sideband cooling schemes, and proves that dynamical cavity cooling is of a very different origin.

1.2.5 Polariton cooling

[52] The Doppler shift is a fundamental effect ubiquitous in wave phenomena [53]. In optics, an atom with resonance frequency ω_A moving in free space with velocity \mathbf{v} along a monochromatic plane-wave laser field with wave number \mathbf{k} shows resonant absorption at the Doppler shifted frequency $\omega = k/c = \omega_A + \mathbf{k}\mathbf{v}$. The shifted resonance forms the basis of the above mentioned Doppler cooling mechanism. In Chap. 6 we revisit the velocity-dependence of the atom-field interaction in the presence of a strongly coupled cavity, and find that the very Doppler effect in the atomic absorption is modified.

This “anomalous” Doppler effect appears in the standard Doppler cooling geometry when a cavity is coupled to the atom with its axis orthogonal to the atomic motion. In this case the atom-field coupling is basically constant and the resonator field exerts no force in the direction of the atomic motion. On the other hand, here cavity loss plays only a minor role in the dynamics. Surprisingly, the somewhat weird modification of the atomic dynamics by the presence of the cavity still leads to a significant improvement of Doppler cooling in the direction orthogonal to its axis. Its physical origin can be traced back to the velocity-dependent delayed reflection of the light emitted by the atom back on the atom. We emphasise that the geometry of the cavity hardly enters the problem at all, so instead a cavity we can imagine various sorts of resonant systems coupled to the atom, such as rings, waveguides or microspheres.

Although atomic spontaneous emission is the only effective dissipation channel, owing to the anomalous Doppler effect, the temperature drops below the Doppler limit. This property is reminiscent of the polarisation-gradient cooling, where dynamical time lag of the population of the magnetic Zeeman-sublevels with respect to the momentary light polarisation is responsible for the low temperature. Analogy can be drawn also to the ground-state cooling of trapped particles by electromagnetically induced transparency [54], where an intense laser field is used to produce a Fano-like resonance in a Λ -atom. In the present case, it is the role of the passive cavity to modify the internal structure of the electronic degrees of freedom, producing the polariton resonance with a complex profile. The role of the cavity as an additional dissipation channel is not so essential here. Hence the cooling mechanism can be called “polariton cooling”.

We note that the enhanced cooling in the Doppler geometry by a coupled cavity as anticipated by us was recently observed experimentally by Nussmann et al. [55].

1.2.6 The atom-cavity system as a quantum seesaw

[56] A spatially modulated laser field far red detuned from an atomic resonance creates a designable optical potential to trap and manipulate ultra-cold atoms [57]. For

a periodic lattice potential this enables tailored implementations of the Bose-Hubbard Hamiltonian [58] to study quantum phase transitions [59] or ideas of quantum information processing [44]. Our atom-cavity system can also be regarded as a dynamical optical lattice where the atomic configuration acts back on the lattice potential due to the coupled atom-field dynamics. In the regime of strong light-matter interaction (strong-coupling CQED), which is experimentally accessible nowadays [31, 60], even a single-photon cavity field exerts significant forces on atoms and the quantum properties of the field can no longer be ignored [36, 61].

One striking consequence of the lattice potential’s dynamical nature is the spatial self-organisation of a laser-illuminated atomic ensemble first anticipated by Domokos and Ritsch [35]. Above a threshold pump intensity, the atoms, spontaneously breaking the continuous translational symmetry of the cloud, form one of two regular patterns in a phase transition [62]. These patterns scatter the maximum field from the pump into the cavity, which has one of the two possible phases, as observed experimentally by [63]. The atoms find their stable configuration by a feedback mechanism: the potential is created or at least modified by the cavity field which is composed of the interference of components scattered from the pump by different atoms. Accumulating around every other antinode the scattering into the cavity mode is enhanced by constructive interference (superradiance), and the potential at the lattice sites occupied by atoms is maximally deepened. In the present work the self-organisation process is overviewed more in detail in Appendix C.

In Chap. 7 we describe an effect which may have deep impact on the self-organising process when the atoms have a kinetic energy less than the recoil energy, ie their wave function is flat on the wavelength scale, eg when using a BEC as an initial state [41]. For a “classical”, or mean-field description of the field no self-organisation would occur because of the destructive interference of the field amplitudes scattered into the cavity by different parts of the atomic wave function. However, this conclusion is invalid since the cavity field realizes a *quantum feedback* [64] for the atomic motion, in which entanglement is a crucial element. Scattered field amplitudes with opposite phases do not cancel but entangle to different atomic wave functions [65]. The quantum average of the field amplitude is still zero, but the photon number is not, which is clearly incompatible with the mean-field description. Field components of the superposition create different forces, which pull the atomic wave functions towards the corresponding self-organised configurations. Hence self-organisation is started immediately even at $T = 0$ and without measurement induced projections [66] — in fact, no spontaneous symmetry breaking occurs. The effect can be generic for a wide class of quantum phase transitions whenever the quantum state acts back on its control.

Ultimately, this system is an experimentally accessible implementation of a “quan-

tum seesaw". The seesaw is a generic example of a system where the particle is subject to a dynamically varying potential (feedback). In its unusual quantum version, the seesaw undergoes an entanglement-assisted decay from the unstable equilibrium towards the left- and right-tilted positions. In Chap. 7 we concentrate on the analogy between the one-atom-in-a-cavity system and a quantum seesaw since this stems from our own work with the MCWF simulation, while its possible impact on self-organisation was studied in a cooperation [56]. This study, however, is by no means complete because strictly speaking we have not yet been able to go to a thermodynamic limit with the coupled quantum atom-field dynamics taken into full account, where a quantum phase transition could be expected. This will be a major direction of our future work, and an outlook on the fully quantum mechanical version of self-organisation with some preliminary results is displayed in Chap. 8:

1.2.7 Many-body aspects — Outlook

In this Chapter after displaying the general framework for describing quantum mechanically many atoms interacting with the cavity field we continue with a negative result: we argue that a standard Hubbard-type description of the atoms [58, 61, 67, 68] cannot give account for quantum self-organisation. This is because this latter heavily relies on the dynamical nature of the cavity-generated lattice potential, while the Hubbard approach may work in the limit when this is only a perturbation.

In fact, the cavity-mediated interaction between the atoms is a strong one, with no chance to be accounted for by some perturbative treatment. As we have seen it in itself can result in a phase transition. This calls into our mind the possibility of a treatment by some renormalisation method. We show that in momentum space the system can be mapped to a lattice model where the cavity plays the role of a bosonic impurity: it allows for scattering between certain lattice sites. The density matrix renormalisation group (DMRG) method developed recently has been applied with great success for such impurity models [69, 70], though in solid state physics both impurity and lattice sites are usually fermionic. As an outlook of the work, we outline the possibility of a DMRG calculation for the system.

1.2.8 Appendices

In the Appendices we discuss such material connected to our work, which is not our own work, or if it is, it is not fully worked out and published, so that it cannot be incorporated into the main stream of the work or appear in the Theses. The hydrodynamic approach for self-organisation displayed in Sec. C.1 is particularly interesting since it yields analytic expression for the critical point of the phase-transition. A version of this

has been published in Ref. [62].

PART I

Preliminaries

System

In most of what follows we shall consider one single two-level atom moving in one dimension in a strongly coupled high-finesse single-mode cavity field as depicted in Fig. 2.1. We shall see that in most cases no reference is made as to the internal structure of the atom and we may as well consider an arbitrary linearly polarisable particle. Eventually, in Chap. 8 we shall consider a set of such atoms (particles), which do not interact with each other. x is the direction of the cavity axis and z is one transverse direction. In the actual numerical calculations ^{85}Rb were considered with the $5^2\text{S}_{1/2}, F = 3 \leftrightarrow 5^2\text{P}_{3/2}, F = 4$ transition since this is most widely used in optical CQED experiments.

2.1 System parameters

In the general case we may use two lasers to drive the system. The first one is the cavity pump, a laser beam injected directly to the cavity via one of its mirrors. It yields an effective pumping strength η for the given mode. The second one is a standing wave laser field, a 1D optical lattice, which is perpendicular to the cavity axis, and hits the atom directly. It will be often referred to as the atomic or transverse pump. It yields a position-dependent effective pumping strength $\eta_t(\mathbf{r})$ for the given atomic transition.

A theoretically important nuance is that the frequency of the two pumps be the same because we shall want eliminate their time dependence simultaneously by transforming to a rotating frame (interaction picture). The atomic and cavity detunings are defined as $\Delta_A = \omega - \omega_A$, $\Delta_C = \omega - \omega_C$, ω_A and ω_C being the resonance frequency of the atom and the cavity, respectively. Dissipation channels are atomic spontaneous emission with rate 2γ and cavity decay with rate 2κ .

A crucial parameter is the single-photon Rabi frequency g of the atom-mode interaction, often termed as the coupling constant between the two. With more fundamental

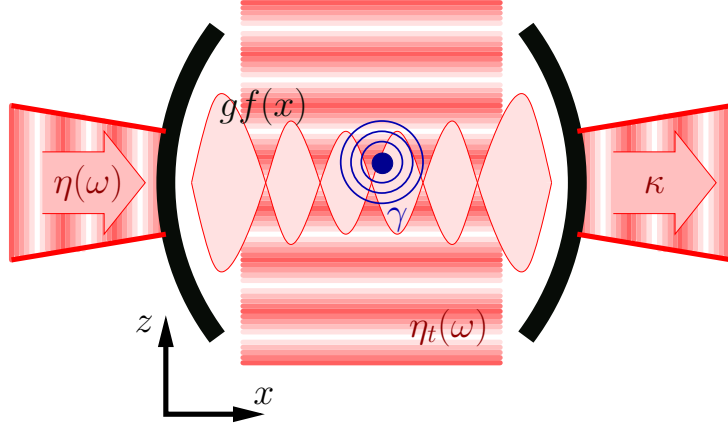


Figure 2.1: Scheme of the system atom-cavity.

parameters it can be expressed as

$$g = \sqrt{\frac{\omega_c}{2\hbar\epsilon_0\mathcal{V}}} \langle e | \mathbf{d} | g \rangle \mathbf{e}. \quad (2.1)$$

\mathcal{V} is the volume of the cavity mode. $|g\rangle$ and $|e\rangle$ are the ground and excited state of the atom, respectively. \mathbf{d} is the atomic dipole moment operator and \mathbf{e} the polarisation vector of the mode. We see for example that one way to increase the coupling between atom and mode is to decrease the mode volume \mathcal{V} .

In the actual applications of the model, the transverse profile of both cavity mode and atomic pumping laser is neglected, so that they depend only on coordinate x and z , respectively. They are straightforwardly taken to be sine modes:

$$f(x) = \sin(K_x x), \quad (2.2a)$$

(the mode function of the cavity mode)

$$\eta_t(z) = \eta_t \sin(K_z z). \quad (2.2b)$$

We note that one of the complex g , η , and η_t can be chosen real and the phases of the remaining two then describe relative phases. While Vukics et al. [34] discussed the possibility of tuning one of the three relative phases, the one between the atomic and cavity pump, and they did discover some interesting related effects, these will not make part of the present work. Therefore, to make it simple, in all what follows all three of g , η , and η_t will be chosen real.

For the considered atomic transition $\gamma = 2\pi \times 3 \text{ MHz}$. Optical driving means a wavelength of about 780 nm corresponding to a frequency $\omega = 2\pi \times 4 \cdot 10^8 \text{ MHz}$.

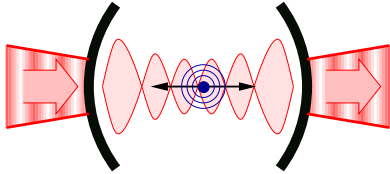
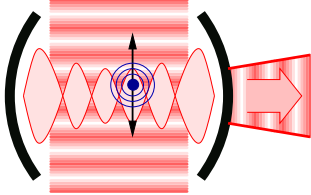
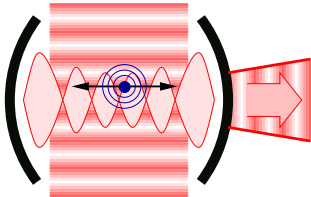
cavity pumped, atom moving in direction x : Configuration CX		$\eta_t = 0, z = \frac{\pi}{2}$
atom pumped, moving in direction z : Configuration AZ		$\eta = 0, x = \frac{\pi}{2}$
atom pumped, moving in direction x : Configuration AX		$\eta = 0, z = \frac{\pi}{2}$

Table 2.1: System configurations.

2.2 Configurations

While models are developed for the full system as described above, in the actual applications we always make some restrictions. In particular, we consider only such cases when either the cavity or the atom is pumped.

When only the cavity is pumped then there is no force acting on the atom in the z direction, so this need not be considered. This simplest will be referred to as Configuration CX in the following.

When the atom is pumped, however, it scatters field from the pump into the cavity mode, so forces will act in both directions. In Ref. [34] it has been proved, however, that cross effects between the two directions have no impact on the statistical properties of the system. Therefore, in the atom pumping case as well, we shall consider the two directions separately.

The system configurations considered in this work are summarised in Tab. 2.1.

Models

In this Chapter we first introduce the “standard” model, Model 0, for the atom-cavity system, which is the origin of all the further models. In the low atomic saturation regime the atomic inner degree of freedom can be eliminated yielding Model 1. Both models have a respective semiclassical approximation Models 0sc and 1sc, in which the atoms are considered as classical point-like particles, and the field is classical.

3.1 Full model — Model 0

Time evolution of this dissipative quantum system is in principle governed by the Master equation:

$$\dot{\rho} = \frac{1}{i\hbar} [H, \rho] + \mathcal{L}\rho. \quad (3.1)$$

We give the two terms in dipole and rotating-wave approximations and in the frame rotating with the frequency of the pumps in terms of cavity field operator a and atomic lowering, raising, and population inversion operators σ , σ^\dagger , and σ_z . The Hamiltonian term describing coherent evolution reads

$$H = \frac{\mathbf{p}^2}{2\mu} - \hbar\Delta_A \sigma_z - i\hbar\eta_t(\mathbf{r}) (\sigma^\dagger - \sigma) - \hbar\Delta_C a^\dagger a - i\hbar\eta (a - a^\dagger) - i\hbar g f(\mathbf{r}) (\sigma^\dagger a - a^\dagger \sigma), \quad (3.2a)$$

where the terms describe atomic external and internal degrees of freedom (free and pumped), free field, pumping of the mode, and atom-mode interaction, respectively.

The Liouvillian term governing dissipative processes reads

$$\mathcal{L}\rho = \kappa \left(2a\rho a^\dagger - [a^\dagger a, \rho]_+ \right) + \gamma \left(2 \int d^2\mathbf{u} N(\mathbf{u}) \sigma e^{-ik_A \mathbf{u} \mathbf{r}} \rho e^{ik_A \mathbf{u} \mathbf{r}} \sigma^\dagger - [\sigma^\dagger \sigma, \rho]_+ \right), \quad (3.2b)$$

where the first term describes cavity decay and the second one atomic spontaneous emission. μ is the atomic mass; $\mathbf{r} = (x, z)$ and \mathbf{p} are atomic position and momentum operators. The model defined by these two equations is the root of all approaches to the atom-cavity system presented in this Chapter.

The second term of Eq. (3.2b) contains momentum recoil due to spontaneous emissions: when the atom spontaneously emits a photon, it gets a momentum opposite to that of the photon to fulfil momentum conservation. The unit vector \mathbf{u} is the direction of the spontaneously emitted photon, and $N(\mathbf{u})$ the direction distribution characteristic to the given atomic transition: this is taken to be isotropic for the sake of simplicity.¹

$k_A = \omega_A/c$ occurring in the same term is the wave number corresponding to the atomic transition. We have two other wave numbers defined by the mode functions (2.2). Note that for each pair of the frequencies ω , ω_C , and ω_A the rotating wave approximation to be valid, it is required that the difference of the two be much smaller than the sum of the two. We can therefore neglect the difference between the three wave numbers and choose $k_A = K_x = K_z$. We then have one single length scale in the system (until it is much less than the length of the cavity).

3.2 Semiclassical approach to Model 0 — Model 0sc

In a possible approximative approach to the model (3.2), the atomic centre-of-mass motion is approximated by Brownian motion, and the corresponding Langevin equation is constructed from approximate solutions of the Heisenberg-Langevin equations for cavity-mode amplitude and atomic polarisation [30, 33, 34, 52]. This approach we term as "semiclassical" because the atom is a classical point-like particle and the field is also classical (it is in a coherent state), but the origin of *noise* in their dynamics is purely quantum mechanical.

3.2.1 Langevin equation for the atomic motion

In the limit of cold atoms, but with a temperature well above the recoil limit $kT_{\text{rec}} = \hbar K^2/(2\mu)$, the atomic wave packet has a coherence length well below optical wavelengths. Accordingly, its position and momentum can be characterised by expectation values of the corresponding operators [14]. As the atoms are slow, the motion can be well approximated by a Brownian motion described by a set of Langevin equations including the force to first order in velocity:

$$\dot{\mathbf{r}} = \frac{\mathbf{p}}{\mu}, \quad (3.3a)$$

$$\dot{\mathbf{p}} = \mathbf{f} + \beta \mathbf{p} + \Xi, \quad (3.3b)$$

where \mathbf{f} is a conservative force, β is a linear friction tensor (a 2×2 matrix in the 2D case), and Ξ is a noise term supposed to be white noise:

$$\langle \Xi(t_1) \circ \Xi(t_2) \rangle = \mathbf{D} \delta(t_1 - t_2), \quad (3.4)$$

¹For an $S \leftrightarrow P$ transition this means that the atomic dipole points into the y direction.

where \mathbf{D} is the diffusion tensor. The central issue is to calculate the coefficients of the Langevin equations, that certainly depend on position \mathbf{r} of the atom.

Coefficients of the Langevin equation (3.3) all originate from expectation values of the force operator, which, in turn, is derived from the Hamiltonian (3.2a):

$$\mathbf{F} = -\nabla H = i\hbar\nabla\eta_t(\mathbf{r}) \left(\sigma^\dagger - \sigma \right) + i\hbar g \nabla f(\mathbf{r}) \left(\sigma^\dagger a - a^\dagger \sigma \right). \quad (3.5)$$

The first term describes the force exerted by the pump laser directly impinging on the atom. The second force term stems from the atom-cavity field interaction. The conservative part of the force can be found from the steady-state quantum average of this operator, $\mathbf{f} = \langle \mathbf{F} \rangle$. The friction coefficient β can be calculated as the linear response of the force \mathbf{f} to a time-dependent perturbation caused by the atomic motion [for details of the calculation see 30, 33].

In this approach the classical noise is linked directly to the quantum noise of the internal variables. Its correlations has been shown to vanish exponentially with a characteristic time of γ^{-1} or κ^{-1} [33]. Hence, if in Eq. (3.3) the shortest characteristic time of the evolution of \mathbf{r} and \mathbf{p} is much longer than γ^{-1} and κ^{-1} , it is well justified to replace the coloured classical noise Ξ with a white noise, as we have already done in Eq. (3.4). This is fulfilled for slow atoms, that is, when the velocity $Kv \ll \gamma^{-1}, \kappa^{-1}$.

3.2.2 Heisenberg-Langevin equations

Many techniques can be applied to obtain approximations for the coefficients of Eq. (3.3). In each case, however, first the internal atom-field dynamics has to be solved somehow, which contains the atomic motion in a parametric form. In the Heisenberg picture the internal variables satisfy the following quantum Langevin equations:

$$\dot{a} = \frac{i}{\hbar} [H, a] - \kappa a + \xi = (i\Delta_C - \kappa) a + gf(\mathbf{r}) \sigma + \eta + \xi, \quad (3.6a)$$

$$\dot{\sigma} = \frac{i}{\hbar} [H, \sigma] - \gamma \sigma + \zeta = (i\Delta_A - \gamma) \sigma + 2gf(\mathbf{r}) \sigma_z a + 2\eta_t(\mathbf{r}) \sigma_z + \zeta, \quad (3.6b)$$

$$\begin{aligned} \dot{\sigma}_z &= \frac{i}{\hbar} [H, \sigma_z] - \gamma \left(\sigma_z + \frac{1}{2} \right) + \zeta_z \\ &= -gf(\mathbf{r}) \left(\sigma^\dagger a + a^\dagger \sigma \right) - \eta_t(\mathbf{r}) \left(\sigma^\dagger + \sigma \right) - \gamma \left(\sigma_z + \frac{1}{2} \right) + \zeta_z. \end{aligned} \quad (3.6c)$$

The noise operators describe white noise, so that their two-time correlation functions are proportional to the delta function and the rate of the corresponding dissipation channel (atomic spontaneous emission or cavity decay), conforming to the

fluctuation-dissipation theorem:

$$\langle \xi(t_1) \xi^\dagger(t_2) \rangle = 2\kappa \delta(t_1 - t_2), \quad (3.7a)$$

$$\langle \zeta(t_1) \zeta^\dagger(t_2) \rangle = 2\gamma \delta(t_1 - t_2), \quad (3.7b)$$

$$\langle \zeta_z(t_1) \zeta_z(t_2) \rangle = 2\gamma \left(\langle \sigma_z \rangle + \frac{1}{2} \right) \delta(t_1 - t_2). \quad (3.7c)$$

The only non-vanishing cross-correlations are

$$\langle \zeta_z(t_1) \zeta^\dagger(t_2) \rangle = 2\gamma \langle \sigma^\dagger \rangle \delta(t_1 - t_2), \quad (3.7d)$$

$$\langle \zeta(t_1) \zeta_z(t_2) \rangle = 2\gamma \langle \sigma \rangle \delta(t_1 - t_2). \quad (3.7e)$$

All other correlations vanish.

The system (3.6) cannot be solved explicitly in its exact form, therefore we resort to approximations.²

3.2.3 Bosonisation of the atomic dipole

In most of the cases of interest the so called bosonisation technique can be applied to simplify the equations of motion [72]. In this approximation the population inversion operator is replaced by its expectation value $\langle \sigma_z \rangle$. Since the commutator of the σ operators becomes a c-number: $[\sigma, \sigma^\dagger] = -2\sigma_z \longrightarrow -\langle 2\sigma_z \rangle$, the atomic dipole operator can be considered as a bosonic annihilation operator, hence the name. Eqs. (3.6a,b) then become linear in the operators and contain the average population inversion merely as a parameter to be determined from Eq. (3.6c) in a self-consistent manner. In this way difficulties stemming from the quantum correlation term $a\sigma_z$ disappear.

The use of this approximation is particularly useful in the limit of low saturation, when the population is mostly in the ground state, and the two-level system can be extended to an infinite latter (boson mode) without significantly altering the outcome [72]. The population inversion then can be further approximated by constant $-1/2$, disregarding its dynamics, and for the amplitude a of the resonator mode and the polarisation σ of the atom we are left with two linear Heisenberg-Langevin equations:³

$$\dot{a} = (i\Delta_C - \kappa) a + gf(\mathbf{r}) \sigma + \eta + \xi, \quad (3.8a)$$

$$\dot{\sigma} = (i\Delta_A - \gamma) \sigma - gf(\mathbf{r}) a - \eta_t(\mathbf{r}) + \zeta. \quad (3.8b)$$

²We note that for a single atom moving in 1D, the Langevin equation has been numerically constructed by Doherty et al. [71] in such a way that the internal dynamics was simulated while putting the atomic motion on an appropriately dense spatial grid. What we do here is different: we want a model which yields explicit expressions for the coefficients of Eq. (3.3).

³In the limit of extremely weak excitations when the dynamics can be restricted to the subspace of one single (atomic *or* photonic) excitation, $\langle \sigma_z a \rangle = -1/2 \langle a \rangle$ is exactly fulfilled [28].

Further progress is made by solving the system (3.8) in different orders of the atomic velocity. For this the time derivation on the LHS is replaced by the hydrodynamic derivation

$$\frac{d}{dt} \longrightarrow \frac{\partial}{\partial t} + \mathbf{v} \nabla, \quad (3.9)$$

while on the RHS variables are cast in the form

$$a = a^{(0)} + \mathbf{v} \mathbf{a}^{(1)} + \mathcal{O}(v^2), \quad (3.10a)$$

$$\sigma = \sigma^{(0)} + \mathbf{v} \boldsymbol{\sigma}^{(1)} + \mathcal{O}(v^2), \quad (3.10b)$$

where $\mathbf{a}^{(1)}$ and $\boldsymbol{\sigma}^{(1)}$ are 2D vectors, which express the impact of atomic motion on the cavity field and atomic polarisation up to first order in the atomic velocity, ie the non-adiabatic response of the two to the atomic motion. The first-order expansion is a good approximation as long as $Kv \ll \gamma, \kappa$.

Putting these expressions back to Eq. (3.5), taking expectation values, and keeping terms up to first order in velocity we obtain the Langevin force, that is, the coefficients \mathbf{f} and $\boldsymbol{\beta}$ of Eq. (3.3).

3.2.4 Adding the recoil diffusion

Since for the internal degrees of freedom the Heisenberg-Langevin approach is used, the recoil diffusion has to be added to the diffusion matrix by hand — in the Lindblad approach it was inherent, cf Eq. (3.2b). The recoil-induced part of the diffusion we shall consider to be proportional to identity, which is in equivalent to the assumption that in the Liouvillean (3.2b) the $N(\mathbf{u})$ direction distribution is isotropic. The recoil contribution reads:

$$D_{\text{rec}} = \frac{2}{5} \hbar^2 k_A^2 \gamma \langle \sigma^\dagger \sigma \rangle. \quad (3.11)$$

The diffusion originating from the quantum noise of the internal variables we call dipole diffusion and is denoted by \mathbf{D}_{dip} . Hence, the diffusion matrix in Eq. (3.4) reads

$$\mathbf{D} = \mathbf{D}_{\text{dip}} + D_{\text{rec}} \mathbf{1}. \quad (3.12)$$

3.2.5 Semiclassical field & polarisation

Important results of Model 0sc, which are often referred to throughout this work are the expectation values of the cavity field operator a and atomic lowering operator σ for a point-like immobile atom at point \mathbf{r} . These expressions are gained from the system (3.8) by taking expectation values and solving for $\langle a \rangle$ and $\langle \sigma \rangle$:

$$\langle a \rangle = - \frac{\eta (i\Delta_A - \gamma) + g f(\mathbf{r}) \eta_t(\mathbf{r})}{(i\Delta_A - \gamma)(i\Delta_C - \kappa) + g^2 f^2(\mathbf{r})}, \quad (3.13a)$$

(The first term stands for the field directly injected to the cavity by the cavity pump, the second one is the field scattered by the atom from the atomic pump into the cavity.)

$$\langle \sigma \rangle = \frac{\eta_t(\mathbf{r})(i\Delta_C - \kappa) - gf(\mathbf{r})\eta}{(i\Delta_A - \gamma)(i\Delta_C - \kappa) + g^2 f^2(\mathbf{r})}. \quad (3.13b)$$

When there is no coupling ($g = 0$), we get the well-known expressions of Lorentzian resonances for both expectation values. With $g \neq 0$ another type of resonance arises: The real part of the denominator vanishes at a given atomic position \mathbf{r} under the resonance condition $\gamma\kappa - \Delta_A\Delta_C + g^2 f^2(\mathbf{r}) = 0$. A necessary condition for this resonance to occur is that the sign of the detunings be the same.

3.3 Eliminated model — Model 1

In the case of relatively high atomic detunings, any direct simulation of the full problem defined by Eqs. (3.2) requires very small time steps, making the simulation a fruitless tiptoeing.⁴

Since in this case the atomic saturation is low (Eq. 3.13b), we can simplify the problem by adiabatically eliminating the upper atomic level (the internal atomic dynamics). In this approximation we are left with a moving linearly polarisable particle with induced polarisation expressed from Eq. (3.8b):

$$\sigma \approx \frac{g \mathcal{E}(\mathbf{r})}{i\Delta_A - \gamma}. \quad (3.14)$$

$\mathcal{E}(\mathbf{r}) = f(\mathbf{r})a + \eta_t(\mathbf{r})/g$ is the dimensionless total electric field at point \mathbf{r} .⁵

⁴Naturally, this problem cannot be solved by using interaction picture as it is easy to see starting from a Jaynes-Cummings part of the Hamiltonian (3.2a):

$$H = -\hbar\Delta_A \sigma_z - i\hbar\eta_t(\mathbf{r})(\sigma^\dagger - \sigma).$$

We can change to interaction picture using the first term (Δ_A is the big frequency): $U_I(t) = e^{-i\Delta_A t \sigma_z}$. The interaction-picture Hamiltonian then reads

$$H_I(t) = U_I(t) H U_I^\dagger(t) + i\hbar \frac{dU_I(t)}{dt} U_I^\dagger(t) = -i\hbar\eta_t(\mathbf{r})(\sigma^\dagger e^{-i\Delta_A t} - \sigma e^{i\Delta_A t}),$$

where we have used the operator expansion theorem [see eg 73] and $[\sigma_z, \sigma] = -\sigma$, $[\sigma_z, \sigma^\dagger] = \sigma^\dagger$. We see that the big frequency survives, now in the time dependence of the Hamiltonian.

Note also that this survival of the big frequency is due to the fact that two neighbouring levels coupled by the non-diagonal part of the Hamiltonian are separated by the big energy gap $\hbar\Delta_A$. On the other hand, it is of course possible to get rid of eg the big frequency $n\Delta_C$ of the free evolution of the n th Fock state component, since here the separation $\hbar\Delta_C$ of neighbouring levels coupled by the interaction is small. The same is true for the kinetic part of the Hamiltonian where with the interaction picture we gain that the frequency grows proportionally to k instead of k^2 . This will indeed be exploited in Sec. 4.1.3, see Eq. (4.6).

⁵The physical electric field reads

$$\mathbf{E} = i\sqrt{\frac{\hbar\omega_C}{2\varepsilon_0\mathcal{V}}}(\mathbf{e}\mathcal{E} - \text{h.c.}).$$

We put this expression back into the Hamiltonian and Liouvillean as expressed in Eqs. (3.2) to obtain effective operators governing the coupled atomic CM and field dynamics:

$$\begin{aligned}
H_{\text{eff}} &= \frac{\mathbf{p}^2}{2\mu} - \hbar\Delta_C a^\dagger a - i\hbar\eta (a - a^\dagger) + \hbar U_0 \mathcal{E}^\dagger(\mathbf{r}) \mathcal{E}(\mathbf{r}) \\
&= \frac{\mathbf{p}^2}{2\mu} + \hbar\eta_{\text{eff}} \sin^2(Kz) - \hbar(\Delta_C - U_0 \sin^2(Kx)) a^\dagger a - i\hbar\eta (a - a^\dagger) \\
&\quad + \hbar\sqrt{U_0 \eta_{\text{eff}}} \sin(Kx) \sin(Kz) (a^\dagger + a), \quad (3.15a)
\end{aligned}$$

(with $\eta_{\text{eff}} = \frac{\eta^2 \Delta_A}{\Delta_A^2 + \gamma^2}$)

$$\begin{aligned}
\mathcal{L}_{\text{eff}}\rho &= \kappa \left(2a\rho a^\dagger - [a^\dagger a, \rho]_+ \right) \\
&\quad + \Gamma_0 \left(2 \int d^2\mathbf{u} N(\mathbf{u}) \mathcal{E}(\mathbf{r}) e^{-iK\mathbf{u}\mathbf{r}} \rho e^{iK\mathbf{u}\mathbf{r}} \mathcal{E}^\dagger(\mathbf{r}) - [\mathcal{E}^\dagger(\mathbf{r}) \mathcal{E}(\mathbf{r}), \rho]_+ \right). \quad (3.15b)
\end{aligned}$$

Here the internal atomic dynamics is incorporated into the light-shift coefficient

$$U_0 = \frac{g^2 \Delta_A}{\Delta_A^2 + \gamma^2}, \quad (3.16a)$$

and the incoherent scattering rate

$$\Gamma_0 = \frac{g^2 \gamma}{\Delta_A^2 + \gamma^2}. \quad (3.16b)$$

In this model the atomic pump creates a classical potential for the atom in the z direction. There is a potential in the x direction, too, but it being proportional to $a^\dagger a$, it is more than a normal potential. As we shall see later, its (quantum) dynamical nature leads to many interesting phenomena, including the dynamical cavity cooling effect (cf Sec. 5.1) or a reduction of trapping times (Sec. 5.2.5). The corresponding term can also be interpreted as the cavity resonance shifted by the atom, at most at an antinode by U_0 . The last term of the Hamiltonian is an interference term between cavity mode and atomic pump, which also yields both pumping for the mode and potentials for the atom in both directions.

For further reference we now quote the Hamiltonians corresponding to the three system configurations treated in this work:

$$H_{\text{CX}} = \frac{p_x^2}{2\mu} - \hbar(\Delta_C - U_0 \sin^2(Kx)) a^\dagger a - i\hbar\eta (a - a^\dagger), \quad (3.17a)$$

$$H_{\text{AZ}} = \frac{p_z^2}{2\mu} + \hbar\eta_{\text{eff}} \sin^2(Kz) - \hbar(\Delta_C - U_0) a^\dagger a + \hbar\sqrt{U_0 \eta_{\text{eff}}} \sin(Kz) (a^\dagger + a), \quad (3.17b)$$

$$H_{\text{AX}} = \frac{p_x^2}{2\mu} - \hbar (\Delta_{\text{C}} - U_0 \sin^2(Kx)) a^\dagger a + \hbar \sqrt{U_0 \eta_{\text{eff}}} \sin(Kx) (a^\dagger + a). \quad (3.17\text{c})$$

We see that H_{AZ} and H_{AX} are intimately connected, the only difference being that in the AZ case there is a classical lattice potential generated by the atomic pump, which in the AX case is replaced by the dynamical potential mentioned above.

It is important to note that after the elimination (3.14), the problem is not specific to a two-level atom any more. The system (3.15) describes a general linearly polarisable (but possibly quantum mechanical) particle such as a molecule or a microscopic silicon ball. The interaction of such systems with the electromagnetic field has been a field of intense interest [74, 75, 76]. Cooling of molecules by optical means is an unsolved problem [77, 78, review: 79]. Their interaction with a cavity field may provide a viable alternative for cooling.⁶

For an arbitrary linearly polarisable particle the polarisation is proportional to the electric field: $\mathbf{P} = \varepsilon_0 \chi \mathbf{E}$, the only parameter being the complex susceptibility. The parameters Δ_{A} , γ and g defined in Sec. 2.1 make no sense, since here is no definite atomic transition any more. In the present model, however, these three parameters occur only in the combinations U_0 and Γ_0 . It is easy to see that their connection with χ is

$$\hbar U_0 = -\frac{\hbar \omega_{\text{C}}}{V} \Re\{\chi\}, \quad \hbar \Gamma_0 = -\frac{\hbar \omega_{\text{C}}}{V} \Im\{\chi\}. \quad (3.18)$$

To derive these equations we have used Eqs. (2.1), (3.14) and the fact that for a two-level atom the polarisation $\mathbf{P} = \mathbf{d} = (\langle e | \mathbf{d} | g \rangle \sigma + \text{h.c.})$. Turning this calculation around we obtain the complex susceptibility for a two-level atom:

$$\chi = -\frac{|\langle g | \mathbf{d} | e \rangle|^2}{\hbar \varepsilon_0 (\Delta_{\text{A}} + i\gamma)}. \quad (3.19)$$

3.4 Semiclassical approach to Model 1 — Model 1sc

Finally, starting from Model 1, we describe the simplest possible model that seizes the coupled dynamics of a moving linear dipole and the single-mode field in the resonator. This approach was developed in [29].

Owing to its simplicity, the model can be solved even for several independent particles. In this case, though there is no direct interaction between the particles, they interact with the very same cavity mode, which, in turn, acts back on the atoms. This can create interesting collective phenomena, and indeed, the model proved to be very

⁶Note that standard laser cooling schemes cannot be applied to molecules: Molecules do not have closed optical transition cycles, therefore the electronic transitions should not be saturated. Standard laser cooling schemes do not work in the limit of vanishing saturation.

useful, for example, in predicting the effect of collective cooling of an atomic ensemble by self-organisation [35], which has been observed experimentally by Black et al. [63].

Besides giving a physical insight into the nonlinear dynamics, this semiclassical model is expected to give quantitatively good estimates for various physical observables in its well-defined range of validity, ie for relatively large photon numbers ($\gtrsim 4$) and for broad enough momentum distribution.

The eliminated model (3.15) is solved by a semiclassical approach, and the resulting equations describe the fluctuating, Brownian-like motion of the atom *and* the photon field taking into account the correlation between the different noise terms consistently with quantum theory. The labelling “semiclassical” here is for the same reason as for the approach presented in Sec. 3.2.5: both particle and field are classical, but the correlated noises in their dynamics are of quantum mechanical origin.

In the present approach an equation for the joint atom-mode Wigner function is derived from the effective Master equation

$$\dot{\rho} = \frac{1}{i\hbar} [H_{\text{eff}}, \rho] + \mathcal{L}_{\text{eff}} \rho, \quad (3.20)$$

(cf Eqs. 3.15) and truncated to obtain a Fokker-Planck equation, which is classical in form, but the origin of the noise terms is purely quantum mechanical. Thereafter, the equivalent Langevin equations are solved:

$$\dot{\mathbf{r}} = \frac{\mathbf{p}}{\mu}, \quad (3.21a)$$

$$\dot{\mathbf{p}} = -\hbar U_0 \nabla |\mathfrak{E}(\mathbf{r})|^2 + 2\hbar\Gamma_0 \Im \{ \mathfrak{E}^*(\mathbf{r}) \nabla \mathfrak{E}(\mathbf{r}) \} + \boldsymbol{\xi}, \quad (3.21b)$$

$$\dot{\alpha} = (i\Delta_C - \kappa) \alpha - (iU_0 + \Gamma_0) f(\mathbf{r}) \mathfrak{E}(\mathbf{r}) + \eta + \zeta. \quad (3.21c)$$

Here $\alpha = \langle a \rangle$ is the amplitude of the coherent cavity field, and $\mathfrak{E}(\mathbf{r}) = \langle \mathcal{E}(\mathbf{r}) \rangle = f(\mathbf{r}) \alpha + \eta_t(\mathbf{r})/g$. The noise terms obey second-order correlation laws:

$$\langle |\zeta|^2 \rangle = \kappa + f^2(\mathbf{r}) \Gamma_0, \quad (3.22a)$$

$$\langle \boldsymbol{\xi} \zeta \rangle = i\hbar\Gamma_0 f(\mathbf{r}) \nabla \mathfrak{E}(\mathbf{r}), \quad (3.22b)$$

$$\langle \xi_i \xi_j \rangle = 2\hbar^2 K^2 \Gamma_0 |\mathfrak{E}(\mathbf{r})|^2 \overline{u_i^2} \delta_{ij} + 2\hbar^2 \Gamma_0 \Re \{ \partial_i \mathfrak{E}^*(\mathbf{r}) \partial_j \mathfrak{E}(\mathbf{r}) \}. \quad (3.22c)$$

Here $\overline{u_i^2} = \int d^2\mathbf{u} N(\mathbf{u}) u_i^2$. In the RHS of the last row, the first term stands for recoil diffusion (cf Sec. 3.2.4), while the second one is the diffusion originating from dipole force fluctuations. The efficient way to simulate these noise processes is given by Domokos and Ritsch [30].

It is interesting to look at the dimensionless version of the deterministic part of

Eqs. (3.21):

$$\frac{d\tilde{\mathbf{r}}}{d\tilde{t}} = \tilde{\mathbf{p}}, \quad (3.23a)$$

$$\frac{d\tilde{\mathbf{p}}}{d\tilde{t}} = \tilde{\omega}_{\text{rec}} \left(-\tilde{U}_0 \tilde{\nabla} |\mathfrak{E}(\tilde{\mathbf{r}})|^2 + 2\tilde{\Gamma}_0 \Im \left\{ \mathfrak{E}^*(\tilde{\mathbf{r}}) \tilde{\nabla} \mathfrak{E}(\tilde{\mathbf{r}}) \right\} \right), \quad (3.23b)$$

$$\frac{d\alpha}{d\tilde{t}} = (i\tilde{\Delta}_{\text{C}} - 1) \alpha - (i\tilde{U}_0 + \tilde{\Gamma}_0) f(\tilde{\mathbf{r}}) \mathfrak{E}(\tilde{\mathbf{r}}) + \tilde{\eta}, \quad (3.23c)$$

where the dimensionless variables are:

$$\tilde{t} = \kappa t, \quad \tilde{\mathbf{r}} = K \mathbf{r}, \quad \tilde{\mathbf{p}} = \frac{K \mathbf{p}}{\kappa \mu}, \quad (3.24)$$

and all the frequency-like parameters have been made dimensionless by κ . Note that the recoil frequency $\omega_{\text{rec}} = \hbar K^2 / \mu$ has appeared as the relevant parameter instead of K and μ , and so there are six parameters in the full system: ω_{rec} , Δ_{C} , η , η_t/g , U_0 , Γ_0 . In the very far detuned regime Γ_0 is much smaller than all the rest, so that in this case we are left with only five parameters.

PART II

Achievements & Results

The quantum simulation

In Sec. 4.1 we describe how we have adapted the MCWF method for the atom-cavity system. We note that for practical considerations we simulate one dimension at a time. In Sec. 4.2 we overview the proper quantities characterising the statistical and quantum properties of the system, which we will use later when producing numerical results. Here, for convenience, we use Configuration CX. As an example the same configuration is used in Sec. 4.4 where we check the validity of the ergodic hypothesis for the system by studying transient behaviour (relaxation).

4.1 The MCWF method for the system

4.1.1 Discrete momentum basis

The method we shall describe for one dimension (x), but here this stands for either the cavity or the transverse direction because at this level they are completely equivalent.

We consider the joint state vector of the atom-cavity system:

$$|\Psi(t)\rangle = \sum_{n,k} \Psi(t, n, k) |n\rangle |k\rangle, \quad (4.1)$$

where $|n\rangle$ is the n th Fock state of the mode. The state of the atomic CM motion is most conveniently expanded in momentum basis ($|k\rangle$ stands for the basis element). The effect of the kinetic-energy operator should certainly be calculated in this basis, besides the (3.15) operators contain only sine functions of the operators x and z , which are also very easily represented in momentum basis.

For the simulations one certainly needs to discretize the momentum basis for the expansion (4.1). Suppose that during the whole time evolution, the atom is confined in some region of length L , an integer multiple of the cavity wavelength. Then the smallest wave number to be considered is $\Delta k = 2\pi/L$.

The evolution (3.20), however, couples only momentum components separated by K or $2K$, since in the system (3.15) the position operator is contained only in the form

$\sin(Kx)$, $\sin^2(Kx)$, and $\exp(iKx)$ — and the same for z . This means that the momentum part of the Hilbert space can be separated to subspaces containing momentum components with increment K , and the time evolution does not mingle these subspaces.

In state-vector language the above arguments can be translated as the expansion

$$\begin{aligned} |\Psi(t)\rangle &= \sum_{u=0}^{K/\Delta k} |\Psi^{(u)}(t)\rangle = \sum_{u=0}^{K/\Delta k} \sum_{v=-\infty}^{\infty} |\Psi_v^{(u)}(t)\rangle |vK + u\Delta k\rangle \\ &= \sum_{u=0}^{K/\Delta k} e^{i u \Delta k \hat{x}} \sum_{v=-\infty}^{\infty} |\Psi_v^{(u)}(t)\rangle |vK\rangle, \quad (4.2) \end{aligned}$$

where $|\Psi_v^{(u)}(t)\rangle$ is still a vector in the mode's Fock space. Expanding the initial condition $|\Psi(0)\rangle$ as above, the time evolution of different $|\Psi^{(u)}(0)\rangle$ components can be calculated independently, and the solution reassembled at the end.

Since $e^{i u \Delta k \hat{x}}$ does not commute with the kinetic part of the Hamiltonian, the evolution of each component will be slightly different. In the present work we shall not consider the implications of this feature since we always restrict ourselves to only one component, say, $|\Psi^{(0)}(t)\rangle$. Hence, in the actual simulations our momentum basis is $\{vK\}_{v \in \mathbb{Z}}$. Since our smallest momentum is $\hbar K$, it is easy to see that in real space this basis translates to considering a space of one cavity wavelength $-\pi < Kx < \pi$ with periodic boundary condition.

In Sec. 8.3 we shall see that using the reflectional symmetry of the Hamiltonian in momentum space, even the $\{vK\}_{v \in \mathbb{Z}}$ subspace falls into two independently evolving subspaces. Obviously, ergodicity in its exact sense cannot hold for such a system. This is, however, not a concern here, since the time evolution in the two subspaces is very similar, so that ergodicity holds to a very good approximation.

4.1.2 Jump operators

The operator (3.15b) being in the canonical form (A.2), with the index m running over the continuum of directions \mathbf{u} with one supplementary point for the cavity decay, we can readily determine the jump operators needed for the MCWF simulation of the (3.15) system. In the second term of (3.15b) it is sufficient to replace the directional integration by a sum of only three terms with $u_x = -1, 0, 1$, the 0 term having double weight. This change we make not only for the sake of simplicity, but it is also necessary because the projection of an arbitrary direction vector \mathbf{u} on the x axis being a non-integer number in general would invoke wave numbers that are not included in our discrete momentum basis.

We then obtain four jump operators, the first one corresponding to cavity decay

with operator:

$$J_C = \sqrt{2\kappa} a, \quad (4.3a)$$

the rest are the atomic spontaneous emission operators with three different recoil directions:

$$J_A(u_x = -1, 0, 1) = \sqrt{2\Gamma_0} e^{-iK u_x x} \mathcal{E}(x), \quad (4.3b)$$

the $u_x=0$ jump having double probability. The probability of cavity decay is proportional to the photon number

$$P_C = 2\kappa \langle a^\dagger a \rangle \Delta t, \quad (4.4a)$$

while the total probability of atomic decays reads

$$P_A = \langle J_A^\dagger J_A \rangle \Delta t = 2\Gamma_0 \langle \mathcal{E}^\dagger(x) \mathcal{E}(x) \rangle \Delta t. \quad (4.4b)$$

4.1.3 Some technical aspects

The Hamiltonian part of the time evolution is integrated by an adaptive step-size Runge-Kutta method. In particular, we used the `rkqs` routine from Numerical Recipes [80], which relies on the Cash-Karp algorithm. The time step Δt is chosen by this routine so that the relative error in each step be less than a prescribed value (10^{-6} in our case). The time step we bounded from above as well so that the total (cavity and atom) probability of jumps remain small ($P_C + P_A \approx 0.1$), which is an important condition for the MCWF method to give good statistics.

An important technical detail is that the kinetic part of the Hamiltonian (3.15a) may contribute arbitrary big frequencies depending on the resolution of the atomic motion, which results in instability in the stepper routine. The effective way to evade this problem is to adopt interaction picture defined by the diagonal part of the Hamiltonian. The unitary operator transforming between the two pictures reads:

$$U_I(t) = e^{i\left(\frac{p^2}{2\mu} + Z a^\dagger a\right)t}, \quad (4.5)$$

where $Z = (iU_0 + \Gamma_0)/2 - i\Delta_C + \kappa$. For reference we quote the non-Hermitian Hamiltonian part of the wave function's evolution in interaction picture in Fourier space (for

2D including both cavity and atomic pumps):

$$\begin{aligned}
\dot{\Psi}_I(n, \mathbf{k}) = & \eta \left(e^{Zt} \sqrt{n} \Psi_I(n-1, \mathbf{k}) - e^{-Zt} \sqrt{n+1} \Psi_I(n+1, \mathbf{k}) \right) + \frac{iU_0 + \Gamma_0}{2} \\
& \times \left\{ \frac{n}{2} \left(e^{i\frac{2(k_x-K)}{\mu}t} \Psi_I(n, k_x - 2K, k_z) + e^{-i\frac{2(k_x+K)}{\mu}t} \Psi_I(n, k_x + 2K, k_z) \right) \right. \\
& + \frac{\eta_t^2}{2g^2} \left(e^{i\frac{2(k_z-K)}{\mu}t} \Psi_I(n, k_x, k_z - 2K) + e^{-i\frac{2(k_z+K)}{\mu}t} \Psi_I(n, k_x, k_z + 2K) \right) \\
& - i\frac{\eta_t}{g} \sqrt{n} \left(e^{i\frac{(2k_z-K)}{2\mu}t+Zt} \Psi_I(n-1, k_x, k_z - K) \right. \\
& \quad \left. - e^{-i\frac{(2k_z+K)}{2\mu}t+Zt} \Psi_I(n-1, k_x, k_z + K) \right) \\
& \left. - i\frac{\eta_t}{g} \sqrt{n+1} \left(e^{i\frac{(2k_z-K)}{2\mu}t-Zt} \Psi_I(n+1, k_x, k_z - K) \right. \right. \\
& \quad \left. \left. - e^{-i\frac{(2k_z+K)}{2\mu}t-Zt} \Psi_I(n+1, k_x, k_z + K) \right) \right\}. \quad (4.6)
\end{aligned}$$

At the beginning of each time step we accord the two pictures, and come back from interaction picture after each one to monitor whether there must be a jump or not. If yes, the jump operator in normal picture is applied. In this, the idea is not to put too big numbers into the arguments of exponential functions, which would be the case if we were constantly in interaction picture and evolved a trajectory for long times, and which could result in numerical problems.

Note that since the entire Hamiltonian is implemented in Fourier space, during the actual evolution of the system, no FFT is needed, which is a huge gain in both computational time and accuracy. This is different from the case when one tries to solve a general Schrödinger equation where the kinetic part must be implemented in Fourier space while the potential in normal space. In that case one needs a quite intricate fourth order method reminiscent of the Runge-Kutta method with 8 (!) embedded FFTs per time step [81]. In this method the kinetic part is implemented with interaction picture, but there is no possibility of implementing adaptive time step.

With the MCWF simulation we can simulate one dimension for the atomic motion at a time, which can be either the cavity direction x or the transverse one z . Indeed: since we usually use about 100 momentum components to resolve the atomic motion, taking the additional dimension would invoke an increase by the same factor in the dimension of the Hilbert space. This would render the problem too big for nowadays computers. In practice we have three different programs for Configurations CX, AZ, and AX.

4.2 Statistical & quantum properties

In the remaining part of this Chapter, for the sake of simplicity, we consider Configuration CX.

4.2.1 Density operator

A significant novelty in our approach is that we are able to calculate and numerically treat the density operator of the system to decipher statistical and quantum properties. This we may do in two different ways giving the same result according to the ergodic hypothesis — which is certainly to be verified for the system:

- When interested in steady-state properties of the system we run only one trajectory $|\Psi(t)\rangle$ for a long time T and take the steady-state density operator as the time average

$$\rho_{ss} = \frac{1}{T - T_{rel}} \int_{T_{rel}}^T dt |\Psi(t)\rangle \langle \Psi(t)|, \quad (4.7)$$

where T_{rel} is an appropriately chosen relaxation time.

- When studying time dependence (relaxation) we run several (N_{traj}) trajectories $|\Psi_i(t)\rangle$ to calculate the time dependent

$$\rho(t) = \frac{1}{N_{traj}} \sum_{i=1}^{N_{traj}} |\Psi_i(t)\rangle \langle \Psi_i(t)|. \quad (4.8)$$

Having obtained the density operator we may verify whether and how much it describes a steady state by substituting it into the RHS of (3.20) and checking whether it vanishes. Note that though it is not possible to simulate (3.20) directly since it would necessitate very many evaluations of the RHS, evaluating it *once* with a given ρ is possible. A good measure is the trace norm of the operator

$$\|\dot{\rho}\| = \text{Tr} \{ \dot{\rho}^2 \}. \quad (4.9)$$

Monitoring this quantity is the proper way to determine whether we have already averaged enough trajectories or for sufficiently long times.

4.2.2 Characterising statistical properties in steady state

From the steady-state density operator we can calculate steady-state averages and probability distributions of observables. From the cavity-cooling point of view a central quantity is the number of excitation quanta $\langle n \rangle$ in the atomic motion. This quantity

is related to the phase-space volume occupied by the atom as

$$\langle n \rangle = \frac{\Delta x \Delta p}{\hbar} - \frac{1}{2}. \quad (4.10)$$

The calculation of $\Delta p = \sqrt{\langle p^2 \rangle - \langle p \rangle^2}$ is straightforward, for the momentum distribution examples are plotted in Fig. 4.1 along with fitted Gaussians (Maxwell-Boltzmann distribution). We see that though the distribution is not exactly thermal, the fit is quite good, so it makes quite good sense to define a „kinetic temperature” via the equipartition theorem as

$$kT = \frac{\langle p^2 \rangle}{\mu}. \quad (4.11)$$

A strong argument for using this quantity is that it is actually measured in „destructive” measurements when the cavity pump is switched off abruptly and the expansion of the atomic cloud is monitored.¹

About the calculation of $\Delta x = \sqrt{\langle x^2 \rangle - \langle x \rangle^2}$ some remarks are necessary. Our potential in (3.15a) being proportional to $f^2(x) = \sin^2(Kx)$ and since we use red atomic detuning so that U_0 is negative (high-field seeker atoms), we have two potential wells (antinodes of the mode) at $Kx = \pm\pi/2$ as depicted by the solid line in Fig. 4.2. As expected, in such a potential a two-peak distribution establishes as steady-state probability distribution of x . Examples for this are plotted by dashed lines in Fig. 4.2. We immediately see that in steady state $\langle x \rangle = 0$. To see how close the atom is to the ground state of *one* well, the $\Delta x = \sqrt{\langle x^2 \rangle}$ should be calculated for one well. This is straightforwardly done as follows: Suppose we have a two-peak probability distribution $p_{\text{tp}}(x) = a p_{\text{op}}(x - \pi/2) + b p_{\text{op}}(x + \pi/2)$ with $a + b = 1$ then the two-peak expectation value of x^2 is

$$\begin{aligned} \langle x^2 \rangle_{\text{tp}} &= \int dx x^2 p_{\text{tp}}(x) = \int dx x^2 \left(a p_{\text{op}}\left(x - \frac{\pi}{2}\right) + b p_{\text{op}}\left(x + \frac{\pi}{2}\right) \right) \\ &= \int dx \left(a \left(x + \frac{\pi}{2}\right)^2 + b \left(x - \frac{\pi}{2}\right)^2 \right) p_{\text{op}}(x) \\ &= \langle x^2 \rangle_{\text{op}} + \frac{\pi^2}{4} + (a - b) \pi \langle x \rangle_{\text{op}}, \end{aligned} \quad (4.12)$$

that is, if $a = b$ or $\langle x \rangle_{\text{op}} = 0$ (in our case both conditions happen to be satisfied) the desired one-peak average is calculated by subtracting $\pi^2/4$ from the two-peak average. If not otherwise stated, in what follows $\langle x^2 \rangle$ is always meant in the one-peak sense.

¹Note that the temperatures in the orthogonal directions are not necessarily the same, $T_x \neq T_z$. It is because of the external driving, which renders the system out of equilibrium: there is no thermalisation between the two directions.

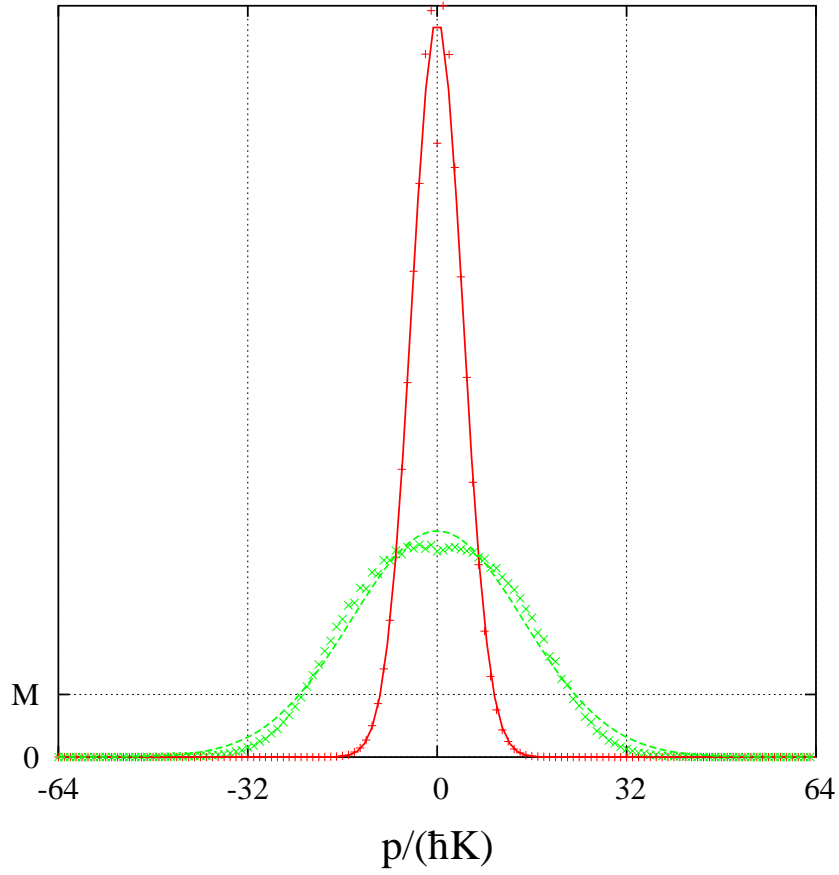


Figure 4.1: Simulated steady-state momentum distributions (points) along with fitted Maxwell-Boltzmann distributions (lines), with M denoting the mean value. For parameters refer to Tab. 4.1 — the narrow peak @ $(\kappa, \eta) = (0.025, 0.025)\gamma$; the wide one @ $(\kappa, \eta) = (0.3, 0.6)\gamma$.

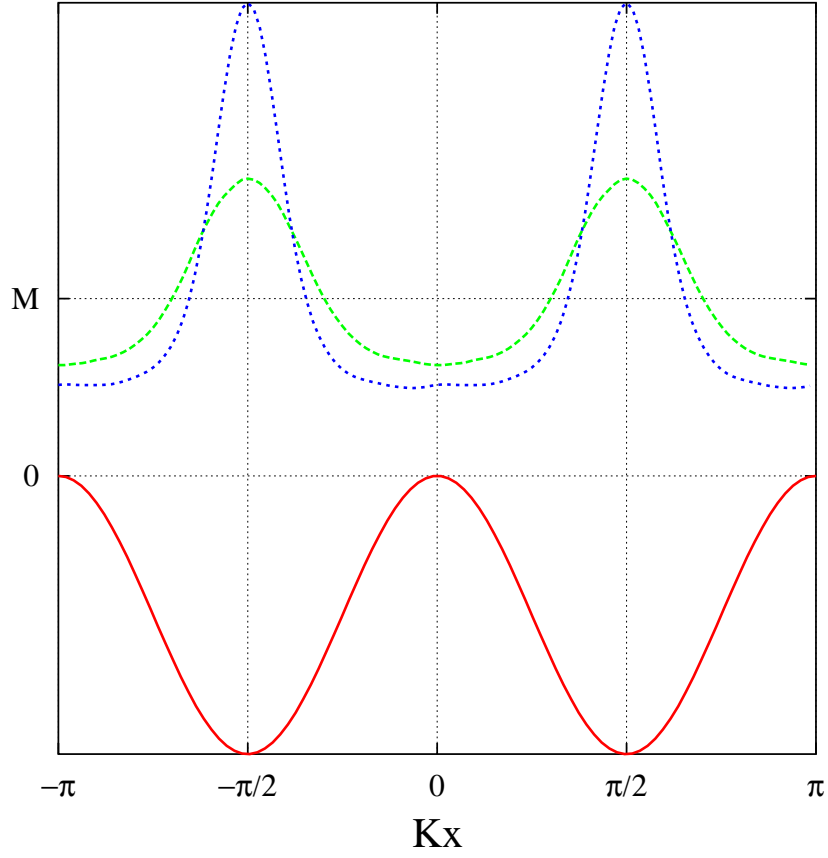


Figure 4.2: Solid line: potential felt by the atom in arbitrary units (calculated). Dashed lines: steady-state probability distributions of x (simulated), $M = 1/(2\pi)$ denoting the mean. Parameters as in Tab. 4.1 — the narrow peaks @ $(\kappa, \eta) = (0.025, 0.05)\gamma$; the wider ones @ $(\kappa, \eta) = (0.1, 0.1)\gamma$.

4.2.3 Characterising entanglement and other quantum properties

It is an interesting question and one which is to be answered only by a quantum mechanical simulation whether the steady state is a coherent or incoherent mixture of the two peaks or, more generally, what are the coherence properties of the steady-state atomic distribution. To study this, we calculate the reduced density operator for the atomic motion:

$$\rho(x_1, x_2) = \langle x_1 | \left(\sum_n \langle n | \rho | n \rangle \right) | x_2 \rangle, \quad (4.13)$$

and define the coherence function as

$$\chi(x) = \int d(K\xi) |\rho(\xi, \xi + x)|. \quad (4.14)$$

Examples for the coherence function are plotted in Fig. 4.3. The most important characteristics derived from this function are the coherence length L of one peak, which is the width of the main peak around zero, and the value $\chi(\pi)$ which is indeed a characteristic of the coherence between the two peaks. However, our simulations has shown that to obtain $\chi(\pi)$ nicely enough, huge statistics is needed, so it is better to perform one more integration and characterise the coherence between the two peaks by the average:

$$C = \frac{2}{\pi} \int_{\frac{\pi}{2}}^{\pi} d(Kx) \chi(x). \quad (4.15)$$

Another important point concerning the quantum nature of the atom-cavity system is whether in steady state there is some entanglement between the atomic motion and the cavity field. For mixed bipartite states as the one we have here, this question is a hard one and there has been a remarkable effort in the literature devoted to the problem of establishing computable measures of entanglement. Since by proper algebra packages the full eigenvalue problem of ρ can be fairly solved, in our case the most appropriate entanglement measure is clearly the negativity [82, 83], calculated from the partial transpose of the density operator

$$\langle n_1, k_1 | \rho^{\text{PT}} | n_2, k_2 \rangle = \langle n_1, k_2 | \rho | n_2, k_1 \rangle \quad (4.16)$$

as the sum

$$\text{negativity} = \left| \sum_i \lambda_i \right| \quad (4.17)$$

of the negative eigenvalues λ_i of ρ^{PT} . For the eigenvalue problem, we used the `zgeev` routine from the **Linear Algebra PACKage** [84], which is capable of finding the full eigensystem of even an 1000×1000 matrix in almost no time at all.

The other question addressed appropriately by a quantum simulation is whether the state of the cavity field is classical (coherent state) as it is assumed in most of the

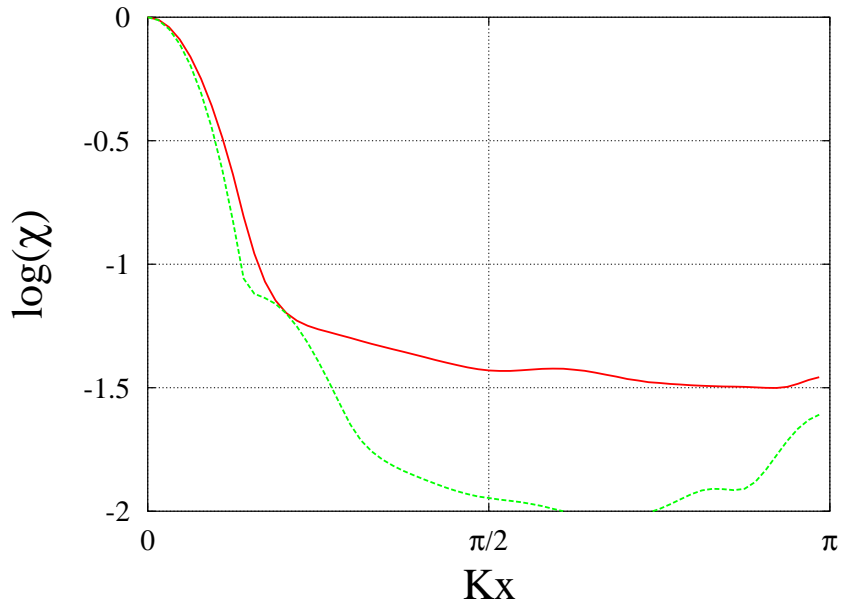


Figure 4.3: Typical behaviour of the coherence function $\chi(x)$ on logarithmic scale. The width of the main peak gives the coherence length of the wave packet in one potential well. The function falls rapidly from $x = 0$ then up to $Kx = \pi$ it grows again slightly, indicating small but non-vanishing coherence between the wave packets in the two wells. Parameters as in Tab. 4.1 but $\kappa = 0.025\gamma$ — solid line @ $\eta = 0.025\gamma$; dashed line @ $\eta = 0.05\gamma$.

semiclassical models. Instead of addressing the full problem, here we shall treat a weaker one: whether the photon statistics is Poissonian, that is, whether the state is an incoherent mixture of coherent states with different phases. For Poissonian statistics the variance equals the mean, so a good measure of nonclassicality is the Mandel Q parameter [73] defined as:

$$Q = \frac{\Delta(a^\dagger a) - \langle a^\dagger a \rangle}{\langle a^\dagger a \rangle}. \quad (4.18)$$

Note that the Hamiltonian (3.15a) containing $a^\dagger a$ as the only higher order term in the field operator a , for an immobile atom or even a separable atom-mode state there would be no way for the field to become else than a coherent state, the driving η being coherent. Therefore, if we observe nonclassicality ($Q \neq 0$) it must be due to atom-mode entanglement, whence this quantity is certainly intimately connected to the negativity.

4.3 System parameters for the MCWFS

In what remains from this Chapter and also in Chap. 5 we consider Configuration CX. Besides studying the quantum regime of the system, our aim is also to compare the newly developed MCWF solution of Model 1 for the case of cavity cooling of one single atom with the predictions of Model 1sc as presented by Domokos et al. [29].

Since for the MCWFS photon number is a crucial quantity, we quote the expectation value of the field here again from Eq. (3.13a) for Configuration CX and with the parameters of Model 1 — recall that this is for a fixed point-like atom situated at point x :

$$\langle a \rangle = \frac{\eta}{(iU_0 + \Gamma_0) \sin^2(Kx) - (i\Delta_C - \kappa)}. \quad (4.19)$$

We shall use mostly the same work point for parameters as the authors of the above Reference: Δ_A should be big enough ensuring small saturation ($\lesssim 0.05$) so that we can use Model 1. Good cavity (small κ) and strongly coupled atom (big g) are considered. $\Delta_C = U_0$ is taken, fulfilling the resonance condition and making that the maximum of the semiclassically expected field (4.19) sets in when the atoms are situated at the antinodes of the field, and its value reads

$$\langle a \rangle \left(Kx = \pm \frac{\pi}{2} \right) = \frac{\eta}{iU_0 + \Gamma_0 - i\Delta_C + \kappa} = \frac{\eta}{\kappa + \Gamma_0} \approx \frac{\eta}{\kappa}, \quad (4.20)$$

the third equality holding unless κ is so small that it becomes comparable with the incoherent scattering rate: $\Gamma_0 = 0.015\gamma$ with our parameters.

We take rubidium 85 atom. For reference, the parameters used in this Section are summarised in Tab. 4.1.

In the semiclassical case there is a lower bound on the photon number ($\gtrsim 4$) for the model to be valid, thus, roughly, $\eta/\kappa \gtrsim 2$ had to be considered. Here there is no

Δ_A	-20γ
Δ_C	$U_0 = -0.312\gamma$
κ	0.1γ
η	$\kappa, 2\kappa$
g	2.5γ
m	$415 \frac{\hbar\gamma}{K^2}$

Table 4.1: Parameters used throughout Chap. 4 and in Sec. 5.2.

limit in principle, however, there is a practical upper bound because too big photon numbers would lead to a very high dimensional Hilbert space, making the problem intractable. Therefore $\eta/\kappa = 1$ and 2 are considered with 1 and 4, respectively, for the semiclassically expected photon number. In the $\eta/\kappa = 2$ case the Fock basis is truncated already at as high as the 10th element, which, together with the roughly 100 discrete momentum components results in a 10^3 dimensional Hilbert space — 10^6 complex numbers for the density matrix. This being still feasible, the two approaches can be compared in this case.

4.4 Relaxation & ergodicity

First we study relaxation of an ensemble of systems started from zero cavity field and incoherent mixture of wave packets evenly distributed in space, corresponding to Doppler temperature, no entanglement, and $C = 0$ — no coherence in the atomic distribution. This is, on one hand, to determine the relaxation time of the system needed in (4.7), on the other hand, to practically verify the ergodic hypothesis. Time dependence of statistical averages and quantum characteristics calculated from the ensemble averaged density operator are plotted in Fig. 4.4. Along with the relaxation the steady state value is also indicated by a constant solid line calculated by averaging one single trajectory for a very long time (about $2 \cdot 10^6/\gamma$ in this case).

What we observe here is that statistical averages fairly relax to the steady-state value: the kinetic temperature and the localisation on a scale of about $1000/\gamma$, the photon number on a much faster scale of $100/\gamma$. Quantum characteristics: negativity, coherence, and $\|\dot{\rho}\|$, however, do not relax to the steady-state but to some higher value. This value certainly tends to the steady-state value with increasing number of trajectories as we also demonstrate in Fig. 4.4(d-f). The conclusion to be drawn is therefore that to obtain the off-diagonal elements of the density operator (phase of wave function) much bigger statistics is needed than for the diagonal elements (modulus of wave function)

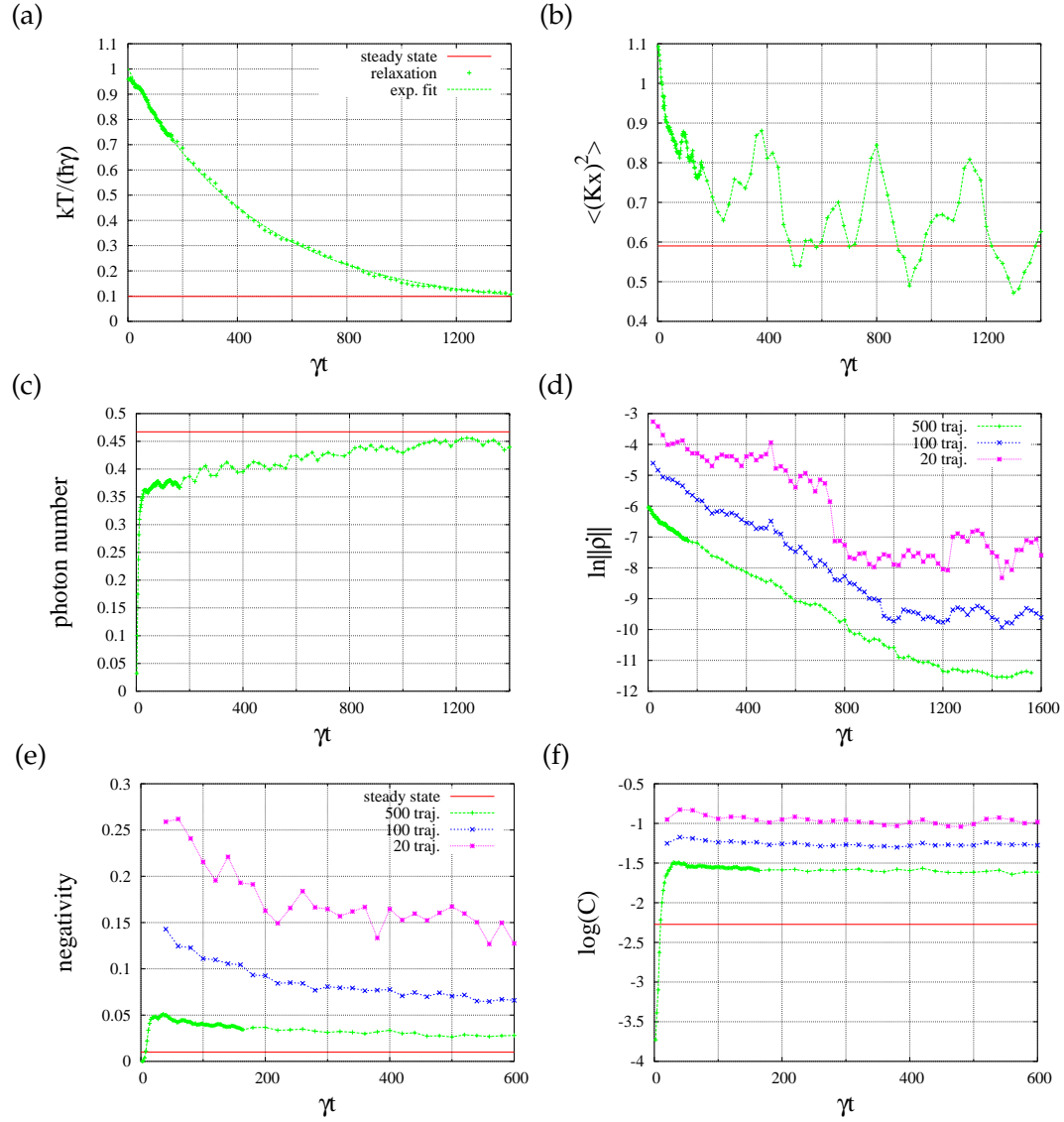


Figure 4.4: Relaxation of the system started from the zero-photon state and incoherent mixture of Doppler-temperature wave packets evenly distributed in space. Average of 500 trajectories. Steady-state values are indicated by solid lines. Quantum characteristics (negativity, C) of the system do not relax to the steady state value ($-\infty$ for the latest one on a logarithmic scale), but the value they relax to tends to the steady state as we increase the number of trajectories. Parameters: Tab. 4.1.

— quantum characteristics are the only that actually rely on off-diagonal elements. This huge statistics is not practical any more, that is the reason why in the following we shall be using time averaging whenever possible. The fact that the steady-state coherence and negativity is smaller than the values finite numbers of trajectories relax to, is definitely what we expect by intuition: individual trajectories naturally exhibit these properties while more and more incoherent averaging deteriorates them.

An interesting fact in itself is, however, that the dissipative atom-mode dynamics is able to *create* coherence even from a completely incoherent initial condition as we observe in Fig. 4.4(f). The fact that the steady state exhibiting low temperature and weak but non-vanishing coherence between the two trapping sites is reached even from a relatively hot and completely incoherent initial condition is a good indication of its robustness and the justness of the ergodic hypothesis.

4.5 Thesis

Thesis I

Based on the Monte Carlo Wave Function method we have created a simulation to study one atom moving in a single-mode cavity field with the atomic internal degree of freedom eliminated. It takes into account the whole coupled atom-field dynamics on a fully quantum mechanical basis. Exploiting the special form of the potentials, the whole evolution of the wave function could be implemented in momentum space with adaptive time step which is a huge gain both in terms of CPU time and accuracy as compared to conventional methods for solving Schrödinger equations. We are able to calculate and numerically treat the full joint atom-field steady-state density operator to decipher quantum properties of the system pertaining to coherence, entanglement, and nonclassicality.

Quantum regime of cavity cooling

Throughout this Chapter we consider Configuration CX. First we describe shortly the mechanism of the so called *dynamical cavity cooling* occurring in this simplest configuration [27]. In Sec. 5.2 we shall examine the dependence of system observables on the bandwidth of the relevant dissipation channel. Here, to enter the quantum regime, we decrease the cavity photon number, while in the high-enough photon number regime accessible also with Model 1sc, we shall compare results of Model 1sc and the MCWF solution of Model 1. As we shall see, the correspondence is remarkable in Model 1sc's expected range of validity. In Sec. 5.3 by increasing the atom-field coupling g with the Rabi frequency kept constant, we enter the quantum regime of cavity cooling.

5.1 Dynamical cavity cooling — mechanism

Cavity cooling owes to the friction force exerted by the cavity field on the atom. The resulting temperature is eventually determined by the ratio of the friction and the diffusion coefficients. In a cavity, diffusion stems not only from recoil, but also from dipole force fluctuations.

In Configuration CX the friction force is due to the dynamic potential term proportional to $\sin^2(Kx) a^\dagger a$ in Hamiltonian (3.17a). Suppose that Δ_C , $U_0 < 0$ and the atom is initially moving fast along the cavity axis.

The condition Δ_C , $U_0 < 0$ makes that an antinode of the field is both a potential minimum and an atom situated here maximises the cavity field, since it pulls the cavity towards resonance (cf Eq. 4.19). For a moving atom, however, due to the dissipative dynamics of the field, it adapts itself only on a timescale κ^{-1} to the atomic motion. Therefore, the field reaches its maximum value every time shortly *after* the atom has passed an antinode of the mode (potential minimum), and when it starts climbing the ramp, it is already becoming steeper than the previous slope it has rolled down on. On average it climbs higher hills than the slopes on which it rolls down, hence losing

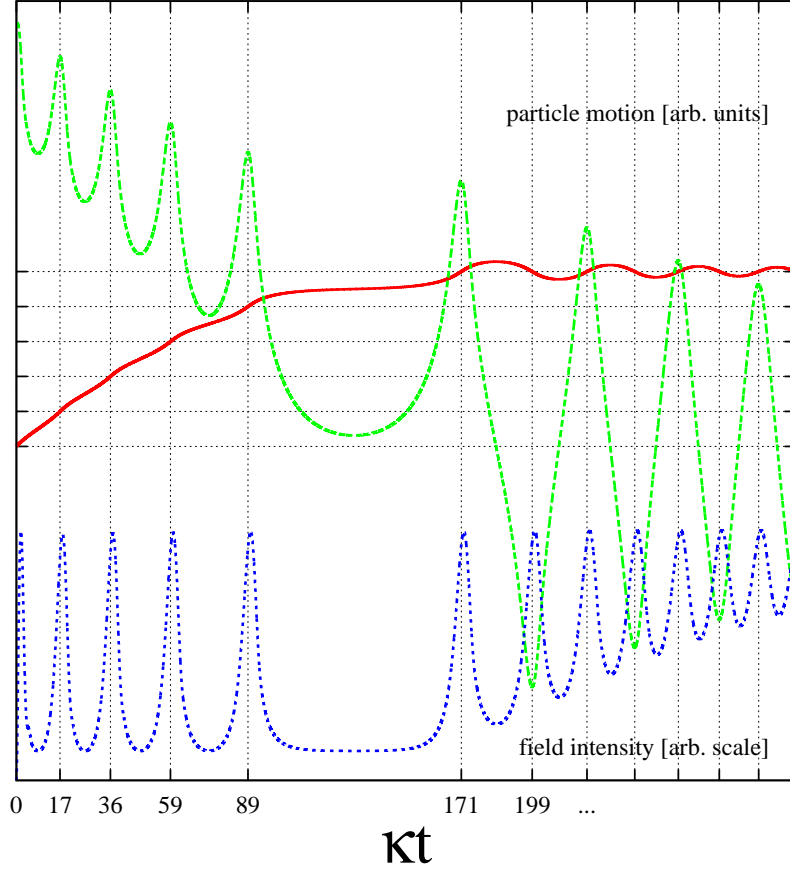


Figure 5.1: Capturing an initially fast atom by the cavity cooling mechanism: time evolution of the field intensity (dotted line), particle position (solid line) and particle momentum (dashed lines). The dotted vertical lines mark the time instants when the atom crosses the field antinodes (horizontal dotted lines). The field intensity reaches its maximum value always shortly afterwards. @ $(\omega_{\text{rec}}, U_0, \Delta_C, \eta) = (5 \cdot 10^{-3}, -3, -4, 1.5)\kappa$.

kinetic energy.¹

Eventually the atom gets stopped and oscillates in a single well around an antinode, where the kinetic energy slowly further decreases. The described process is visualised in Fig. 5.1 where we have used Model 1sc without noise to calculate the trajectory.

Note that all this is without spontaneous emission and the energy is carried away by the cavity damping. The philosophy here is that in strongly coupled systems, all subsystems share all available dissipation channels, the final temperature scaling with the decay rate of the dominating channel. Since in the far atomic detuning regime spontaneous emission is strongly suppressed ($\Gamma_0 \ll \kappa$), the final temperature will scale with κ , which can be much smaller than γ .

Recall that in free-space Doppler cooling the limiting temperature reads [14]:

$$kT_D = \frac{\hbar\gamma}{2} \left(\frac{\Delta_A}{\gamma} + \frac{\gamma}{\Delta_A} \right) \begin{cases} \longrightarrow \frac{\hbar\Delta_A}{2} & \text{for } |\Delta_A| \gg \gamma \\ \geq \hbar\gamma & \text{equality for } \Delta_A = \gamma \end{cases}, \quad (5.1)$$

that is, the minimum temperature is γ , while in the far detuned regime (low saturation) the cooling is quite inefficient. In the following, the limiting temperature $\hbar\gamma$ will be often referred to as the “Doppler temperature”.

5.2 Role of the cavity

The basic idea behind cooling atoms in a resonator is that the kinetic energy can be dissipated via the cavity loss channel because of the strongly-coupled atom-field dynamics. Therefore, the dependence of observables on the bandwidth κ of the relevant dissipation channel must manifest the cavity cooling mechanism.

5.2.1 Scaling of parameters

To distill this effect, the local electromagnetic field intensity should be invariant. Therefore, in the following we keep η/κ constant, cf semiclassically expected field (4.20), while studying steady-state properties of the system as a function of the cavity decay rate κ . Since the photon number is constant, unlike in the next Section we can simulate the whole κ range with the MCWF simulation.

The semiclassical equations (3.21) of Model 1sc serve as a good starting point. Here, for reference, we quote them for Configuration CX. The atom moves under the action

¹From the above discussion it follows that the smaller the κ the smaller the capture range of the cooling mechanism: Indeed atoms with a velocity $\gtrsim \kappa/K$ will pass the field node *before* the cavity field adapts itself, and instead of a ramp find themselves again on a slope.

of the field as

$$\dot{x} = \frac{p}{\mu}, \quad (5.2)$$

$$\dot{p} = -\hbar K U_0 |\alpha|^2 \sin(2Kx) + \xi_p, \quad (5.3)$$

where $|\alpha|^2$ is the cavity photon number. It is kept closely constant by the assumption $\eta/\kappa = \text{const}$. This means that the magnitude of the mechanical forces acting on the atom is kept invariant. This action can be achieved with few photons making many round-trips and hitting the atom many times (small κ limit), or with many photons making only a few round-trips (large κ limit). One can view this situation as with increasing κ the role of the cavity is gradually switched off and the free-space Doppler cooling scheme is rendered.

Results are plotted in Figs. 5.2, 5.3, 5.4, and 5.5 at two different pump strengths $\eta/\kappa = 1$ and $\eta/\kappa = 2$. Stars indicate Model 1sc results in the $\eta/\kappa = 2$ case, which fairly fit on the quantum data in the range $\kappa \gtrsim 0.1\gamma$. Semiclassical data cannot be produced for smaller values of κ , nor for the $\eta/\kappa = 1$ setting, because of the too low photon numbers involved, shown in Fig. 5.2. Note also that the simulated photon numbers, plotted by points, are always below the line representing the expected ones calculated from the formula (4.20). The reason is that in the simulation there is a finite extension of the atomic distribution (regardless whether it is incoherent as in the semiclassical model or has some coherence as in the quantum-mechanical one) while in (4.20) we have assumed a point-like atom fixed at an antinode.

5.2.2 Temperature, motional excitation quanta

With increasing κ the system tending to the free-space Doppler cooling scheme, the temperature increases as $kT \approx \hbar\kappa$ (see Fig. 5.3(a)). This numerical result verifies that the final achievable temperature scales with the bandwidth of the dominating loss channel. In the limit of $\kappa \rightarrow 0$, the temperature is fairly low and tends to the other decay rate of the system, $kT \rightarrow \hbar\Gamma_0$.

In a harmonic potential, which sets in close to the attractive antinodes of the cavity mode, the virial theorem makes a connection between the localisation $\langle x^2 \rangle$ and the mean kinetic energy $\langle p^2 \rangle$ (proportional to the temperature T). Both are appropriate measures for characterising the thermal properties of the system. However, for weak enough intensities, in particular in the limit of $\kappa \approx 0$, the optical potential vanishes. Therefore, the fact that how much the atomic motion is quantised (how close we are to an eventual BEC) should be expressed not in terms of the temperature but rather the number of excitation quanta which is related to the phase-space volume $\Delta x \Delta p$ occupied by the ensemble as (4.10). It is plotted in Fig. 5.3(b) and is valid for the full range

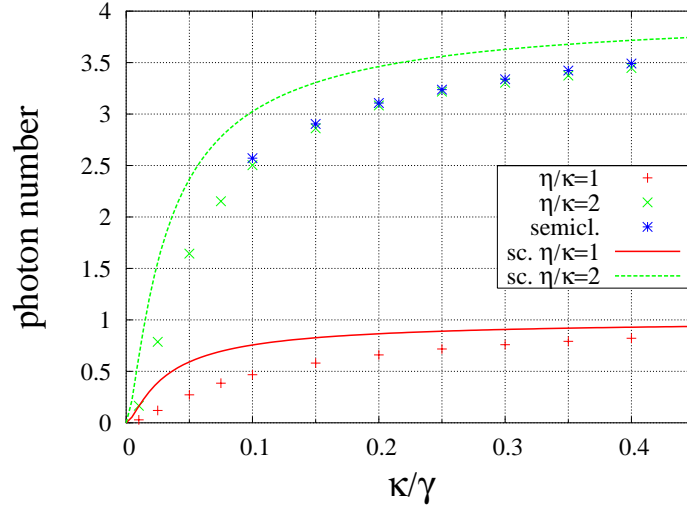


Figure 5.2: Photon number of the field as a function of κ @ $\eta = \kappa$ and $\eta = 2\kappa$. Further parameters: Tab. 4.1. Points correspond to MCWF simulations, stars to Model 1sc ones while lines are the predictions (4.20) calculated for a point-like atom fixed at an antinode. Difference is due to finite extension of the atomic distribution.

of the variation of κ since it does not rely on any assumption about the harmonicity of the potential. The number of excitation quanta in the atomic motion goes down to as low as about three where the behaviour of the system is hardly semiclassical any more.

5.2.3 Localisation

The localisation of the atom exhibits a non-trivial behaviour. For $\kappa \gtrsim 0.1\gamma$ the width of the position distribution $\langle x^2 \rangle$ increases in accordance with the Model 1sc results, as we see in Fig. 5.4(a). Owing to the quantum solution, we learned that the increasing degree of delocalisation is an incoherent effect because at the same time the coherence length L of the wave packet in one well decreases (Fig. 5.4(b)). Large κ is therefore indeed the limit of the atom becoming a classical point-like particle (corresponding to coherence length $L = 0$) which results in the semiclassical simulation working well.

Now with the fully quantum mechanical simulation the regime $\kappa \lesssim 0.1\gamma$ can also be explored. In this limit, due to the decreasing photon number resulting in decreased average potential strength, $\langle x^2 \rangle$ grows again (Fig. 5.4(a)), but now together with increasing L and C (Fig. 5.4(b) and (c)) giving a wide coherent distribution: coherent wave packet in one well, and considerable amount of coherence between the two wells as well.

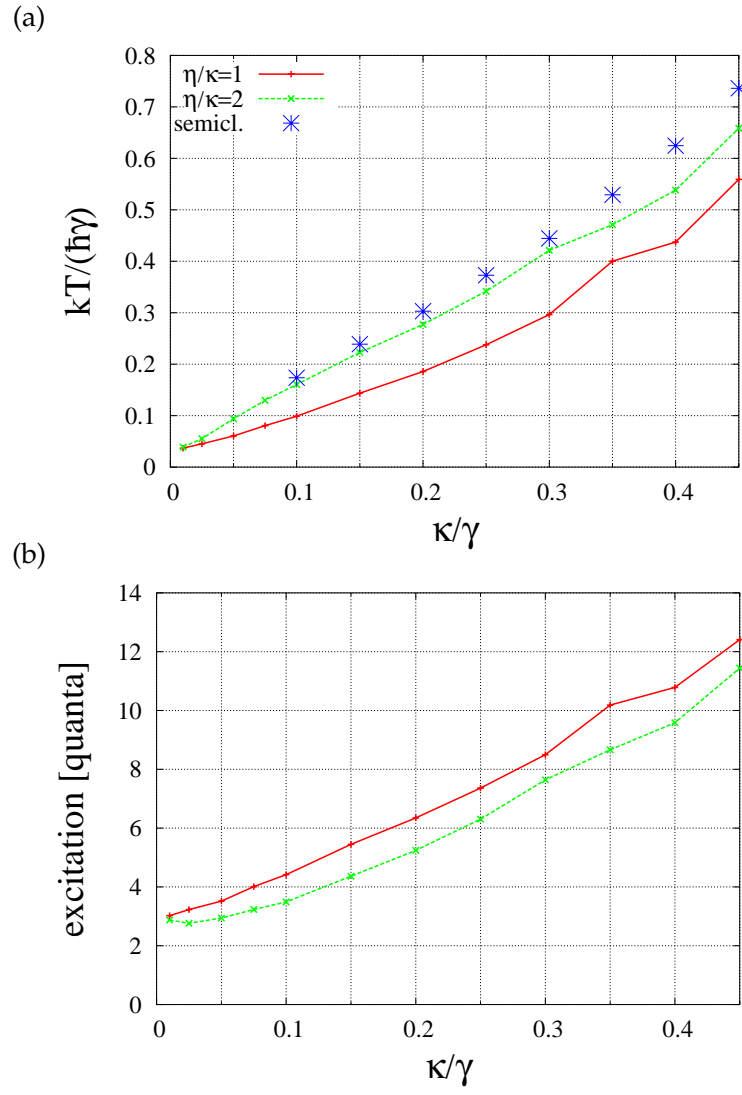


Figure 5.3: Same as in Fig. 5.2 for (a) kinetic temperature and (b) number of excitation quanta in the atomic motion. Stars correspond to Model 1sc simulations.

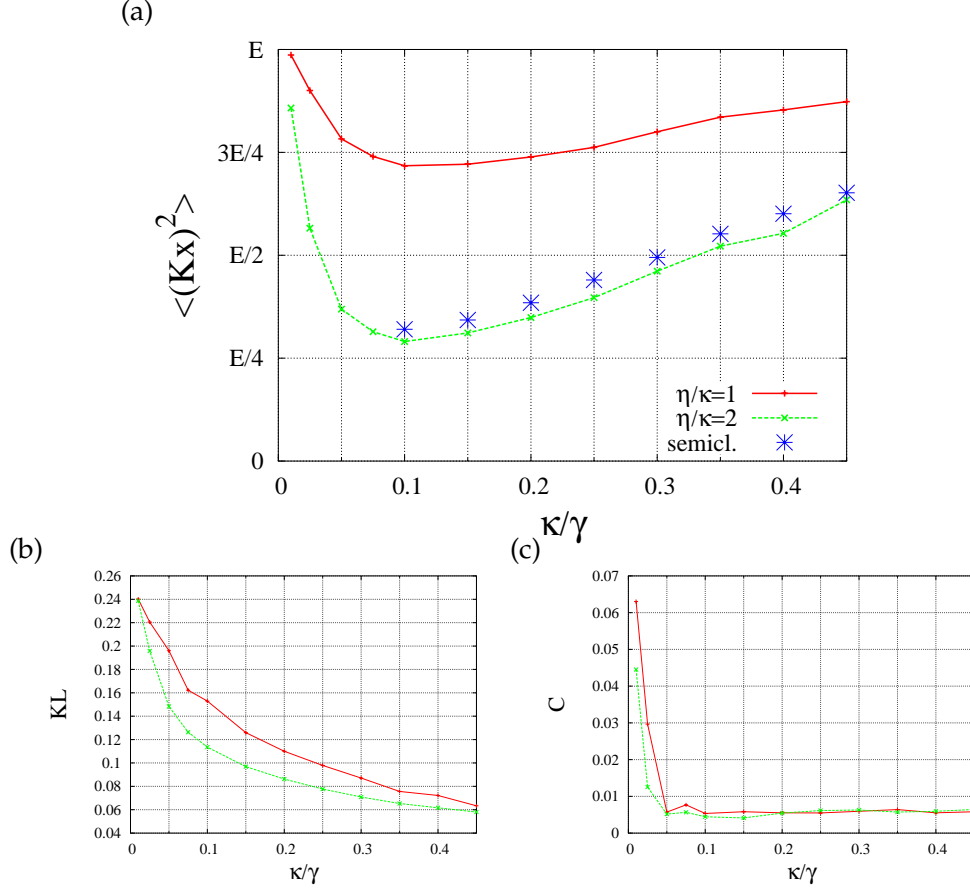


Figure 5.4: Same as in Fig. 5.2 for (a) localisation of the atom, (b) coherence length, and (c) coherence between adjacent trapping sites. The scale of $\langle (Kx)^2 \rangle$ is such that 0 corresponds to delta distributions in both wells, while $E = \pi^2/12$ corresponds to even distribution. Stars correspond to Model 1sc simulations. The correspondence is remarkable, save that the semiclassical model is certainly unable to reproduce the increase in $\langle (Kx)^2 \rangle$ for very small κ values.

5.2.4 Quantum measures

Finally, Fig. 5.5 is devoted to the important stationary quantum properties of the coupled system. In Fig. 5.5(a) the negativity of the simulated steady-state density operator's partial transpose has been plotted as a function of κ . For comparison we have also plotted (lines without points) the negativity of such a highly entangled pure reference state in which every photon number component of the wave function is in the ground state of the potential $\hbar U_0 f^2(x) a^\dagger a$, and the photon number distribution is Poissonian with mean equalling the semiclassically expected photon number. For small κ – though the entanglement in the reference state is certainly much stronger in general – these curves follow roughly the same behaviour as the simulated ones: the amount of entanglement decreases due to decreasing photon number. This is evident, since with very low photon numbers the weight of Fock state components higher than zero being negligible, the state of the system is very close to the separable state $|0\rangle_{\text{mode}} |\Phi\rangle_{\text{atom}}$.

For increasing $\kappa \gtrsim 0.1\gamma$, the negativity monotonically decreases. The picture that can be adopted here is that while coherent time evolution tends to increase the entanglement, jumps destroy it. This is because the potential in the Hamiltonian (3.15a) is proportional to the photon number operator $a^\dagger a$, and therefore each photon number component of the wave function feels different potential strength and evolves differently in time making an entangled state even from an initially separable one. If jumps are too frequent (increasing κ), however, there is no time for a given photon number component to evolve according to its own potential because it is readily shifted to a lower level.

The Mandel Q parameter of the cavity field (Fig. 5.5(b)) follows roughly the same behaviour as the negativity, proving our former assertion that the source of nonclassicality of the field is entanglement between the atomic motion and the cavity field.

In the $\kappa \rightarrow 0$ "quantum" regime of very low temperature, wide coherent atomic distribution, and maximum atom-mode entanglement and nonclassicality of the cavity field, cooling time certainly becomes a crucial question: whether the steady state characteristically exhibiting quantum features can be reached in a reasonable time from a relatively hot and essentially "classical" atomic cloud. For this we again refer to Fig. 4.4(a) where we have already dealt with an example of the relaxation of both the statistical and quantum features of the system at $\kappa = 0.1\gamma$ being on the very limit of the "semiclassical" and "quantum" regimes. The dependence of trapping and relaxation times on κ will be systematically studied in the next Subsection.

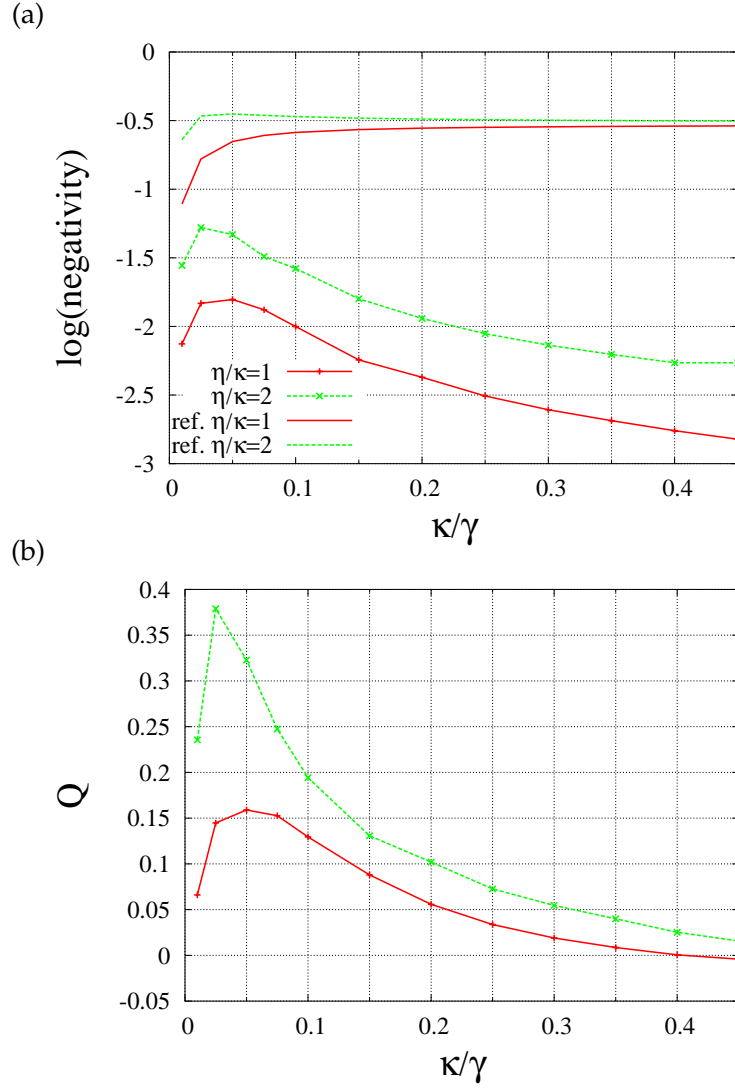


Figure 5.5: Same as in Fig. 5.2 for (a) negativity (of the partial transpose) and (b) Mandel Q parameter of the field. In (a) data plotted with lines without points correspond to negativity calculated for such a highly entangled reference state in which we assume that each photon number component is in the ground state of the corresponding potential and the photon number distribution is Poissonian with mean calculated from the semiclassical model. The entanglement of the actual state is certainly very low compared to the reference.

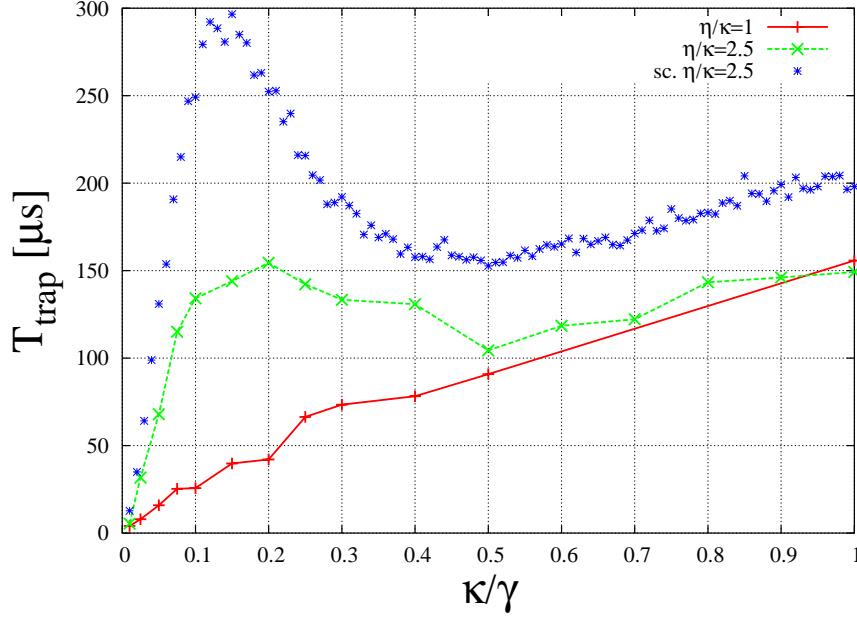


Figure 5.6: Trapping time of the atom as a function of κ @ $\eta = \kappa$ (solid line) and $\eta = 2.5\kappa$ in the MCWF case (dashed line) and Model 1sc case (stars without line).

5.2.5 Trapping & cooling times

Trapping time of the atom at a given trapping site (antinode of the field) is an important quantity that can also be accessed in experiments. It has been thoroughly studied in Model 1sc by Domokos et al. [29] since, as a function of the cavity decay rate κ , it exhibits a maximum. This behaviour was attributed to the role of the cavity, ie it is a manifestation of the role of atom-cavity correlations in the dynamics. Here we revisit this problem using the quantum model, and in the following set of results we simulate the transient dynamics of an ensemble.

The atom being a quantum mechanical particle, it is not altogether obvious how we define the atom being trapped. Still, if we start with a wave packet confined in one well then we observe that the probability of finding the atom in the other well is zero at the beginning and grows in time. From the time dependence of this probability, though it is not simply exponential, a characteristic time can certainly be extracted. This characteristic time will be identified with the trapping time.

We note that since we consider two trapping sites situated at $Kx = \pm\pi/2$ and periodic boundary condition, the probability of finding the atom in a given well is unambiguously linked to the expectation value of the position $\langle x \rangle$, so that we only have to monitor this latter during the simulation. Our results are plotted in Fig. 5.6 with

$\eta/\kappa = 1$ and $\eta/\kappa = 2.5$ together with Model 1sc data for the latter case. Trapping times were determined by fitting on the average of about 300 trajectories.

Both the quantum and semiclassical models exhibit a peak in the trapping time as a function of κ in the $\eta/\kappa = 2.5$ case, while there is no peak for $\eta/\kappa = 1$. There are three effects underlying these results. For very small κ , the photon number is low, see Fig. 5.2, resulting in a shallow potential well and fast escapes, accordingly. In the range of κ where the photon number is about $(\eta/\kappa)^2$ the trapping time depends on the cavity cooling mechanism. The larger the photon loss rate κ , the shorter the atom is captured at its initial site. The drastic drop of trapping times at about $\kappa > 0.1\gamma$ outlines the role of the number of photon round-trips, hence that of the atom-photon correlations.

Finally, the slowly increasing trapping times for very large κ is an artifact of the present approach starting from a state of a well-trapped atom. In this regime the cavity field becomes closely adiabatic making the dipole-force diffusion and cavity cooling slow. Transient relaxation becomes longer, and this is why it takes also longer for the atom to reach its steady temperature.

In general, trapping times predicted by the Model 1sc are always longer than the ones predicted by the quantum solution of Model 1. One is immediately tempted to explain the difference by the atom penetrating the average potential barrier $U_0 \langle a^\dagger a \rangle$, but this explanation turns out to be false since due to the big mass, the Gamow factor is very big making the probability of tunnelling negligible. Rather, a possible explanation originates from the *graininess* of the electromagnetic field. The potential being proportional to the photon number *operator*, the lower Fock state a component of the wave function corresponds to, the weaker potential it feels. In particular, the 0th Fock state component does not feel any potential at all, wherefore it simply spreads being a free wave packet.

From this consideration we may readily imagine a way for the atom to escape (at least partly) from its actual trap other than being thrown over the potential barrier by an appropriate fluctuation (this latter is the only way in the semiclassical model): Let us restrict ourselves to 0- and 1-photon components. Suppose that the system starts from the 1 photon state where the atom feels a potential of strength U_0 and is confined in one well. After some while a jump occurs, so that the wave packet trapped by the 1-photon potential falls to the 0-photon level where there is no potential any more. Therefore it starts to spread, so that there appears some portion of the wave function also in the other well. It may happen that before an other jump takes place (which would simply erase the 0-photon component), the 0-photon component gets pumped up to the 1-photon level where after a while the portion of the wave function in the other well also becomes a small trapped wave packet.

Cooling time of the system is certainly an other important time scale from both theo-

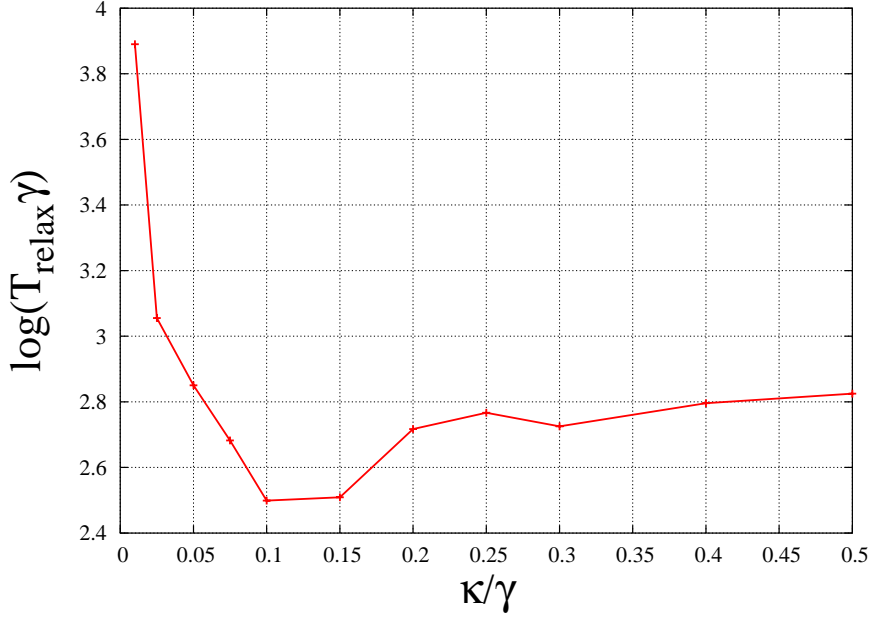


Figure 5.7: Cooling time of the kinetic temperature as a function of κ @ $\eta/\kappa = 1$.

retical and experimental point of view: Whether, the system started from a warm cloud of essentially classically behaving atoms, the cold steady-state exhibiting quantum features can be reached before the system is heated out by environmental noise sources. To study this as a function of the cavity decay rate κ we start from evenly distributed wave packets of short coherence length whose width correspond to Doppler temperature. An example for this situation was already presented in Sec. 4.4 where we have shown that the relaxation of the kinetic temperature is fairly exponential (see Fig. 4.4(a) with the fit of an exponential function on the simulated data). The characteristic time of this exponential is used as cooling time in the following.

Results for the cooling time as a function of the cavity decay rate κ are plotted on a logarithmic scale in Fig. 5.7. As we see the cooling time falls abruptly with increasing κ and reaches a minimum at about the limit of the „quantum” regime $\kappa \lesssim 0.1\gamma$. The origin of this minimum behaviour is the same as that of the maximum behaviour in the trapping time wherefore we refer to the above discussion.

In this Subsection we have shown that the $\kappa \approx 0.1\gamma$ regime is not only the regime of low temperature, considerable mode-atom entanglement, and coherence of the atomic distribution, but also trapping time is maximal and cooling time is minimal in this regime.

5.3 The cavity FORT

In the following we show that Configuration CX in the far-off-resonance regime with varying g but Rabi frequency kept constant can be looked on as a free-space far-off-resonance trap ($g = 0$) in which the trapping laser field has been replaced by a dynamical cavity field (big g limit). Owing to the dynamical cavity cooling mechanism described in Sec. 5.1, the trapping field itself also cools the atoms, allowing for trapping in steady-state, which is in sharp contrast to what we see in free-space traps. In this Section we use Model 1sc to describe the system when the photon number is large and the MCWF solution of Model 1 presented in the previous Chapter for the complementary low photon number regime. From now on we are considering such driving that is far detuned from the atomic resonance but nearly resonant with the cavity field.

5.3.1 Free-space FORT

Far-off-resonance dipole traps (FORT) are commonly used for long-time capturing and localisation of neutral atoms by laser light fields [85]. The basic idea behind tuning the laser frequency very far below the atomic resonance resides in the fact that the depth of the trap potential and the spontaneous photon scattering rate scale differently with the detuning Δ_A . The former is proportional to Ω^2/Δ_A while the latter to Ω^2/Δ_A^2 where Ω is the Rabi frequency of the atom-laser coupling². As a consequence, deep traps can be formed at a reduced level of recoil noise generated by spontaneous emissions in the large detuning limit. This scheme of almost conservative trapping preserves the coherence of the atomic CM motion. This is vital for all-optical Bose condensation [86], and also for processing quantum information with neutral atoms carrying a q-bit in their internal degree of freedom. Furthermore, because of the large detuning, the trapping potential captures simultaneously atoms in different Zeeman sublevels of the ground state, an important element of the condensation of Cs [87], or different isotopes to create fermion-boson mixtures of Yb [88].

Nevertheless, in steady state the atoms would not be localised at the antinodes of the field in a FORT because Doppler cooling is inefficient in the large Δ_A limit. Long trapping times are obtained only for an initially cold ensemble because the relaxation process, ie spontaneous photon scattering is very slow. Its rate is usually so low that, in fact, the trapping time is limited rather by technical noise in the experiments [89].

In this Section we show that Configuration CX can be considered as a generalised FORT scheme. The square of the Rabi frequency, $\Omega^2 = g^2 \langle a^\dagger a \rangle$, is a key parameter, which is determined by the local energy density of the electromagnetic field at the

²All this can be verified by looking at Eq. (3.13b) and (3.17b), in the case when $g = 0$ and $\eta = 0$, since then the system is simply an atom moving in a standing-wave laser field, the Rabi frequency being $\Omega = \eta$.

atomic position. However, a given energy density can be provided in a variable manner since it depends not only on the number of photons but also on, roughly speaking, the “volume” of a photon. Consider now Configuration CX, where the field is enclosed in a Fabry-Perot resonator with the photons having a well defined finite mode volume. The shorter the cavity length, the smaller number of photons are needed to reach a given local field density. Simply, photons are “recycled” by mirror reflections and hit the atom more frequently in a unit of time. The opposite limit of infinite mode volume and infinite number of photons, keeping their ratio constant, corresponds to the standard optical lattice of a free standing-wave laser field.

We will show that, keeping the Rabi frequency Ω invariant but reducing the mode volume, the atomic motion is dramatically influenced. The main effect is that a strong localisation and stable trapping of atoms *in steady state* becomes possible, at a very small degree of perturbation of the atomic ground state. Let’s emphasise that the strong-coupling regime of CQED is not needed. Even for a moderate coupling between the cavity photons and the atomic dipole, the trapping time gets longer by many orders of magnitude than it would be in a free-space FORT with the same Rabi frequency. The effect relies on the correlations between the atomic motion and the field which yield, on top of the far-off resonance trapping, the dynamical cavity cooling mechanism described in Sec. 5.1, experimentally demonstrated recently [31]. In this generalisation of FORT the necessary and sufficient cooling is provided by the trapping field itself without the need for additional near-resonant fields [90, 91], or for a magic wavelength [92, 93].

In contrast to the standard FORT scheme, in Configuration CX the laser field does not directly interact with the atom. It pumps a cavity mode which is dynamically coupled to the atom. The cavity resonance frequency ω_C may differ from the laser frequency, thus as compared to free-space FORT a new system parameter, the detuning Δ_C appears.

5.3.2 Scaling of parameters

Our starting point is again the system (5.2). Since $U_0 \propto g^2 \propto 1/\mathcal{V}$ (cf Eq. 2.1), one can recognise the local energy density $\hbar\omega_C |\alpha|^2 / \mathcal{V}$ in the force term. In the following we attempt to keep this constant while varying the mode volume \mathcal{V} from large values (\equiv standard FORT) towards the “cavity FORT” regime, where much fewer photons create the same local field density. We note that, for simplicity, the cavity loss rate κ is assumed to be constant.³

³ In fact, as it is easy to verify $\kappa = cT/L$, where L is the cavity wavelength and T is the transmission coefficient of the mirrors. The latter has also to be varied when varying \mathcal{V} to keep κ constant.

In the cavity FORT regime, the field amplitude α is a dynamical variable, its evolution couples to the atomic position as

$$\dot{\alpha} = (i\Delta_C - \kappa - (iU_0 + \Gamma_0) \sin^2(Kx)) \alpha + \eta + \xi_\alpha \quad (5.4)$$

(cf Eq. 3.21c). With properly setting the pump field η and the detuning Δ_C , the stationary mean α can be adjusted at will for a fixed position of the atom. The coupled equations of motion, on average, can be kept closely invariant under the variation of \mathcal{V} . The only point for which this cannot be done exactly is the correlated fluctuations of the atomic position and the field amplitude α (cf Eq. 3.22b).

The Rabi frequency, which we want to keep constant, can be expressed in terms of the single-photon Rabi frequency g as $\Omega^2 = g^2 |\alpha|^2$. In Fig. 5.8 the steady-state properties of a single trapped atom are plotted for varying g , representing the variation of the mode volume \mathcal{V} via $g \propto 1/\sqrt{\mathcal{V}}$. The detuning is set to

$$\Delta_C = -\kappa + U_0. \quad (5.5)$$

Since in this case $|\alpha|^2 \propto \eta^2$, (see Eq. 4.20), the pumping strength must be varied as $\eta \propto 1/g$ to keep Ω^2 constant. From Eq. (3.14) it is easy to see that the mean atomic excitation $\langle \sigma^\dagger \sigma \rangle = |\langle \sigma \rangle|^2$, ie the probability P_e of the two-level system being in the excited state, is also kept constant by this assumption. It is about 0.05 for the whole range of this plot with a small residual variation due to the localisation effect, ie the atoms are not always at the very antinode of the field where they are maximally coupled to the mode.

5.3.3 Temperature, localisation

The kinetic temperature drops several orders of magnitude for increasing g , finally reaching the limiting temperature of about the linewidth of the dominating dissipation channel $kT \approx \hbar\kappa$. Recall that in free-space Doppler cooling, which sets in for $g \rightarrow 0$ the limiting temperature is $kT \approx \hbar\Delta_A/2$ for large detuning $|\Delta_A| \gg \gamma$. The temperature reduction can be attributed to the action of the coupled atom-field dynamics.

For low enough temperature trapping becomes possible, which is demonstrated by the localisation plot in Fig. 5.8b. The measure is the mean spread $\langle (Kx/\pi)^2 \rangle$ in units of $E = 1/12 \approx 0.08$ which is the mean spread of the uniform distribution. A mean spread significantly below E expresses that the atom is localised in the vicinity of an antinode. Note that the localisation is destroyed again for large values of g where the mean intensity corresponds to only few photons. Such a minimum behaviour would not be possible were the atom moving in a normal potential because the virial theorem ensures a monotonic connection between the mean kinetic and the potential energy. Here, however, the potential in the Hamiltonian (3.17a) is proportional to $a^\dagger a$. Hence

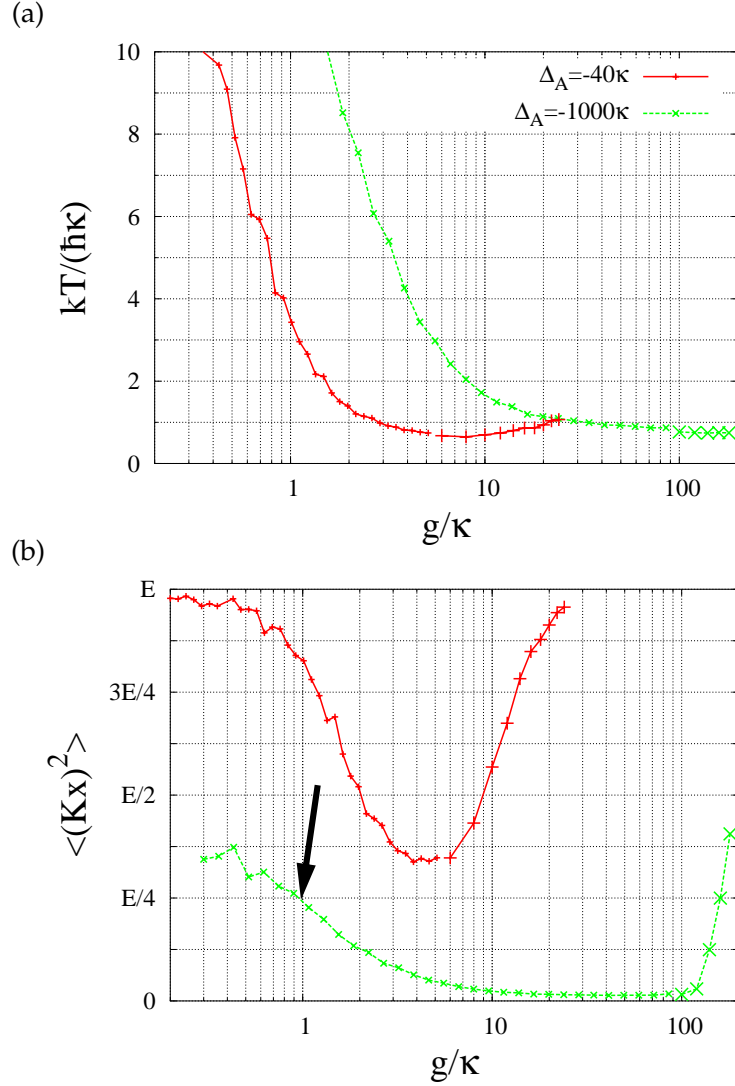


Figure 5.8: (a) Steady-state kinetic temperature and (b) localisation of the atomic centre-of-mass motion as a function of the coupling constant to the cavity mode. The localisation is given in units of $E = \pi^2/12$ corresponding to a uniform distribution. The two curves were generated at different atomic detunings, $\Delta_A = -40\kappa$ (solid line) and $\Delta_A = -1000\kappa$ (dashed line), and $\kappa = \gamma/2$ was set for both. The bigger marks (for large g values) originate from the MCWF simulations, the smaller ones from Model 1sc. $P_e = 5\%$ on the whole range of g .

the part of the joint atom-cavity wave function which is associated with the 0th photon number state does not feel any potential and spreads freely.

The cooling mechanism, responsible for the steady-state localisation, can be analytically shown to survive in the large detuning limit, $\Delta_A \gg \gamma$ [see also 26 in a different context]. In a calculation similar to the one carried out in Model 0sc (cf Eq. 3.10a), the linear response of the field amplitude to the atomic motion can be calculated from Eq. (5.4), which, when put back into the force operator, yields a linear friction force with a coefficient

$$\frac{\beta}{2\gamma P_e} = \frac{\hbar K^2}{2\mu\gamma} 4 \cos^2(Kx) \frac{2g^2(\Delta_C - U_0 \sin^2(Kx))(\kappa + \Gamma_0 \sin^2(Kx))}{\left((\Delta_C - U_0 \sin^2(Kx))^2 + (\kappa + \Gamma_0 \sin^2(Kx))^2\right)}, \quad (5.6)$$

where we normalised it to the rate of spontaneous photon scattering. A similar result, without the normalisation to P_e was obtained in Refs. [94, 95]. It follows that the optimum cavity detuning is

$$\Delta_C \approx -\kappa - \Gamma_0 + U_0 \approx -\kappa + U_0, \quad (5.7)$$

which is exactly what we used for the plots in Fig. 5.8. The maximum friction coefficient, spatially averaged, is

$$\frac{\beta}{2\gamma P_e} = \frac{\hbar K^2}{2\mu\gamma} \left(\frac{g}{\kappa}\right)^2, \quad (5.8)$$

which proves the invariance of the friction coefficient per saturation as a function of the atomic detuning. Dislike with Doppler cooling in free laser fields, going away from resonance with the saturation kept constant does not make the damping processes vanish. For $g \sim \kappa$, the friction force equals the maximum of the Doppler friction force. Since the relation of g and γ is irrelevant here, strictly speaking, the regime of strong-coupling CQED is not even necessary. Optical lattices in resonators fulfilling $g \gtrsim \kappa$ [eg 93, 96, 97] are suitable for this type of generalised FORT scheme.

Stable trapping is achieved if the steady-state temperature is well below the trap depth. The former can be estimated by taking the large Δ_A limit of the results of Refs. [27, 28]. It yields, for uniform distribution,

$$kT = \hbar\kappa \left(1 + \frac{\kappa\gamma}{g^2}\right), \quad (5.9)$$

which is in accordance with the limiting temperature in Fig. 5.8a. In an intermediate range of g the simulated temperature is in fact lower, an effect due to the localisation where (5.9) holds only approximatively. As the temperature scales with κ , it can be independently controlled and chosen far below the trap depth, the latter being about $\hbar U_0 |\alpha|^2 = \hbar \Delta_A P_e$.

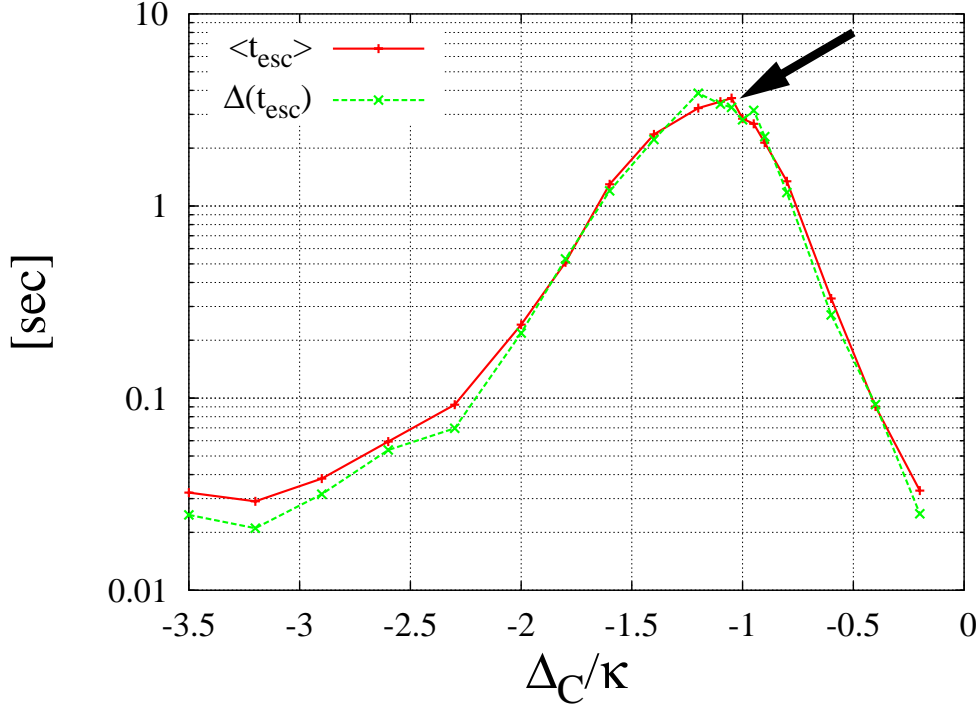


Figure 5.9: Trapping times as a function of the detuning of the field from the cavity resonance. Parameters are $\Delta_A = -1000\kappa$ and $g = \kappa = \gamma/2$, corresponding to the point indicated by arrow in Fig. 5.8. $P_e = 5\%$ on the whole range of Δ_C .

5.3.4 Resonance in the trapping time

The role of the cavity cooling mechanism can be seized in the variation of steady-state properties as a function of the detuning between the pump laser frequency and the cavity resonance. In Fig. 5.9 we plot the mean escape time of the atom from a trapping site, which is an experimentally accessible quantity. In the simulations the initial distribution represents atoms at the antinode with a small velocity spread. It is the dipole force fluctuations and, to less extent, the spontaneous recoil noise which heats up the atom to escape. A significant peak can be observed at about $\Delta_C \approx -\kappa$. The variance of the escape times is also presented in the same plot. From the fact that the mean and the variance are almost equal we can deduce that the distribution of the escape times is close to an exponential one, which is expected in a steady state. The parameters were set such that the point for detuning $\Delta_C = -\kappa + U_0$ in this plot (see arrow) corresponds to the point indicated by arrow in Fig. 5.8b. Note that, for reducing the numerical effort, this working point is far from the strongest localisation. In fact, the magnitude of

the atomic detuning Δ_A is also far below the one used in FORT. Though using larger detunings would yield much longer trapping times, it would make the simulations intractably long.

5.3.5 The $|\Delta_A| \rightarrow \infty$ limit

For very large detuning the trap frequency ν (cf model developed in Appendix B) starts to dominate the other frequencies of the system (resolved sideband limit). For about 5% saturated Rb atoms the limit is $\Delta_A \gtrsim 10^4 \gamma$, but it can be pushed to higher detunings Δ_A by reducing the saturation. In the resolved sideband limit the validity of the analytical calculations (Eq. 5.6) breaks down, since they rely on the assumption of small atomic velocity ($kv \ll \kappa$). The simulations presented throughout this Section would work in this limit as well. With different tuning, $\Delta_C \approx -2\nu$, cavity sideband cooling is possible though very inefficient in the given geometry (only two-phonon transitions are allowed — see Appendix B). In this case the use of an external probe field tuned to the red sideband is a straightforward solution. Cavity cooling in the resolved sideband limit is considered elsewhere [26, 49, 50], here we concentrate only on the cooling mechanism around $\Delta_C = -\kappa$.

5.4 Theses

Thesis II

We have shown that the regime where the cavity decay rate is smaller than the spontaneous decay rate by about an order of magnitude is the limit where quantum effects such as atom-field entanglement and finite coherence length of the atomic wave packet commence to play a role in the dynamics. This quantum-classical transition regime is optimal for cavity cooling and trapping since here besides the fairly low temperature, localisation and trapping time is maximal while cooling time is minimal. In the quantum field regime we have shown that even when there is on average only one photon in the cavity, it still fully exhibits the cavity cooling effect. We have found good agreement between the results of former semiclassical simulations and MCWF ones in the regime of bigger cavity decay rate.

Thesis III

We have shown that if an atom is trapped by a quantum field, the trapping time differs significantly from the one measured for a classical field of the same intensity. The atom can escape via the zero photon component of the field which yields no potential. The

effect can serve as a proof for testing the graininess of the field.

Thesis IV

We proved that in the standard dynamical cavity cooling scheme the cooling force at a fixed rate of spontaneous photon scattering does not vanish in the regime of very far detuning associated with large optical potential depths. This is at sharp variance with standard Doppler cooling. From another point of view, the very popular far-off-resonance dipole trap scheme was generalised and its efficiency was shown to be greatly enhanced, embedding a cooling mechanism, if the field is enclosed in a cavity. The embedded cooling mechanism provides for trapping in steady state, which means that in an experiment trapping would be limited only by technical noise.

Thesis V

We have demonstrated cavity cooling and trapping with a model in which there is no reference to the internal structure of the particle to be cooled. Hence, cavity cooling is shown to be applicable for general linearly polarisable particles, in particular, for molecules.

Polariton cooling

From now on in the work we are considering the case when the atoms are driven. In this Chapter we show the existence of a cavity cooling and trapping mechanism in Configuration AZ. The effect is surprising in the sense that a passive cavity, though yielding forces on the atom only in the direction of its axis, still yields cooling and trapping in the direction orthogonal to its axis. The effect has been recently observed experimentally by Nussmann et al. [55].

While in Sec. 5.3 we have found that a nearly resonantly driven cavity provides for cooling and trapping in the direction of its axis, here we find that the same is true in the case when the atoms are pumped and in the direction orthogonal to the cavity axis. Clearly, common in the two schemes is that the spectrum of the coupled atom-field system has resonances other than the Lorentzian of a simple polarisable medium — responsible for simple Doppler cooling —, regardless of the geometry of the scheme.

6.1 Anomalous Doppler-effect

Configuration AZ can be considered as the standard Doppler cooling geometry, where the atom interacts with two counter-propagating red detuned plane wave fields of frequency ω composing a standing wave along the direction z , plus a passive cavity aligned in the x direction. An interesting question to ask is whether and how the properties of the standard Doppler scheme are modified by this addition. In this section we are using Model 0sc to study this question since it turns out to be useful to keep the atomic internal degree of freedom for the interpretation of the findings.

6.1.1 The effect as anticipated by Model 0sc

In Configuration AZ, for the atom moving with velocity v_z , the linear velocity-dependence of the mean polarisation is equivalent with the first-order expansion (3.10b). Cal-

culated from Model 0sc and up to first order in Kv_z it reads

$$\left\langle \sigma^{(0)} + v_z \sigma_z^{(1)} \right\rangle = \frac{\eta_t}{(i\Delta_A - \gamma) + \frac{g^2}{i\Delta_C - \kappa} - iKv_z \left(1 - \frac{g^2}{(i\Delta_C - \kappa)^2} \right)}, \quad (6.1)$$

where the atom is supposed to be at the antinode of the pump field. This corresponds to a Lorentzian resonance of an effective two-level atom with frequency

$$\omega_D = \omega_A + \frac{g^2 \Delta_C}{\Delta_C^2 + \kappa^2} + Kv_z \left(1 - \frac{g^2(\kappa^2 - \Delta_C^2)}{(\Delta_C^2 + \kappa^2)^2} \right) \quad (6.2)$$

and linewidth

$$\gamma_D = \gamma + \frac{g^2 \kappa}{\Delta_C^2 + \kappa^2} + Kv_z \frac{2g^2 \kappa \Delta_C}{(\Delta_C^2 + \kappa^2)^2}. \quad (6.3)$$

For $g = 0$, Eqs. (6.2) and (6.3) reduce to the usual Doppler-shifted resonance curve with $\omega_D = \omega_A + Kv_z$ and $\gamma_D = \gamma$. However, when the atom is coupled to the cavity mode, the additional terms shown above appear. The ones independent of the velocity correspond to the cavity-induced lineshift and line broadening well-known from CQED. Their consequences on cavity cooling have been extensively covered in previous literature [22, 25, 28], therefore, we shall not discuss them here.

Rather, we focus on the transverse velocity-dependent correction to the standard Doppler term in Eq. (6.2), which carries striking new features. It is proportional to $g^2/(i\Delta_C - \kappa)^2$, a complex number yielding both lineshift and modification of the linewidth. The maximum lineshift is $-Kv_z g^2/\kappa^2$, reached at resonance $\Delta_C = 0$. This can cancel or even dominate the standard Doppler shift Kv_z in the case of $g \geq \kappa$ (good cavity). Such a condition is satisfied in existing CQED setups. In this limit, the pump field is “red shifted” when the atom moves opposite to the wave propagation, which is a seriously counterintuitive behaviour. The usual sign of the Doppler shift, which is necessary for the cooling to work, is recovered only for a detuning $|\Delta_C| > \kappa$, and even here its magnitude can be considerably altered.

A second interesting consequence is the velocity-dependence of the spontaneous emission rate (6.3) into free-space modes independent of cavity geometry. It even depends on the direction of motion relative to the pump field propagation. This motion-induced effect is clearly different from the one predicted in Refs. [98, 99], where the atom moves along the sinusoidal mode of the cavity, yielding sidebands on the atomic resonance and enhanced inelastic scattering at the sideband frequencies.

6.1.2 Microscopic picture

The key to the anomalous behaviour is the interference of the pump and cavity fields. The amplitude of the cavity field depends on the coordinate z since it is generated by scattering on the atom. For an immobile scatterer, the cavity and pump fields, as well

as the resulting atomic polarisation exhibit the same z -dependence. For $g \sim \kappa$, the cavity photons can be reabsorbed, or even multiple absorption-emission cycles can occur, which combines the interference with the cavity memory effect. This can even lead to a destructive interference of the two fields cancelling atomic polarisation [100]. For a moving atom the phase of the pump varies instantaneously with the atomic position, while the cavity field adapts only on a time scale κ^{-1} . Hence there appears a phase lag between the pump and the cavity components of the field impinging on the atom. This interference phase changes as a function of the atomic velocity, which can be seen explicitly in an analytic form by rewriting the above expression for the polarisation as

$$\langle \sigma^{(0)} + v_z \sigma_z^{(1)} \rangle = \frac{\eta_t + g \langle a^{(0)} \rangle}{i(\omega - \omega_A - K v_z) + \gamma} + \frac{v_z g \langle a_z^{(1)} \rangle}{i(\omega - \omega_A) + \gamma}, \quad (6.4)$$

here again, the atom at the antinode of the pump field. The first term is the polarisation induced by the total adiabatic field, containing the velocity dependence in the naively expected way (standard Doppler shift). The anomalous dependence is contained in the second term, which describes the non-adiabatic response of the field to the atomic motion (cf Eq. 3.10a).

Doppler cooling of two-level atoms makes use of the dependence of the photon scattering rate on the velocity, as described by the Doppler effect. It can be improved by a cavity which increases the photon emission rate at the cavity resonance frequency set blue detuned to the pump frequency [25]. In such an inelastic scattering process the photon energy difference has to be compensated by the loss of atomic kinetic energy, hence the cavity yields an efficient dissipative channel for the atomic motion. However, this interpretation is valid only in the “bad-cavity” limit, $g \ll \kappa$. In this limit the correction to the Doppler shift can be neglected and the simple expression κv can be used to leading order in g/κ . In the good cavity limit $g/\kappa \gtrsim 1$, however, the real shift calculated above deviates substantially from the standard form. The velocity-selectivity of the optical force changes qualitatively, which implies a completely new scaling of the laser cooling properties.

6.2 Cooling

Let us now discuss the dynamical consequences of the anomalous Doppler effect. We have numerically simulated the coupled stochastic equations of Model 0sc. In Fig. 6.1 the kinetic temperature is plotted against the coupling strength g of the atom-cavity interaction.

The drastic reduction in the temperature for increasing coupling constant g demonstrates the impact of the anomalous Doppler term on the mechanical forces. As shown

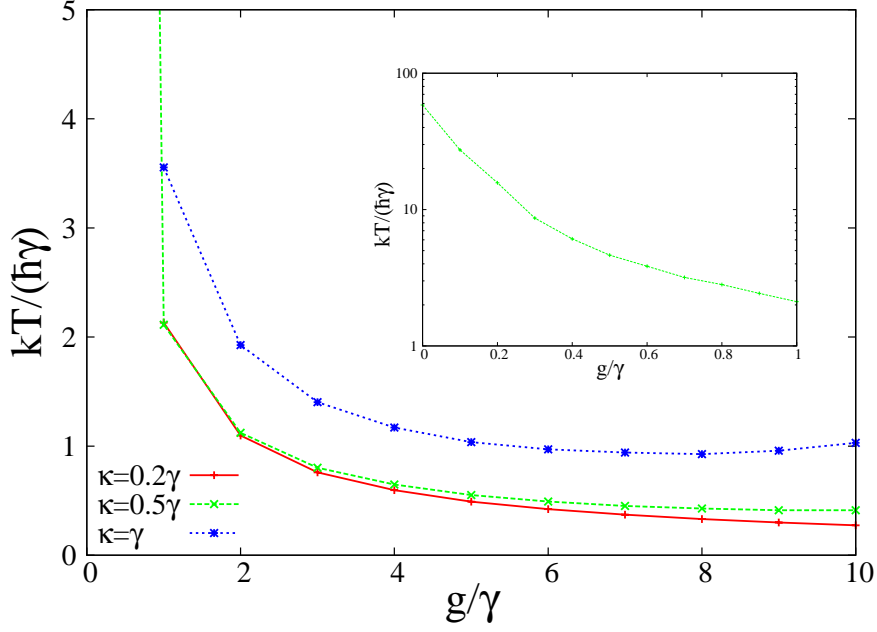


Figure 6.1: Steady-state kinetic temperature of the atomic centre-of-mass motion as a function of the coupling constant to the cavity mode. @ $(\Delta_A, \Delta_C, \eta_t) = (-350, -0.6, 90)\gamma$.

in the inset, from $g = 0$ to $g = \gamma$ the temperature changes one and a half order of magnitude¹. It finally drops below the Doppler limit $kT_D = \hbar\gamma$ (cf Eq. 5.1). Accordingly, we have found that the trajectories exhibit longterm trapping (up to seconds) of the particles in the direction of the pumping field: see Fig. 6.2 for the trapping probability of an atom.

The result is in sharp contrast to free-space Doppler cooling, where the temperature is always higher than the potential depth prohibiting trapping (cf Sec. 5.3.1). Hence the effect cannot be simply seen as replacing our atom–cavity system by a single entity with modified linewidth and transition frequency. Note also that the cooling gets most efficient in the limit of $\kappa \rightarrow 0$, where the cavity dissipation channel is completely closed.

6.3 The polariton

Because of the large detuning, $\Delta_A \gg \gamma$, direct excitation of the atom is negligible. By coherent scattering on the atom, the pump can quasi-resonantly excite a “photonic polariton” at the resonance condition, $\Delta_C \Delta_A = g^2$, associated with the lower dressed state of the coupled atom-cavity mode system — see also the resonance in the field and

¹Note that $g = 0$ corresponds to simple Doppler cooling where according to the formula (5.1) the temperature should be $175\hbar\gamma$, considerably higher than the one plotted here. Model 0sc is unable to reproduce this since it works only for small velocities.

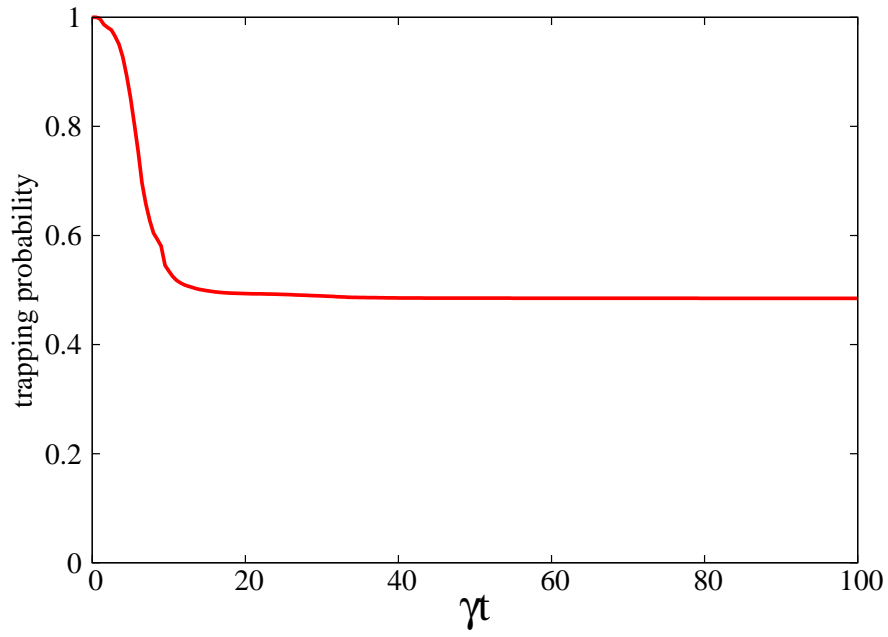


Figure 6.2: Trapping probability of an atom derived from an ensemble of about 32k atoms initially at Doppler temperature and homogeneously distributed on the section of length λ around 0. The fraction of atoms still in this section is plotted against time. About one half of the atoms remain trapped for seconds. @ $(g, \kappa) = (5, 0.5)\gamma$, other parameters as in Fig. 6.1.

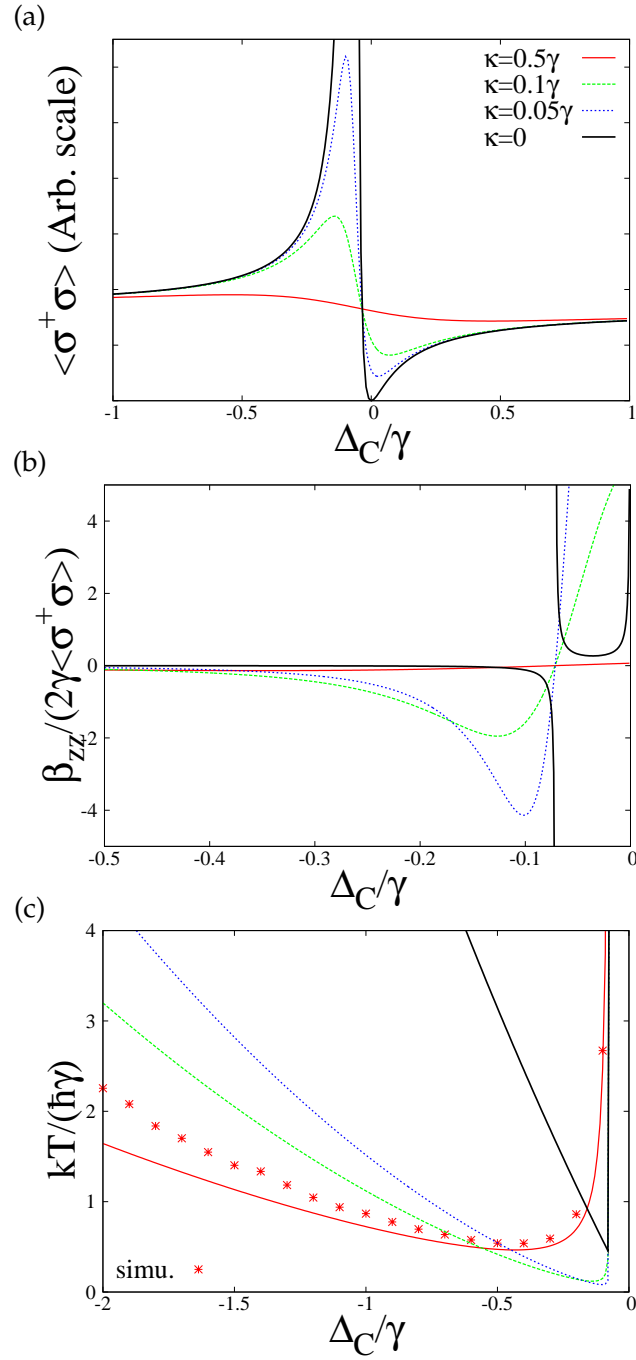


Figure 6.3: (a) The polariton resonance in the mean atomic excitation, (b) the consequent linear friction coefficient normalised to the spontaneous emission rate, and (c) kinetic temperature along the z -direction as a function of the Δ_C . $g = 5\gamma$, other parameters as above. The points in (c) stem from numerical simulation of Model 0sc.

polarisation (3.13). This state is composed dominantly of photonic excitations, the associated small ($\propto g^2/\Delta_A^2$) atomic excitation is plotted against the cavity mode frequency (embedded in Δ_C) in Fig. 6.3(a). Note that for $\Delta_C = 0$ the upper state population is suppressed by destructive interference of the pump and cavity fields, it is strictly zero for $\kappa = 0$ [100].

The linewidth of the polariton resonance is $\kappa + (\gamma - \kappa) g^2/\Delta_A^2$. For vanishing κ , the velocity dependence of the polariton excitation, hence that of the optical force is greatly enhanced in the vicinity of the polariton peak. This results in enhanced friction force (cf β in Eq. 3.3b). The zz component of this, normalised to the mean spontaneous emission rate, is shown in Fig. 6.3(b) for various values of κ . Regions below -1 indicate less than one spontaneous emission in a cooling time $1/\beta_{zz}$. Owing to the sharp resonance, the atomic motion can induce a dramatic increment of the number of photons in the cavity. For the parameters of the figure and for $\kappa = 0.1\gamma$, a number of 180 extra photons are created at Doppler velocity and at a saturation of 0.1. If each photon carries about a recoil energy ($\equiv \hbar^2 K^2/\mu \approx 0.0024\hbar\gamma$) more than the incoming pump photon, a kinetic energy on the order of the Doppler energy $\hbar\gamma$ can be rapidly transformed into internal energy of the system. That is, the energy is being buffered in the form of "photonic polariton" excitations while slowly leaking into the environment.

In Fig. 6.3(c), we used the temperature as a numerical benchmark of the polariton resonance's role in the cooling. The curves are analytically estimated by a semi-empirical approach relying on the hypothesis that the atom is tightly confined in the vicinity of an antinode of the pumping field (generalised Einstein relation — for details see Ref. [34]).

Finally we note that some current experimental setups operate with parameters $g = 5\gamma$, $\kappa = 0.5\gamma$ [55, 96], and $g = 9\gamma$, $\kappa = 2\gamma$ [93]. The ratio g/κ exceeds 1 by far so that the anomalous Doppler shift is directly observable in the fluorescence, while the polariton cooling manifests itself by the appearance of long-time atomic trapping.

6.4 Remarks, Theses

Note that the geometry of the cavity was not really relied on here, the effect occurring in the direction orthogonal to its axis. Therefore, analogous effects are anticipated in other micro-optical setups, where atoms are captured in dipole traps close to resonant optical structures such as rings, waveguides or microspheres by using the corresponding coupled atom-field resonances.

Our preliminary studies with the MCWF solution of Model 1 for Configuration AZ have revealed that it may be possible to achieve ground-state cooling with the polariton cooling effect in the very far detuned regime. Ground-state cooling means that in the

steady state there is basically no excitation quantum in the atomic motion, so that it corresponds to a BEC.

Thesis VI

We have shown that if an atom moves in a monochromatic laser field and is strongly coupled to a mode with weak damping — such as a high-Q cavity mode — nearly resonant with the field then the velocity-dependence of its polarisation deviates substantially from the standard Doppler shift. This “anomalous” Doppler shift is proportional to the square of the ratio of coupling constant and decay rate. Depending on the parameters the Doppler-shift can even change sign: in this case a field counter-propagating to the motion is felt as red-shifted by the atom.

Thesis VII

We have shown that if in the standard Doppler-cooling scheme a resonant object is coupled to the atom then the efficiency of cooling both in terms of limiting temperature and cooling time can be greatly enhanced. In addition, long-time trapping is achieved up to the range of seconds. The effect is based on the anomalous Doppler effect, which at proper but general enough parameters is an enhancement to the standard Doppler effect. An alternative explanation on a higher level of understanding is in terms of a peculiar resonance (polariton) of the coupled atom-cavity system, which in the strongly coupled case is very different from the simple Lorentzian resonance used for Doppler cooling.

The atom-cavity system as a quantum seesaw

In this brief Chapter a quite spectacular effect is displayed which was come across when applying the MCWF simulation developed in Chap. 4 to Configuration AZ or AX. The effect has implications for a quantum version of self-organisation (cf Appendix C), and hence it was the chief motivation for us to undertake quantum many-body studies to be presented in Chap. 8. In the following we use Configuration AZ.

7.1 The quantum-seesaw analogy

With proper but generic enough parameter settings which allow for cooling and trapping the atom, MCWF trajectories independent of the initial condition exhibit the feature that after a certain transient time in the cavity there is no field but still there are photons:

$$\langle a \rangle = 0, \quad \langle a^\dagger a \rangle \neq 0. \quad (7.1)$$

The photon number is roughly the semiclassically expected, that is, the one which is radiated by a point-like atom situated near the antinode of the pumping field. A closer look at the joint atom-field wave function revealed that it eventually assumed the form

$$|\Psi_\pm\rangle \approx \frac{1}{\sqrt{2}} (|\text{left}\rangle |\alpha\rangle \pm |\text{right}\rangle |-\alpha\rangle). \quad (7.2)$$

Here $|\text{left}\rangle$ ($|\text{right}\rangle$) means a well localised atomic wave packet centred on the left (right) antinode of the pumping field — $\langle \text{left} | Kz | \text{left} \rangle = -\pi/2$ ($\langle \text{right} | Kz | \text{right} \rangle = \pi/2$) — in the section of length λ considered in the MCWF simulation (cf the discussion of Fig. 4.2 in Sec. 4.2.2). An atom in state $|\text{left}\rangle$ ($|\text{right}\rangle$) radiates approximately a coherent field $|\alpha\rangle$ ($|-\alpha\rangle$) into the cavity given by Eq. (3.13a). A field in state $|\alpha\rangle$ ($|-\alpha\rangle$) deepens the potential well at the left (right) antinode while flattens the other one. This positive feedback is reminiscent of a seesaw and is also the must of the self-organisation process.

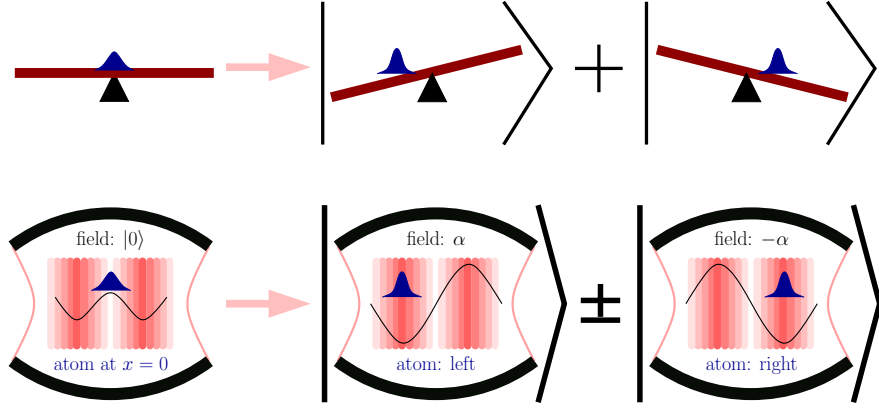


Figure 7.1: Analogy between a quantum seesaw and the atom-cavity system in Configuration AZ. Note that the seesaw itself and the particle on it as well is supposed to have some attraction towards the centre to have a finite steady state. The potential felt by the atom is indicated by solid black lines.

In the fully quantum mechanical version of the seesaw, that is, when both the seesaw and the particle moving on it are quantum objects, the possibility of entanglement allows the system to immediately leave its unstable central equilibrium point and evolve towards left and right simultaneously. Moreover, the decay of the unstable equilibrium occurs without any noise, which is unthinkable for classical spontaneous symmetry breaking phenomena. In Fig. 7.1 we display the analogy between a quantum seesaw and the atom-cavity system in Configuration AZ.

7.2 Role of entanglement and decoherence

The role of entanglement in the initial phase of the dynamics is displayed in Fig. 7.2 where the evolution of the mean photon number and the negativity characterising atom-field entanglement (cf Sec. 4.2.3) is plotted. The plots stem from the ensemble average of 500 trajectories where the initial condition was no field and the atom having a completely flat wave function. According to the above discussion about immediate decay of the unstable equilibrium, photons and entanglement are immediately created. The oscillations in the photon number and negativity are clearly related. The minima correspond to the expected times of the 0th, 1th, 2nd, etc. photon loss via cavity decay. The photon number oscillates around a constant and does not vanish for long times.

On the other hand, dissipation (quantum jumps) destroys entanglement so that the negativity oscillates around a decaying mean¹. Indeed: each cavity decay means the

¹Some residual entanglement remains in the steady state of the system for the same reasons as discussed in Sec. 5.2.4 for Configuration CX.

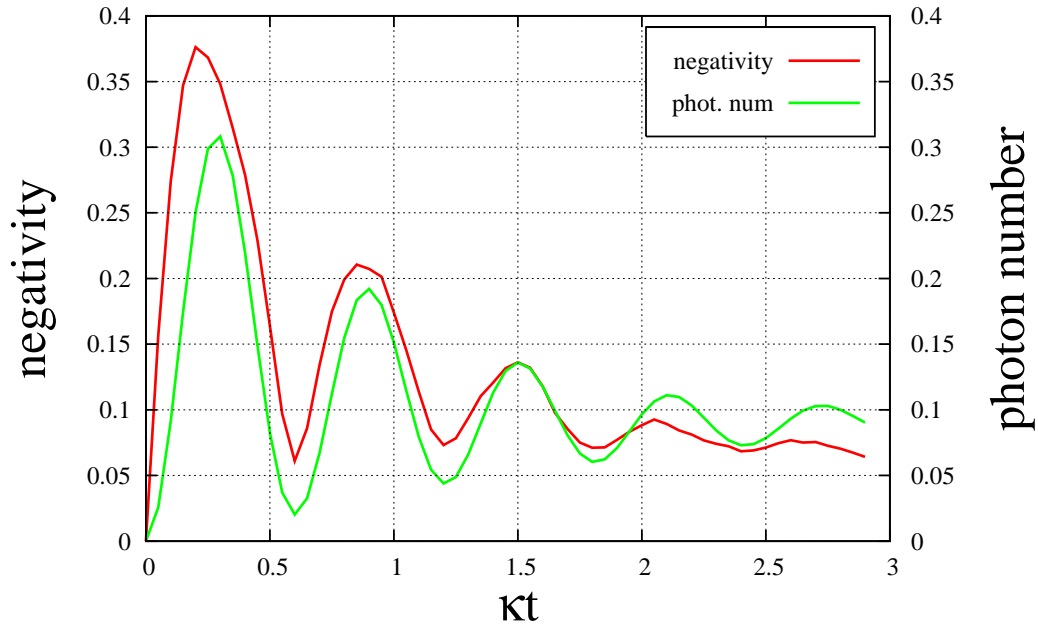


Figure 7.2: Fast dynamic growth of entanglement and photon number for a single atom in the range $0 < \kappa t \lesssim 0.2$. Afterwards, both oscillate around a decaying mean — this is just the behaviour of an under-damped oscillator. The initial condition is flat wave function and field in vacuum state. @ $(U_0, \Delta_C, \eta_t) = (-1.7, -12, 20)\kappa, \Gamma_0 = 0$.

action of the operator a on the state (7.2), which flips the sign of the superposition:

$$J_C |\Psi_+\rangle = \sqrt{\kappa} (\alpha |\text{left}\rangle |\alpha\rangle + (-\alpha) |\text{right}\rangle |-\alpha\rangle) \propto |\Psi_-\rangle, \quad (7.3)$$

$$J_C |\Psi_-\rangle \propto |\Psi_+\rangle. \quad (7.4)$$

It is easy to see that the atomic decay in Configuration AZ also flips the sign, while in Configuration AX it leaves the sign unchanged. The result is that in steady state the system is in the complete mixture:

$$\rho_{ss} = \frac{1}{2} (|\Psi_+\rangle \langle \Psi_+| + |\Psi_-\rangle \langle \Psi_-|). \quad (7.5)$$

Careful analysis of this state reveals that it is impossible to be distinguished from the steady state of a classical simulation performed for one particle. Hence, the conclusion is that quantum properties may play a role in the initial phase of the dynamics, while they are absent from the steady-state.

7.3 Robustness of the final state

Let us start the system from the initial condition $|\text{right}\rangle$ where it begins to radiate the coherent field state $|-\alpha\rangle$. As we see in Fig. 7.3, this state is remarkably stable for a long time, but eventually collapses due to fluctuations, and the system ends up in the state (7.2), which is made obvious by the fact that $\langle z \rangle = \langle a \rangle = 0$, while the photon number is not affected: $\langle a^\dagger a \rangle \approx |\alpha|^2$. Hence in the atom-cavity implementation of the quantum seesaw, even if the seesaw is tilted to one direction with the atomic wave packet completely on that side, fluctuations eventually enable the system to escape from this state to a symmetric final state.

As we see in Fig. 7.3(b) this happens even *with* atomic spontaneous emission, though on a much longer time scale.

7.4 Remarks, Thesis

We note that in Refs. [61, 67] for atoms moving in a cavity a lattice model was developed which, when applied to Configuration AZ, fairly reproduces the quantum seesaw effect, there is even good quantitative agreement with the MCWFS results. The results presented in this Chapter are to be published together with the lattice-model results [56]. In the lattice model it was shown that in the initial phase of the dynamics even the quantum many-body state of the system is important, whether eg it is in a Mott insulator or a superfluid state.

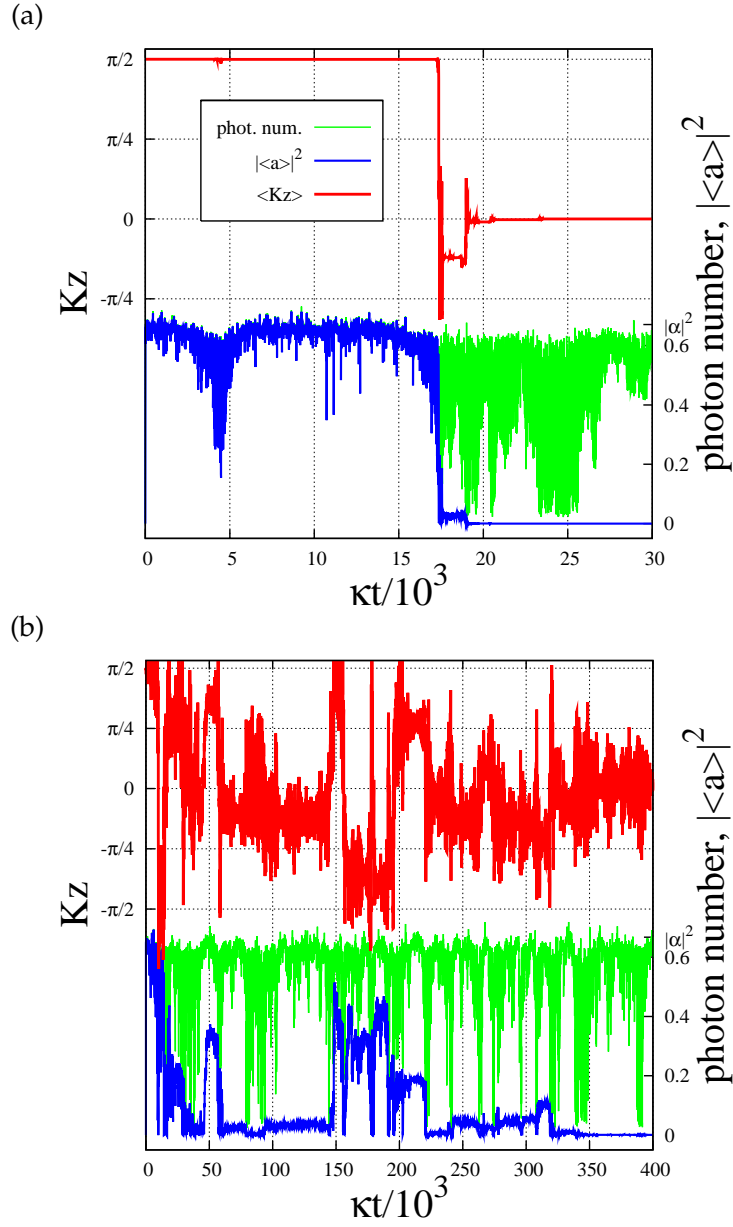


Figure 7.3: MCWF trajectories exhibiting dynamical formation of a the state (7.2) without (a) and with (b) spontaneous emission. The atom is initially well localised in the right well ($\langle Kz \rangle = \frac{\pi}{2}$) and radiates approximately a coherent field with amplitude $-\alpha$ into the cavity. Due to fluctuations it eventually escapes and evolves into the state (7.2), having no mean field but non-vanishing photon number: $\langle a \rangle = 0$, $\langle a^\dagger a \rangle \approx |\alpha|^2$. @ $(U_0, \Delta_C, \eta_t) = (-0.5, -1.2, 20)\kappa$. In (b) $\Gamma_0 = 0.005\kappa$.

Thesis VIII

We have shown that the atom-cavity system in the case of atom pumping realizes a quantum seesaw with the cavity field standing for the seesaw, that is, a system capable of leaving its unstable equilibrium point via entanglement and without any noise. The effect has implications on phenomena in which spontaneous symmetry breaking is inherent, such as the self-organisation of ultra-cold atoms in a cavity field.

Many-body aspects — Outlook

In this Chapter we overview some of our ideas of a fully quantum mechanical description of many atoms in the cavity. Our motivation is to study the self-organisation phenomenon (cf. Appendix C) in the case when both the atomic motion and the cavity field is described quantum mechanically, since Chap. 7 hinted that the possibility of atom-field entanglement has an impact on what is classically spontaneous symmetry breaking and maybe also on the phase transition phenomenon as a whole. The question arises whether there is a quantum phase transition, that is, an abrupt change in the structure of the ground state at some critical point in parameter space. Note that the “ground state” of such a dissipative system is defined as the stationary solution of the Master equation

$$\dot{\rho} = \mathfrak{L}\rho \left(= \frac{1}{i\hbar} [H, \rho] + \mathcal{L}\rho \right), \quad (8.1)$$

that is, the eigenvector of the (super)operator \mathfrak{L} corresponding to 0 eigenvalue.

Our starting point is the second quantised version of the Model 1sc Hamiltonian. Probably the simplest model which has any chance for catching the basic physics of the problem is discussed in Sec. 8.2. Here the cavity field is eliminated and we consider only two possible atomic states corresponding to the $|\text{left}\rangle$ and $|\text{right}\rangle$ states of Chap. 7. In Sec. 8.3 we show that the problem with full atomic motion can be mapped to a lattice model and we discuss the possibility of a DMRG solution of the model.

To make it simple, in the whole Chapter $\Gamma_0 = 0$. Hence, the whole dissipative part of the dynamics is described by the Liouvillian

$$\mathcal{L}\rho = \kappa \left(2a\rho a^\dagger - \left[a^\dagger a, \rho \right]_+ \right). \quad (8.2)$$

Note that even without the spontaneous emission induced recoil diffusion, there is “enough” noise in the system stemming from the cavity-decay induced dipole force diffusion to account for self-organisation.

8.1 The many-atom Hamiltonian

The Hamiltonian describing the fully quantum mechanical dynamics of many atoms interacting with the cavity field stems from (3.15a) and reads

$$H_{\text{mb}} = -\hbar\Delta_C a^\dagger a - i\hbar\eta \left(a - a^\dagger \right) + \int d\mathbf{r} \Psi^\dagger(\mathbf{r}) \left(\frac{\mathbf{p}^2}{2\mu} + \hbar U_0 \mathcal{E}^\dagger(\mathbf{r}) \mathcal{E}(\mathbf{r}) \right) \Psi(\mathbf{r}). \quad (8.3)$$

Here $\Psi(\mathbf{r})$ is an operator which annihilates an atom at point \mathbf{r} . The atoms are supposed to be bosons so that

$$\left[\Psi(\mathbf{r}), \Psi^\dagger(\mathbf{r}') \right] = \delta(\mathbf{r} - \mathbf{r}'). \quad (8.4)$$

Here we are chiefly interested in the interaction transmitted by the cavity field between the atoms since each atom interacts with the very same cavity mode. As explained in Appendix C for the classical case, this indirect interaction itself is capable of generating a phase transition. Direct atom-atom interaction, which would be an additional term in the Hamiltonian of fourth order in Ψ is therefore omitted.

Concerning the problem of scaling with the atom number N we note that were we to consider a Bose-Einstein condensate, the atoms could be described by a classical field $\Psi(\mathbf{r}) = \sqrt{N} \Phi(\mathbf{r})$ where N is the number of atoms and $\Phi(\mathbf{r})$ is the condensate wave function. In this case it is easy to verify that the problem is identical to a one-particle problem, but with parameters rescaled as $g \rightarrow \sqrt{N}g$ and $\eta_t \rightarrow \sqrt{N}\eta_t$.

In the following we shall consider Configuration AZ because it is here that we have a lattice fixed by the transverse pumping field, which will be an important point in the next Section. The Hamiltonian in this case reads

$$H = -\hbar(\Delta_C - NU_0) a^\dagger a + \hbar\omega_{\text{rec}} \int dz \Psi^\dagger(z) \mathcal{H}_0 \Psi(z) + \hbar\sqrt{U_0 \eta_{\text{eff}}} (a^\dagger + a) \mathcal{S}, \quad (8.5)$$

with $\mathcal{H}_0 = \mathbf{p}^2/(2\hbar^2 K^2) + \mu\eta_{\text{eff}}/(\hbar K^2) \sin^2(Kz)$ the dimensionless lattice Hamiltonian, and

$$\mathcal{S} = \int dz \Psi^\dagger(z) \sin(Kz) \Psi(z). \quad (8.6)$$

Note that the total number of atoms is certainly conserved so that the operator $\int dz \Psi^\dagger(z) \Psi(z)$ has been replaced by N .

Sometimes it will be convenient to eliminate the cavity field. It can be done using the above Hamiltonian and the Liouvillean (8.2) — omitting the noise:

$$a = \frac{-i\sqrt{U_0 \eta_{\text{eff}}}}{i(\Delta_C - NU_0) - \kappa} \mathcal{S}. \quad (8.7)$$

We insert it back to the Hamiltonian (8.5):

$$H_{\text{eff}} = \hbar\omega_{\text{rec}} \int dz \Psi^\dagger(z) \mathcal{H}_0 \Psi(z) - \frac{\hbar U_0 \eta_{\text{eff}} (\Delta_C - NU_0)}{(\Delta_C - NU_0)^2 + \kappa^2} \mathcal{S}^2 \quad (8.8a)$$

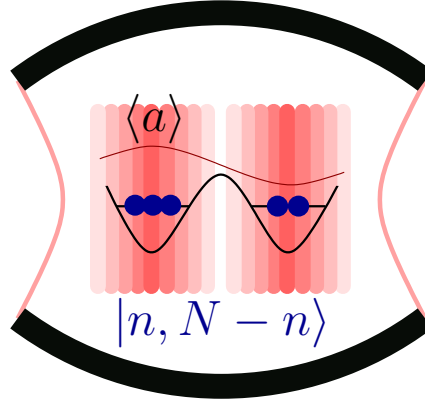


Figure 8.1: Toy many-body model for many atoms interacting with the cavity field in Configuration AZ. A section of length λ is considered with two trapping sites in the transverse pumping field at $Kz = \pm\pi/2$, and one atomic state in each well. The cavity field is eliminated making that for N atoms there are $N + 1$ states of the system.

and Liouvillean (8.2)

$$\mathcal{L}_{\text{eff}}\rho = \frac{U_0 \eta_{\text{eff}}\kappa}{(\Delta_C - NU_0)^2 + \kappa^2} \left(2\mathcal{S}\rho\mathcal{S} - [\mathcal{S}^2, \rho]_+ \right). \quad (8.8b)$$

This system describes a field which has gained self-interaction and dissipative dynamics via the cavity field.

8.2 Toy many-body model

Let us consider the section λ around 0 (cf. Fig. 8.1). In this section the potential stemming from the transverse pumping field has two minima at $Kz = \pm\pi/2$ (note that U_0 is negative). This defines a symmetrical double-well problem in which the ground state $|0\rangle$ is eigenstate of the parity operator with eigenvalue 1 and the first excited state $|1\rangle$ with eigenvalue -1 :

$$\mathcal{H}_0 |0\rangle = \epsilon_0 |0\rangle, \quad \mathcal{H}_0 |1\rangle = \epsilon_1 |1\rangle. \quad (8.9)$$

Using these two states we can define two other states with minimal energy¹ localised in the left and the right well, respectively:

$$|l\rangle = \frac{1}{\sqrt{2}} (|0\rangle + |1\rangle), \quad |r\rangle = \frac{1}{\sqrt{2}} (|0\rangle - |1\rangle), \quad (8.10)$$

and these two states are also orthogonal.

¹This is the difference between $|l\rangle, |r\rangle$ and $|\text{left}\rangle, |\text{right}\rangle$ used in Chap. 7. There, the atom is not necessarily in the ground state of the corresponding potential well.

The toy many-body model consists of the system (8.8) with the restriction to these two states, that is, setting $\Psi = b_l |l\rangle + b_r |r\rangle$. As it is easy to verify, in this case

$$\int dz \Psi^\dagger(z) \mathcal{H}_0 \Psi(z) = J \left(b_l^\dagger b_r + b_r^\dagger b_l \right) + \text{const.}, \quad (8.11a)$$

$$\mathcal{S} = \tilde{J} \left(b_l^\dagger b_l - b_r^\dagger b_r \right), \quad (8.11b)$$

with $J = \epsilon_l - \epsilon_0$ (hopping parameter), and $\tilde{J} = \langle l | \sin(Kz) | l \rangle = -\langle r | \sin(Kz) | r \rangle$. This model is eventually an utterly simplified Bose-Hubbard model [58, 61, 67, 68]. There are only two dimensionless parameters:

$$\mathcal{J} = \frac{U_0 \eta_{\text{eff}} (\Delta_C - NU_0) \tilde{J}^2}{((\Delta_C - NU_0)^2 + \kappa^2) \omega_{\text{rec}} J}, \quad \mathcal{K} = \frac{U_0 \eta_{\text{eff}} \kappa \tilde{J}^2}{((\Delta_C - NU_0)^2 + \kappa^2) \omega_{\text{rec}} J}, \quad (8.12)$$

with dimensionless operators:

$$H = \left(b_l^\dagger b_r + b_r^\dagger b_l \right) - \mathcal{J} \left(b_l^\dagger b_l - b_r^\dagger b_r \right)^2, \quad (8.13a)$$

$$\mathcal{L}\rho = \mathcal{K} \left(2 \left(b_l^\dagger b_l - b_r^\dagger b_r \right) \rho \left(b_l^\dagger b_l - b_r^\dagger b_r \right) - \left[\left(b_l^\dagger b_l - b_r^\dagger b_r \right)^2, \rho \right]_+ \right). \quad (8.13b)$$

Since the states are defined by the fixed potential generated by the transverse pump ($\propto \sin^2$), the model is expected to work well in the limit when this potential dominates the one generated by interference with the cavity field ($\propto \sin$). Therefore, it certainly cannot give account of the fact that the atoms make the potential for themselves (via the scattering-generated cavity field), which so far has been a must of most of this work. In particular, strictly speaking self-organisation is ruled out from this treatment since it occurs in the limit where the \sin potential dominates the \sin^2 one.

On the other hand, since for N atoms there is only $N + 1$ possible states of the system, the model can be solved exactly. The solution consists of exact diagonalisation of the superoperator \mathcal{L} . The dimension of the density matrix space being $(N + 1)^2$ this means the diagonalisation of an $(N + 1)^2 \times (N + 1)^2$ matrix, which is again done using LAPACK. This can be done for up to 20 atoms. Once done, the exact time evolution of the density matrix ρ is known.

As it is easy to verify even analytically, the ground state, that is, the final state of the evolution is a very trivial one which consists of each state $|n, N - n\rangle$ having the same population with vanishing coherences. An example is given in Fig. 8.2. Hence, there is of course no quantum phase transition in this model. The photon number in the final state is proportional N^2 so that this is a superradiant state. The expectation value of the field is, however, zero, due to the symmetry.

Still, in the transient behaviour there is a change which is reminiscent of the self-organisation. Starting the system from the $|N - 1, 1\rangle$, with proper choice of parameters it can be achieved that the population of the self-organised state $|N, 0\rangle$ dominates the dynamics for a long time. An example for $N = 4$ atoms is shown in Fig. 8.3.

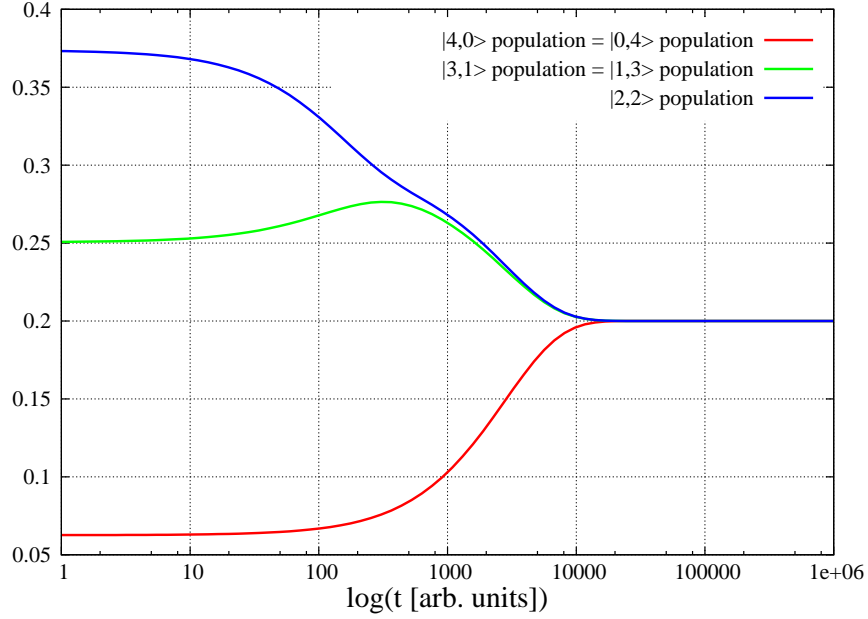


Figure 8.2: The evolution of populations show the setting in of the simplistic final state for $N = 4$ atoms. The initial state is $(b_l^\dagger + b_r^\dagger)^N / 2^{N/2} |0\rangle$ — In the lattice-model literature this is usually called “superfluid” or BEC state. @ $\mathcal{J} = 2000$, $\mathcal{K} = 1000$.

8.3 Mapping to a lattice model

From what was said in Sec. 4.1.1 it is clear that in the many atom case for Configuration AZ the system can be mapped to the lattice system depicted in Fig. 8.4. Since here a section of length λ is the elemental cell in the problem, particle exchange is only band-to-band. There is no particle exchange inside a band and interaction is only generated by that each sublattice interacts with the same cavity mode, that is, a photon emitted by a particle on one sublattice can be absorbed by one on another sublattice. While this interaction alone is capable of generating phase transitions [101], here, just like in Sec. 4.1.1 we nevertheless restrict ourselves to the set of momentum components $\{nK\}_{n \in \mathbb{Z}}$, that is, we set $\Psi = \sum_{n \in \mathbb{Z}} b_n |nK\rangle$. Inserting into Hamiltonian Eq. (8.5) we obtain:

$$H = -\hbar(\Delta_C - NU_0) a^\dagger a + \sum_{n \in \mathbb{Z}} \left(\frac{\hbar\omega_{\text{rec}}}{2} n^2 b_n^\dagger b_n - \frac{\eta_{\text{eff}}}{4} (b_{n+2}^\dagger b_n + b_n^\dagger b_{n+2}) + \frac{\sqrt{U_0\eta_{\text{eff}}}}{2i} (b_{n+1}^\dagger b_n - b_n^\dagger b_{n+1}) (a + a^\dagger) \right). \quad (8.14)$$

In this model the atomic motion is not restricted, so that it fully accounts for the atoms moving in the dynamic potential created by the field. Hence, it is very promising for the description of dynamical phase transitions like the self-organisation. A great

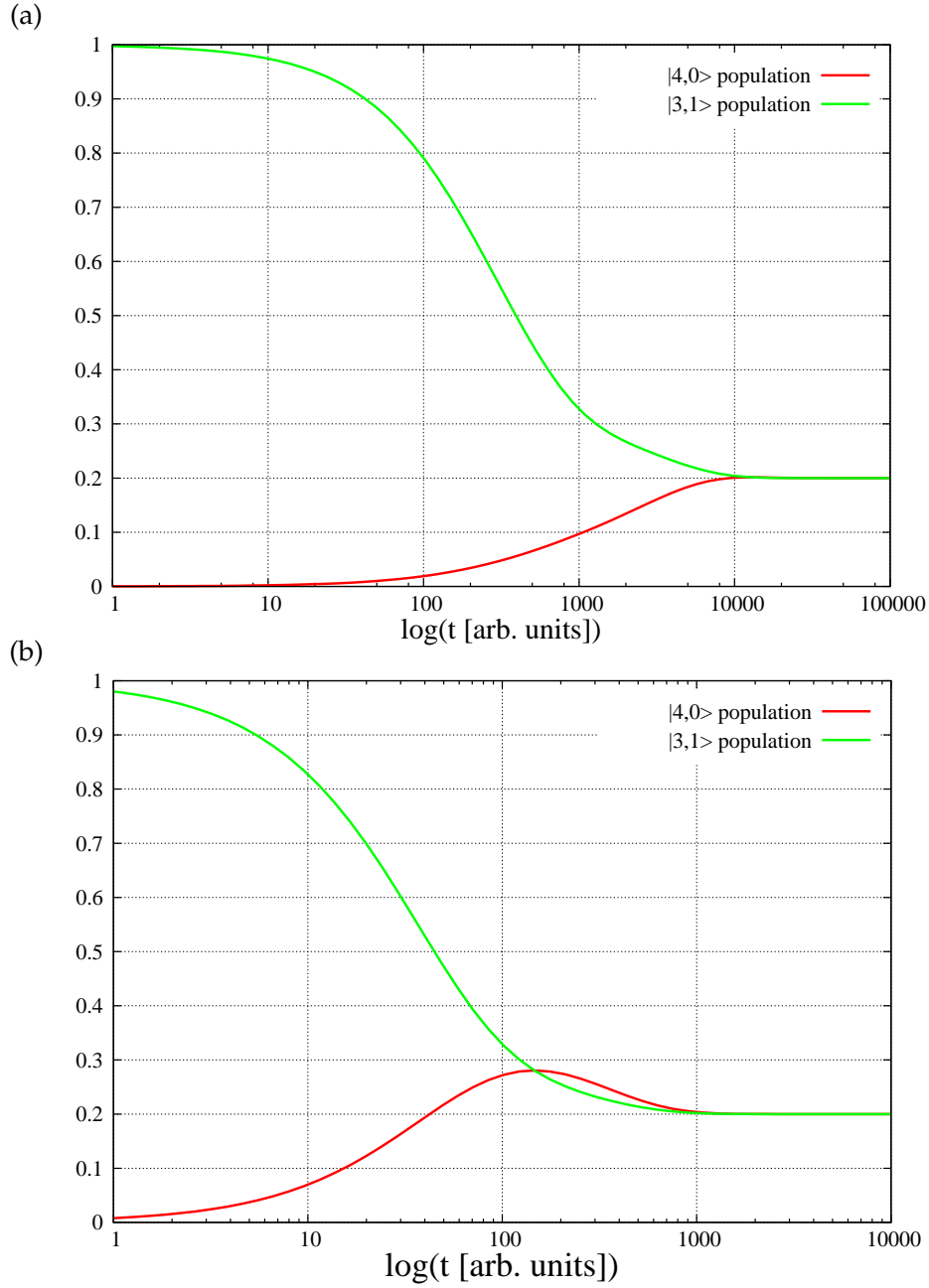


Figure 8.3: Evolution of populations of the states $|3, 1\rangle$ and $|4, 0\rangle$. In part (b) the later dominates the former, an effect reminiscent of self-organisation. @ $\mathcal{K} = 1000$; in (a) $\mathcal{J} = 2000$, in (b) $\mathcal{J} = 200$.

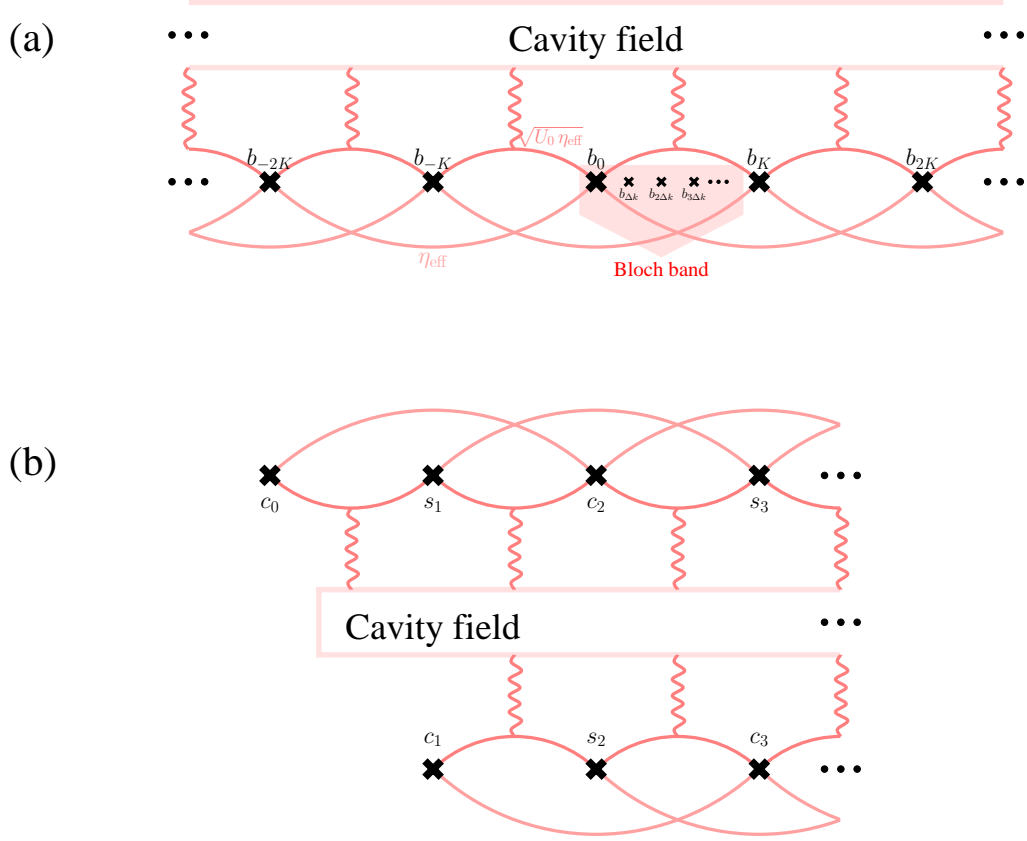


Figure 8.4: (a) Many-atom system in Configuration AZ mapped to a lattice model in momentum-space. Observe that the interaction is between Bloch bands. The one between the next-neighbouring bands is generated by the pump field, while the one between neighbouring bands is associated with the absorption or emission of a cavity photon. In the text we restrict ourselves to the (sub)lattice indicated by the big crosses. (b) Using the symmetry of the Hamiltonian even this sublattice is split into two between which there is no particle exchange.

advantage of using momentum space is that even the first few lattice sites seize the basic physics of the system. E.g. the unorganised state is approximately described by the sites $\pm 2, 0$, while the organised one by the sites ± 1 .

The above Hamiltonian is symmetric with respect to the change $b_n \leftrightarrow b_{-n}$. This feature can be exploited by introducing cosine and sine modes instead of momentum eigenstates:

$$c_0 = b_0, \quad c_{n>0} = \frac{b_n + b_{-n}}{\sqrt{2}}, \quad s_{n>0} = \frac{b_n - b_{-n}}{\sqrt{2}i}. \quad (8.15)$$

In this case even the infinite lattice $\{nK\}_{n \in \mathbb{Z}}$ is separated into two half-infinite sublattices between which there is no particle exchange. One consists of the even c -s and odd s -s, the other vice versa. Between the two sublattices the interaction is again generated by that both interact with the same cavity mode. This we again ignore and restrict ourselves to only one sublattice.

We plan to apply the Density Matrix Renormalisation Group [102] — for a review see Schollwöck's [69] — to this lattice, which aims at the calculation of ground state properties of lattice systems. As already hinted above, the key physics is described by the first few lattice sites while the rest serves as a noise source, which is a must for the phase transition. The finite-system DMRG is to be applied with some prefixed cutoff in momentum. The cavity field is not to be renormalised, and also in the photon number a cutoff is to be introduced: hence, we in fact have a lattice for each photon number component. In the DMRG method, quantum phase transitions are detected by the calculation of site entropies in the ground state [103].

The MCWF method made easy

Suppose a quantum system with dissipative dynamics governed by the Master equation

$$\dot{\rho} = \frac{i}{\hbar} [\rho, H] + \mathcal{L}\rho, \quad (\text{A.1})$$

where the Liouvillian, as it is usual in quantum optics, has the form

$$\mathcal{L}\rho \equiv \sum_m \left(J_m \rho J_m^\dagger - \frac{1}{2} [J_m^\dagger J_m, \rho]_+ \right). \quad (\text{A.2})$$

At time t the system is in a state with normalised wave function $|\Psi(t)\rangle$.

The Monte Carlo Wave-Function method for such an abstract system consist of two steps in order to obtain the wave function at time $t + \delta t$ up to first order in δt :

1. The wave function is evolved with the non-Hermitian Hamiltonian

$$H_{\text{nH}} = H - \frac{i\hbar}{2} \sum_m J_m^\dagger J_m \quad (\text{A.3})$$

to obtain (up to first order in δt)

$$|\Psi_{\text{nH}}(t + \delta t)\rangle = \left(1 - \frac{iH_{\text{nH}} \delta t}{\hbar} \right) |\Psi(t)\rangle. \quad (\text{A.4})$$

Since H_{nH} is non-Hermitian, this new wave function is not normalised. The square of its norm reads

$$\begin{aligned} \langle \Psi_{\text{nH}}(t + \delta t) | \Psi_{\text{nH}}(t + \delta t) \rangle \\ = \langle \Psi(t) | \left(1 + \frac{iH_{\text{nH}}^\dagger \delta t}{\hbar} \right) \left(1 - \frac{iH_{\text{nH}} \delta t}{\hbar} \right) | \Psi(t) \rangle \equiv 1 - \delta p, \end{aligned} \quad (\text{A.5})$$

where δp reads

$$\delta p = \delta t \frac{i}{\hbar} \langle \Psi(t) | H_{\text{nH}} - H_{\text{nH}}^\dagger | \Psi(t) \rangle \equiv \sum_m \delta p_m \quad (\text{A.6a})$$

$$\delta p_m = \delta t \langle \Psi(t) | J_m^\dagger J_m | \Psi(t) \rangle \geq 0 \quad (\text{A.6b})$$

Note that the time step δt should be small enough so that this first-order calculation be valid. The requirement is $\delta p \ll 1$.

2. A possible quantum jump with total probability δp . For the physical interpretation of such a jump see eg Refs. [39, 104]. We choose a (quasi) random number ϵ between 0 and 1, and if $\delta p < \epsilon$, which should mostly be the case, no jump occurs and for the new normalised wave function at $t + \delta t$ we take

$$|\Psi(t + \delta t)\rangle = \frac{|\Psi_{\text{nH}}(t + \delta t)\rangle}{\sqrt{1 - \delta p}}. \quad (\text{A.7})$$

If $\epsilon < \delta p$, on the other hand, a quantum jump occurs, and the new normalised wave function is chosen among the different wave functions $J_m |\Psi(t)\rangle$ according to the probability distribution $\Pi_m = \delta p_m / \delta p$:

$$|\Psi(t + \delta t)\rangle = \sqrt{\delta t} \frac{J_m |\Psi(t)\rangle}{\sqrt{\delta p_m}}. \quad (\text{A.8})$$

In the following we demonstrate that the above two-step stochastic evolution of a wave function is equivalent with the deterministic evolution of the density operator governed by the Master equation (A.1). Let us consider the operator $\sigma(t) \equiv |\Psi(t)\rangle \langle \Psi(t)|$. Let $\bar{\sigma}(t)$ be the average of $\sigma(t)$ over the possible outcomes of the MCWF evolutions all starting in $|\Psi(0)\rangle$. We shall prove that if $\rho(0) = |\Psi(0)\rangle \langle \Psi(0)|$ then $\bar{\sigma}(t)$ coincides with $\rho(t)$ at all times t .¹

If at time t the MCWF wave function is $|\Psi(t)\rangle$ then at time $t + \delta t$

$$\bar{\sigma}(t + \delta t) = (1 - \delta p) \frac{|\Psi_{\text{nH}}(t + \delta t)\rangle \langle \Psi_{\text{nH}}(t + \delta t)|}{\sqrt{1 - \delta p}} + \delta t \delta p \sum_m \Pi_m \frac{J_m |\Psi(t)\rangle \langle \Psi(t)| J_m^\dagger}{\sqrt{\delta p_m}}, \quad (\text{A.9})$$

which, when using Eq. (A.4), gives

$$\bar{\sigma}(t + \delta t) = \sigma(t) + \frac{i\delta t}{\hbar} [\sigma(t), H] + \delta t \mathcal{L}\sigma(t). \quad (\text{A.10})$$

Averaging over the possible values of $\sigma(t)$ we obtain

$$\frac{d\bar{\sigma}(t)}{dt} = \frac{i}{\hbar} [\bar{\sigma}(t), H] + \mathcal{L}\bar{\sigma}(t). \quad (\text{A.11})$$

This is equivalent with the Master equation (A.1). From the above proof it is also clear that in the MCWF method the deterministic part of the damping (loss, dissipation) is accounted for by the non-Hermiticity of the evolution, while the stochastic part (noise, fluctuation) is rendered by the quantum jumps.

¹The generalisation for mixed initial states is then straightforward since every mixed state can be decomposed as a convex combination of pure states. The MCWF evolution in this case should be performed separately for each initial pure-state component.

Cavity sideband cooling

Originally, *sideband cooling* is for an atom strongly-enough confined in a (harmonic) trap and illuminated by a plane wave whose spatial dependence couples the atomic internal and motional degrees of freedom, making that the atomic motion inherits the dissipation of the internal dynamics (spontaneous decay). The detuning between the illuminating light and the atomic transition has to be set to minus the trap vibration frequency (a sideband), hence the name.¹

In this Appendix, using a simple Wigner-Weisskopf approach and perturbation theory, we demonstrate that a similar effect exists in Configuration CX, the cavity field standing for the dissipative internal degree of freedom. We also show that to exhibit this effect, a very different detuning is necessary than what we have used throughout this work, and therefore this effect is very different from our dynamical cavity cooling effect.

We start from the Hamiltonian (3.17a) and add the cavity decay in Wigner-Weisskopf approximation (we omit the atomic decay):

$$H = \frac{p^2}{2\mu} - \hbar (\Delta_C - U_0 \cos^2(Kx) + i\kappa) a^\dagger a - i\hbar\eta (a - a^\dagger), \quad (\text{B.1})$$

where we have taken \cos for the mode function. We assume that the field is big enough to strongly confine the atom in the vicinity of 0, so that we can take $\cos(Kx) \approx 1 - K^2 x^2/2$. We separate the expectation value of the field: $a = \alpha + \tilde{a}$ with $\alpha = i\eta/(\Delta_C -$

¹This effect is accounted for by the simple Hamiltonian

$$H = \hbar\nu b^\dagger b + \hbar\omega_A \sigma^\dagger \sigma + \hbar\eta (\sigma^\dagger e^{-i(\omega t + kx)} + \text{h.c.}).$$

In interaction picture this reads

$$H = \hbar\eta \left(\sigma^\dagger e^{-i\Delta_A t} \sum_n \frac{(\text{const.})^n (b e^{-i\nu t} + b^\dagger e^{i\nu t})^n}{n!} + \text{h.c.} \right) \approx \hbar\eta (\sigma^\dagger b^\dagger P(b^\dagger b) + \text{h.c.}),$$

where for the \approx we have set $\Delta_A = -\nu$ and applied rotating-wave approximation, P is some polynom. The coupling term $\propto \sigma^\dagger b^\dagger$ accounts for cooling in a way described in the text for the cavity sideband cooling case.

$U_0 + i\kappa$) (cf Eq. 4.20) and $\langle \tilde{a} \rangle = 0$. The Hamiltonian then reads

$$H = \frac{p^2}{2\mu} + \hbar |U_0| |\alpha|^2 \frac{K^2 x^2}{2} - \hbar (\Delta_C - U_0 + i\kappa) \tilde{a}^\dagger \tilde{a} + \hbar U_0 \left(\alpha^* \tilde{a} + \alpha \tilde{a}^\dagger \right) \frac{K^2 x^2}{2}, \quad (\text{B.2})$$

where the higher order term $\propto \tilde{a}^\dagger \tilde{a} x^2$ has been dropped. The expectation value of the last term being zero, the atom moves in a classical harmonic potential with frequency $\nu = \sqrt{\hbar |U_0| / \mu K |\alpha|}$. Introducing the ladder operators b for the harmonic potential we arrive at

$$H = \hbar \nu b^\dagger b - \hbar (\Delta_C - U_0 + i\kappa) \tilde{a}^\dagger \tilde{a} + \frac{\hbar \nu}{4} \left(\frac{\tilde{a}}{\alpha} + \frac{\tilde{a}^\dagger}{\alpha^*} \right) (b + b^\dagger)^2. \quad (\text{B.3})$$

The last term is a small perturbation.

Let us consider the state $|n, 0\rangle$ — $n \gtrsim 2$ atomic excitation and 0 photon (in the \tilde{a} sense). The energy of this state is perturbed in second order:

$$\begin{aligned} E_{n,0}^{(2)} &= \frac{\hbar^2 \nu^2}{16 |\alpha|^2} \sum_{m, m \neq n, 0} \frac{|\langle n, 0 | \tilde{a} (b + b^\dagger)^2 | m, m \rangle|^2}{E_{n,0}^{(0)} - E_{m,m}^{(0)}} \\ &\approx \frac{\hbar \omega_{\text{rec}} |U_0| n^2}{16} \left(\frac{1}{2\nu + (\Delta_C - U_0 + i\kappa)} + \frac{1}{-2\nu + (\Delta_C - U_0 + i\kappa)} + \frac{4}{(\Delta_C - U_0 + i\kappa)} \right). \end{aligned} \quad (\text{B.4})$$

The energy has indeed inherited an imaginary part. This is true for every $n > 0$ which means that the population of the excited states is damped, which means cooling towards the ground state. Being of second order, this is a small effect, its best being at the detunings $\Delta_C - U_0 = \pm 2\nu, 0$.

Self-organisation

Self-organisation of ultra-cold atoms in a cavity was first anticipated by Domokos and Ritsch [35], and demonstrated experimentally by Black et al. [63]. Later it was discovered that the process can be considered as a dynamical phase transition between an unorganised and a self-organised atomic distribution with control parameter η_t , and connected phenomena such as spontaneous symmetry breaking, scaling laws, and hysteresis have been identified [62].

The authors of the above theoretical works used Model 1sc, which, owing to its simplicity, allows for the simulation of many atoms interacting with the cavity field. Self-organisation happens in Configurations AZ and AX where the self-organised phase is a $2\pi/K$ periodic atomic distribution as well as in two dimensions in which case a checkerboard-like pattern emerges in the self-organised phase. The process for Configuration AZ is summarised in Fig. C.1.

Self-organisation is due to the competition between the potential proportional to \sin and the one proportional to \sin^2 in the Hamiltonians (3.17b) and (3.17c). When a \sin potential is added to a \sin^2 potential, the original periodicity of π/K is reduced to a periodicity of $2\pi/K$. The original even and odd attracting sites (minima of the \sin^2 potential) will now have different depths, and it can also happen that one set of them become repelling sites (when the \sin dominates the \sin^2).

Every phase transition can be considered as a result of a competition between energy and entropy, the transition happening between a phase with high energy and high entropy and one with low energy and low entropy. In the present case these phases are:

High energy and entropy. In Configuration AX this is simply a homogeneous atomic distribution, while in AZ a distribution with periodicity π/K . Since the cavity is not pumped, cavity field can build up only from the field scattered by the atoms from the cavity pump. In this phase there will be no cavity field since the field scattered by atoms with position difference π/K vanishes due to destructive interference. No cavity field means that the \sin potential being proportional to a

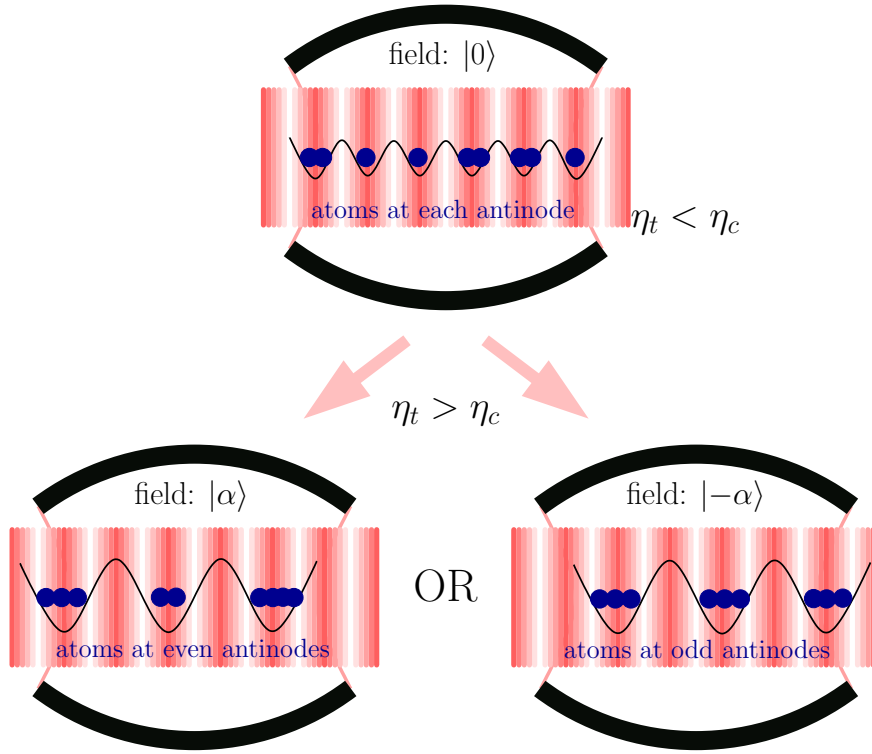


Figure C.1: Self-organisation in Configuration AZ. The solid black line indicates the potential felt by the atoms.

vanishes. In Configuration AX the \sin^2 potential being proportional to $a^\dagger a$ also vanishes while in AZ this remains. This means that the above mentioned atomic distributions are stationary.

Low energy and entropy. This is the self-organised phase. In each Configuration it consists of the atoms occupying every second (either the even or the odd) trapping sites of the \sin^2 potential. In this case each atom scatters with the same phase into the resonator so that constructive interference yields a strong field (super-radiance). With big enough η_t this results in the \sin potential dominating the \sin^2 one, which again with proper parameters yields deep potential wells *at the positions of the atoms*. Which of the two configurations (even or odd) is realized is decided in a spontaneous manner.

From the above discussion it is clear that in each phase the atomic distribution creates a cavity field which, in turn, creates such a potential as to stabilise the given atomic distribution, hence the name “self”-organisation. Note that parameters should be adjusted in a way such that this feedback be positive, in particular, $\Delta_C - NU_0$ should be negative. ($U_0 < 0$ is of course also necessary, or else the atoms seek the *nodes* of the field where they do not scatter into the cavity). Strong coupling is *not* necessary for self-organisation since the coupling parameter is scaled up with the square root of the atom number.

C.1 Hydrodynamical approach

Probably the simplest approach to classical many-body effects such as the self-organisation is considering the atoms as a continuum with density $\rho(\mathbf{r})$ and velocity field $\mathbf{v}(\mathbf{r})$ inside the cavity. In this approach the unorganised phase appears as a stationary solution with every parameter setting, but it becomes hydrodynamically unstable at the transition point.

This approach we shall present for Configuration AX since it is here that we know the unorganised phase exactly (homogeneous distribution). The field equations mostly stem from Eqs. (3.23) of Model 1sc with the substitution $\mathfrak{E}(x) = f(x) \alpha + \eta_t/g$:

$$\delta_\tau \tilde{v} + \tilde{v}(\delta_\xi \tilde{v}) = \tilde{\omega}_{\text{rec}} \left(-\tilde{U}_0 \delta_\xi |\mathfrak{E}(\xi)|^2 - \frac{\mathcal{A}\mu}{\hbar\kappa} \delta_\xi \log \tilde{\rho} \right), \quad (\text{C.1a})$$

$$\delta_\tau \tilde{\rho} + \delta_\xi(\tilde{\rho} \tilde{v}) = 0, \quad (\text{C.1b})$$

$$\frac{d\alpha}{d\tau} = \left(i \left(\tilde{\Delta}_C - \frac{N\tilde{U}_0}{2} \right) - 1 \right) \alpha - i \frac{\tilde{U}_0 \eta_t}{g} \int d\xi \tilde{\rho}(\xi) \sin(\xi). \quad (\text{C.1c})$$

Here N is the number of atoms. Note that Γ_0 has been set to zero since here we do not want to be bothered by the recoil diffusion. This is well justified in the far-enough-detuned regime. The first equation is a diffusive version of the Euler equation, the second one is the continuity equation, while the third one is the hydrodynamic version of Eq. (3.23c). We have written dimensionless equations with $\tau = \kappa t$, $\xi = Kx$, $\tilde{v} = Kv/\kappa$, and $\tilde{\rho} = \rho/K$.

The second term in the right-hand side of Eq. (C.1a) has been added to account for the diffusion in the atomic motion, which now originates solely from the dipole-force diffusion of the cavity field (scaling with κ).¹ Note that strictly speaking the system is at zero temperature (since it does not interact with any finite temperature reservoir), still, as we have seen throughout this work, cavity decay does yield some finite effective temperature. This is necessary since without temperature entropy is not a concern any more (cf 1st law of thermodynamics), and the system always goes for the low energy state hindering any phase transition from occurring. To a more applied level this general principle translates as the dipole force diffusion stabilising the unorganised phase. Since the effective temperature is approximately κ , we can set $\mathcal{A}\mu = \hbar\kappa$.

Now it is very clear that $\tilde{v} \equiv 0$, $\tilde{\rho} \equiv \tilde{\rho}_0$, and $\alpha = 0$ is always a solution of the system (C.1) (unorganised phase). Let us introduce the small fields $v(\xi)$ and $\rho(\xi)$ perturbing this solution (α is also small in the following), and put them back to the system (C.1). The linearised equations for the small fields read

$$\delta_\tau v = \tilde{\omega}_{\text{rec}} \left(-\tilde{U}_0 \frac{\eta_t}{g} \cos(\xi) (\alpha + \alpha^*) - \frac{\delta_\xi \rho}{\tilde{\rho}_0} \right), \quad (\text{C.2a})$$

$$\delta_\tau \rho + \tilde{\rho}_0 \delta_\xi v = 0, \quad (\text{C.2b})$$

$$\frac{d\alpha}{d\tau} = \left(i \left(\tilde{\Delta}_C - \frac{N\tilde{U}_0}{2} \right) - 1 \right) \alpha - i \frac{\tilde{U}_0 \eta_t}{g} \int d\xi \rho(\xi) \sin(\xi). \quad (\text{C.2c})$$

Now the spatial dependence of the fields can be separated since looking at the first two equations it becomes clear that they must assume the form $v = \mathfrak{v}(\tau) \cos(\xi)$ and

¹Let us justify this term as follows: Suppose a continuum is moving in a potential $V(x)$. Then the “diffusive” Euler equation reads

$$\delta_t v + v(\delta_x v) = -\frac{1}{\mu} \delta_x V(x) - \mathcal{A} \delta_x \log(\rho).$$

If $v \equiv 0$ this can be solved for an “equilibrium” ρ :

$$\rho(x) \propto \exp \left(-\frac{V(x)}{\mathcal{A}\mu} \right),$$

which is just the equilibrium distribution for the gas interacting with a reservoir of temperature T with $\mathcal{A} = kT/\mu$.

$\rho = \mathfrak{r}(\tau) \sin(\xi)$. We obtain

$$\frac{d\mathfrak{v}}{d\tau} = \tilde{\omega}_{\text{rec}} \left(-\tilde{U}_0 \frac{\eta_t}{g} 2\Re\{\alpha\} - \frac{\mathfrak{r}}{\tilde{\rho}_0} \right), \quad (\text{C.3a})$$

$$\frac{d\mathfrak{x}}{d\tau} = \tilde{\rho}_0 \mathfrak{v}, \quad (\text{C.3b})$$

$$\frac{d\alpha}{d\tau} = \left(i \left(\tilde{\Delta}_C - \frac{N\tilde{U}_0}{2} \right) - 1 \right) \alpha - i \frac{\tilde{U}_0 \eta_t}{g} \frac{KL}{2} \mathfrak{r}. \quad (\text{C.3c})$$

The last equation has to be split into real and imaginary parts and hence we are left with a system of four real ordinary differential equations for which the eigenfrequencies must be determined. The critical parameter setting is then signalled by the appearance of an eigenfrequency with positive real part. This gives

$$\eta_c = \sqrt{2} \frac{\kappa |\Delta_A|}{\sqrt{Ng}}, \quad (\text{C.4})$$

which is in good agreement with the result of more elaborate studies, such as Model 1sc simulations. Certainly, this hydrodynamical model cannot give account of the hysteresis effect discussed by Asbóth et al. [62].

Összefoglalás — Summary

A disszertációban a 2003-mal kezdődő PhD-éveink alatt végzett munkánkat foglaltuk össze. A következőkben a disszertációt foglaljuk össze, fejezetenként haladva. A címek után megjelenő referenciák azt mutatják, hogy az adott fejezet anyaga milyen publikációkban jelent meg.

A vizsgált fizikai rendszer

Értekezésünkben jobbra az optikai rezonátoros kvantumelektrodinamikai rendszerek egy prototípusát vizsgáltuk, ami egyetlen mozgó kétállapotú atomból áll, és ez egy nyílt (Fabry-Perot típusú) optikai rezonátor egyetlen módusával hat kölcsön.

A 8. fejezetben a többatomos esetet vizsgáltuk, ahol minden atom ugyanazzal a rezonátormódussal hat kölcsön. Bár a közvetlen atom-atom kölcsönhatást az egyszerűség kedvéért elhanyagoltuk, a probléma mégis lényegileg soktestprobléma a rezonátor által közvetített kölcsönhatás miatt. Érdekes, hogy a kölcsönhatás erőssége nem is függ az atomok távolságától, egyedül az atomoknak a rezonátormező legközelebbi duzzadóhelyéhez viszonyított pozíciója a lényeges. Ezt a kölcsönhatást a [32] referenciában kimerítően vizsgálták a legegyszerűbb, kétatomos esetben.

Elméleti modellek

Négy különböző szintű modellt használtunk az adott paramétertartománynak megfelelően. Ezeknek rövid neveket adtunk a hivatkozások megkönnyítése végett: A

- 0. Modell** az atom-rezonátor rendszer standard kvantumoptikai modellje. Meglehetősen kézenfekvő dologról van szó, hiszen két Jaynes–Cummings típusú tag számot ad az atom és a rezonátormező, valamint az atomnak egy esetleges pumpáló mezővel (atomi pumpa) való kölcsönhatásáról. A rezonátor gerjesztését (rezonátor-pumpa) egy egyszerű koherens gerjesztő tag írja le. A disszipatív folyamatokat

a Lindblad-formalizmusban kezeljük. A 0. Modell teljesen veszi figyelembe egy optikai rezonátoros kvantumelektrodinamikai rendszer mindhárom szabadsági fokát: az atomi külső (tömegközépponti mozgás), belső (elektronkonfiguráció) szabadsági fokokat és a rezonátormező szabadsági fokát. A

0sc Modell [30, 33, 34] úgy keletkezik, hogy ez utóbbi két szabadsági fokot elimináljuk. Az egyetlen megmaradó szabadsági fokot, az atom tömegközépponti mozgását is végletesen leegyszerűsítjük a teljes kvantummechanikai leíráshoz képest, mivel az atomot klasszikus pontszerű részecskének tekintjük. A két szabadsági fok eliminálása természetesen nem lehet adiabatikus, hiszen akkor elveszíténénk minden disszipációs csatornát. Ehelyett az atom sebességében első rendig végezzük az eliminálást, ennek következtében a belső szabadsági fokok disszipatív dinamikája átöröklődik az atom mozgására, amely így klasszikus Brown-mozgáshoz hasonlít. A zaj közvetlenül a belső szabadsági fokok kvantumzajából származik. A modell nagy elméleti előnye, hogy a tömegközéppont Brown-mozgását leíró Langevin-egyenlet együtthatóira zárt kifejezéseket szolgáltat. Az

1. Modell [30] abból áll, hogy az atom belső szabadsági fokát *adiabatikusan* elimináljuk, úgyhogy az atomi polarizáció egyszerűen az atom helyén lévő elektromos mezővel lesz arányos. Ez általános lineárisan polarizálható kvantummechanikai részecskével ekvivalens, ezért minden eredmény, amit az 1. Modellből vezetünk le, ilyen általános részecskékre is érvényes, így atomokon kívül pl. molekulákra vagy mikroszkopikus szilikon gömbökre. Az elimináció akkor jogos, amikor a gerjesztő mező frekvenciája nagyon el van hangolva az atomi rezonanciától, hiszen ilyenkor az atomi gerjesztettség kicsi, és az atom belső szerkezete alig észlelhető. Az egész disszertációban többnyire ezt a tartományt tekintettük, mert ez az, ami a rezonátoros hűtés szempontjából a legérdekesebb, hiszen a szabad térbeli lézerhűtési technikák itt nem működnek. A spontán emisszió elfojtott, és a rezonátorbomlás lesz az uralkodó disszipációs csatorna. Az értekezésben az 1. Modell használatával demonstráltuk a rezonátoros hűtést és csapdázást, így ez valóban alkalmazható molekulákra, ami munkánk egyik fontos motivációja volt. Az

1sc Modell [29, 30] az 1. Modell megszorítása, amennyiben mind az atom mozgását, mind pedig a rezonátormezőt klasszikusnak tekintjük, de a 0sc Modellhez hasonlóan a korrelált zaj a dinamikájukban tisztán kvantummechanikai eredetű. Lényeges különbség a 0sc Modellhez képest azonban, hogy itt a rezonátormező dinamikáját nem elimináljuk. Az 1sc Modell a lehető legegyszerűbb olyan modell, ami még képes a csatolt disszipatív atom-rezonátor dinamika alapvető fizi-

káját leírni. Nagy előnye, hogy több (akár több ezer) atomot is jól tud kezelni, így sikeresen alkalmazhatták többatomos rendszerek kollektív jelenségeinek vizsgálatára [35].

A kvantumos szimuláció

[36] A 4. fejezetben azt mutattuk meg, hogyan lehet az 1. Modellnek közelítő, de teljesen kvantummechanikai megoldását adni. Kiindulópontunk a Monte-Carlo hullámfüggvény-módszer (Monte Carlo Wave-Function — MCWF) volt. Ennek előnye, hogy a sűrűségoperátor sztochasztikus hullámfüggvényekkel való mintázása segítségével a probléma dimenziószámát a négyzetgyökére csökkenti.

A szimuláció kifejlesztésével a célunk az volt, hogy feltérképezzük a kvantumos jelenségeket az atom-rezonátor kölcsönhatásban, főként olyan paramétertartományokban, amik kísérletekben már napjainkban is elérhetők, de ahol az 1sc Modell már nem megbízható. Ezt jórészt a 5. fejezetben tettük meg. Eközben természetesen alátámasztottuk a korábbi, az 1sc Modellel kapott eredményeket azokban a tartományokban, ahol ez a Modell érvényes lehet.

Két olyan tartomány van, ahová az 1sc Modellel nem lehet behatolni: Egyrészt a nagyon alacsony fotonszámok tartománya. Itt a mező kvantumos mivolta már nyilvánvalóan nem hanyagolható el. Másrészt azok a tartományok, ahol az atom kinetikus hőmérséklete már olyan alacsony, hogy az atomi mozgás kvantáltságát figyelembe kell venni. Ez különösen igaz az olyan kísérletekben, amikor Bose-kondenzátum hat kölcsön a rezonátorral. Ilyenkor mindkét szabadsági fokot kvantálni kell, hogy az esetleges kvantumos korrelációkról számot adhassunk.

A módszer eredeti megfogalmazásában *számos trajektóriával* kellett a sűrűségoperátort mintázni, értekezésünkben azonban megmutattuk, hogy az állandósult állapotbeli fizikai mennyiségek meghatározásához elegendő *egyetlen trajektórián* hosszabb ideig átlagolni. Ez természetesen az ergodikus hipotézissel egyenértékű, amiről megmutattuk, hogy bár egzaktul nem teljesülhet, gyakorlatilag mégis alkalmazható a rendszerre.

Megközelítésünk lényeges újítása volt, hogy az 1. Modell Hamilton-operátorának speciális alakját kihasználva minden számolást impulzustérben tudunk végezni, ami azt jelenti, hogy a szimuláció lényeges része alatt nem kell Fourier-transzformálni. Ez mind CPU-időben mind pedig számítási pontosságban nagy javítást jelent a hagyományos, parciális differenciálegyenletek megoldását célzó módszerekhez képest.

A rezonátoros hűtés kvantumos tartománya

[36, 51] Az 5. fejezetben az atom-rezonátor kölcsönhatás olyan tartományába léptünk,

ami nem írható le azzal a szemiklasszikus megközelítéssel, ami az 1sc Modell a fent említett két ok valamelyikéből kifolyólag.

Az 5.2. szakaszban a fő motivációnk a [29] referenciában bemutatott munka volt, amelyet a szerzők az 1sc Modell segítségével végeztek. A kvantumozott szimulációkkal mindenekelőtt ellenőriztük az eredményeiket olyan paramétertartományban, ahol mindkét Modell működőképes (Megjegyezzük, hogy az 1. Modell általunk adott kvantumozott megoldásának csak gyakorlati, míg az 1sc Modellnek elméleti korlátai is vannak). Munkájukat két irányba terjesztettük ki: megmutattuk, hogy amikor átlagban csak egyetlen foton van a rezonátorban, akkor is képes kifejteni a rezonátoros hűtéshez szükséges hatást. Másrészt, csökkentve a rezonátor vonalszélességét olyan alacsony hőmérsékleteket értünk el, ahol az atom mozgásában lévő kvantumok száma mindössze körülbelül 3 — ez már nem tekinthető szemiklasszikus mozgásnak.

A fent említett munka szerzői az atom csapdázási idejét is tanulmányozták. Ezeket az eredményeket is megpróbáltuk ellenőrizni, itt azonban lényeges eltérést tapasztaltunk. Arra a következtetésre jutottunk, hogy az eltérés nem magyarázható meg egyedül az atom kvantumozott természetével, vagyis az alagutazás lehetőségével. A lehetséges magyarázat inkább a csapdázó rezonátormező kvantáltságában rejlik. Az általa létrehozott potenciál nem klasszikus potenciál, hiszen a fotonszámoperátorral arányos. A 0. fotonszámkomponenshez így nem is tartozik potenciál. Megmutattuk, hogyan képes az atom ezen a fotonszámkomponensen keresztül megszökni a csapdából. A jelenség jelentősége abban rejlik, hogy a rezonátormező „szemcsézettségének” tesztelésére szolgálhat.

Az 5.3. szakasz munkánk talán legfontosabb része volt. A rezonátor szerepét itt egy másik szemszögből tárgyaltuk: A csatolási állandót változtattuk, de oly módon, hogy a Rabi-frekvencia állandó maradjon. Megmutattuk, hogy ez felfogható úgy, mint átmenet a szabad térbeli messzire hangolt dipólcsapda (far-off-resonance dipole trap — FORT) — ahol nincs hűtés! — és a dinamikus rezonátoros hűtés között. Az erősen csatolt tartományban nagyon kevés foton eredményezi ugyanazt a Rabi-frekvenciát, így ezzel egy időben a kvantumozott mező tartományába is beléptünk. Ebben a szakaszban az 1sc Modellt és az 1. Modell kvantumozott megoldását egymást kiegészítő módon használtuk.

Megmutattuk, hogy a dinamikus rezonátoros hűtés a Doppler-hűtéssel ellentétben nem szűnik meg a nagyon messzi elhangolás tartományában. Ebben a tartományban, ha a spontán fotonszórási rátát állandónak tartjuk, mély optikai csapda jön létre. Ez, a rezonátoros hűtéssel együtt, azt eredményezi, hogy az atom az *állandósult állapotban* is csapdázott marad, ami a szabad térbeli FORT elrendezésben nem lehetséges, hiszen ez utóbbi esetben a hosszú csapdázás mindössze annak köszönhető, hogy az atomok nagyon lassan melegsznek fel, az állandósult állapotban azonban nem csapdázottak.

Polariton-hűtés

[52] A 6. fejezetben azt vizsgáltuk, hogyan alakul az atom-mező kölcsönhatás sebességfüggése erősen csatolt rezonátor jelenlétében. Azt találtuk, hogy az atomi abszorpcióban megszokott igen alapvető Doppler-effektus változik meg.

Ezt az „anomális” Doppler-effektust a hagyományos Doppler-hűtés elrendezésében fedeztük fel, az atomhoz csatolt rezonátor tengelye merőleges volt az atom mozgására. Ebben az esetben az atom-mező csatolás állandó, így a rezonátor nem fejt ki erőt az atom mozgásának irányában. Másrészt itt a rezonátorveszteség nem játszik lényeges szerepet a dinamikában. Ezért volt meglepő, hogy a rezonátor mégis jelentősen megjavítja a Doppler-hűtést a tengelyére merőleges irányban. Ez mind az elérhető hőmérsékletben, mind a hűtési időben, mind pedig a csapdázási tulajdonságokban megnyilvánul. A jelenséget mikroszkopikus szinten a rezonátor- és az atomot pumpáló mező interferenciájával magyaráztuk, amely függ az atom sebességétől.

Hangsúlyozzuk, hogy a rezonátor geometriája itt alig játszott szerepet, helyette szinte tetszőleges rezonáns objektumot elképzelhetünk, például gyűrűket, hullámvezetőket vagy mikrogömböket. Így azt várjuk, hogy az anomális Doppler-effektus túlmutat a rezonátoros kvantumelektrodinamikán, és a mikrooptikai kísérletek sokkal szélesebb körében megfigyelhető.

A Doppler-hűtés elrendezésében az atomhoz csatolt rezonátor által megjavított hűtést, ahogy azt elméletileg megjósoltuk, nemrégiben kísérletileg is megfigyelték [55].

Az atom-rezonátor rendszer mint kvantumlibikóka

[56] Az atom-rezonátor kölcsönhatásban a rezonátor által létrehozott potenciál dinamikus abban az értelemben, hogy az atom mozgása visszahat a potenciálra. A sokatomos esetben az egész atomi konfigurációt figyelembe kell venni, a rezonátormező ilyenkor dinamikus optikai rácsként fogható fel.

Ennek egyik meglepő következménye az, hogy pumpált atomok térbeli önszerveződést mutathatnak rezonátor mezejében [35]. Egy bizonyos kritikus pumpateljesítmény fölött az atomok, spontán megsértve az atomfelhő kezdeti transzlációs szimmetriáját, két lehetséges mintázat egyikét hozzák létre. A jelenség dinamikai fázisátalakulásként fogható fel [62]. A két mintázat maximalizálja a szórást a pumpából a rezonátorba (szuperradiáns módon szórnak), és a rezonátormező a mintázatok kettősségének megfelelően kétféle, egymással ellentétes fázist vehet fel, ahogy ezt kísérletileg is megfigyelték [63]. Az atomok pozitív visszacsatoláson keresztül találják meg a stabil konfigurációjukat: az atomi konfiguráció hat a rezonátormezőre, ez pedig potenciált hoz létre (vagy legalábbis módosítja a pumpa által létrehozott optikai potenciált), ami

hat az atomokra.

A 7. fejezetben egy olyan jelenséget mutattunk be, ami lényeges hatással lehet az önszerveződés fent leírt klasszikus fázisátalakulására abban az esetben, amikor az atomokat kvantumosan kell leírni, vagyis amikor a hullámfüggvényük a mező hullámhosszának skáláján lapos (gondoljunk például egy BEC-re). Ebben az esetben, ha a mezőt klasszikusan, vagyis átlagmezővel íránk le, nem történne önszerveződés, hiszen az atomi hullámfüggvény különböző részeiről szórt mezők az interferencia miatt kioltják egymást. Megmutattuk azonban, hogy ebben az esetben nem tekinthetünk el a rezonátormező kvantumos mivoltától, amely *kvantumos visszacsatolást* hoz létre az atomi mozgás számára. Az összefonódás ebben kulcsfontosságú. A szórt mezők nem oltják ki egymást, hanem különböző atomi hullámfüggvényekkel fonódnak össze. A mező kvantummechanikai átlaga továbbra is zérus, de a fotonszám véges.

Azt találtuk, hogy az önszerveződés még zérus hőmérsékleten is azonnal megindul, hiszen valójában nincs szükség spontán szimmetriasértésre: a két mintázat egyszerre realizálódik (kvantummechanikai szuperpozícióban). A jelenség általános lehet olyan kvantumos fázisátalakulások esetén, ahol a kvantumállapot visszahat a kontrolljára.

A 7. fejezetben elsősorban azzal foglalkoztunk, hogy ez a rendszer a „kvantumlibikóka” kísérleti megvalósítása lehet. A libikóka olyan rendszer, ahol a részecske dinamikusan változó potenciálnak (visszacsatolásnak) van kitéve, hiszen a pozíciójától függ, hogy milyen potenciált érez. A libikóka kvantumos verziójában a középen lévő instabil egyensúlyi helyzetét összefonódáson keresztül hagyja el a részecske, és a libikóka egyszerre dől el balra és jobbra. Hangsúlyozzuk, hogy mindezt egy atom esetén vizsgáltuk, az általunk kifejlesztett MCWF szimulációval. Azt, hogy a kvantumlibikóka jelenség milyen hatással van az önszerveződésre a sokatomos esetben, egy, a későbbiekben megjelenő cikkünkben vizsgáljuk [56]. A vizsgálat azonban nem zárulhat le ezzel sem, mert szigorúan véve még nem sikerült olyan modellt létrehozunk, amellyel sok atom teljesen kvantumos mozgását tanulmányozhatnánk úgy, hogy a teljes csatolt atom-mező dinamikát is figyelembe vegyük. Mindez a jövőbeli munkánk egyik fő iránya lesz, erre a 8. fejezetben tekintettünk ki. A 8.3. szakaszban bemutatott modell nagyon jó jelölt a fent említett probléma tanulmányozására.

A sokatomos eset — Kitekintés

A 8. fejezetben felvázoltuk annak általános keretét, hogy hogyan lehet sok, a rezonátormezővel kölcsönható atom mozgását teljesen kvantummechanikailag leírni. A modell valójában az 1. Modell térelméleti változata.

Ezután egy negatív eredményre jutottunk: az atomi mozgás standard Hubbard-típusú leírása — ez az, ami először az eszünkbe jut — *nem adhat számot* egy esetle-

ges kvantumos önszerveződésről. Ennek egyszerűen az az oka, hogy az önszerveződés a rezonátor által létrehozott potenciál dinamikus mivoltán alapul, a Hubbard-megközelítés azonban ezt a legjobb esetben is csak egy rögzített potenciál perturbációjaként tudja figyelembe venni.

Valójában a már korábban is említett, a rezonátor által közvetített kölcsönhatás az atomok között *erős*, úgyhogy erről perturbatív leírás nem adhat megfelelően számot. Ez a kölcsönhatás önmagában fázisátalakulást eredményez. Mindez természetes módon egy esetleges renormalizáción alapuló leírás lehetőségét juttatta eszünkbe. Megmutattuk, hogy a sok-atom-rezonátorban rendszert felfoghatjuk ugyan rácsmodellnek, csak hogy *impulzustérben*. Itt a rezonátormező (bozonikus) szennyezés szerepét játsza, ami szórást tesz lehetővé bizonyos rácspontok között. Az elmúlt évtizedben kifejlődött sűrűségmátrix-renormalizációs csoport (density matrix renormalisation group — DMRG) módszerét nagy sikerrel alkalmazták szennyezőt tartalmazó modellek megoldásában. A disszertáció kitekintéseként felvázoltuk egy, a rendszerünkre adaptált DMRG számolás lehetőségét.

Acknowledgements

Decidedly in the first place acknowledgement is due to my excellent supervisor, Péter Domokos: his professional help was invaluable. We were also getting on jolly well: it was really a great pleasure for me to work together with him during all these years!

Thanks to Helmut Ritsch, our Innsbruck colleague, for his collaboration in most of the work presented here, for his kindly and generously hosting me several times at his institute and his beautiful place, and for his professional guidance during these periods.

My special thanks to my good fellow and colleague, János Asbóth, for his often unexpected but always valuable remarks concerning the work and physics in general.

Bibliography

- [1] S. Haroche. Cavity quantum electrodynamics. In J. Dalibard, J.-M. Raimond, and J. Zinn-Justin, editors, *Fundamental Systems in Quantum Optics, Proceedings of the Les Houches Summer School, Session LIII*, page 165. North-Holland, Amsterdam, 1992.
- [2] Paul Berman, editor. *Cavity Quantum Electrodynamics*. Academic Press, San Diego, 1994.
- [3] E. M. Purcell. Spontaneous emission probabilities at radio frequencies. *Phys. Rev.*, 69:681, 1946.
- [4] Daniel Kleppner. Inhibited spontaneous emission. *Phys. Rev. Lett.*, 47:233, 1981.
- [5] P. Goy, J. M. Raimond, M. Gross, and S. Haroche. Observation of cavity-enhanced single-atom spontaneous emission. *Phys. Rev. Lett.*, 50:1903, 1983.
- [6] D. J. Heinzen, J. J. Childs, J. E. Thomas, and M. S. Feld. Enhanced and inhibited visible spontaneous emission by atoms in a confocal resonator. *Phys. Rev. Lett.*, 58:1320, 1987.
- [7] D. J. Heinzen and M. S. Feld. Vacuum radiative level shift and spontaneous-emission linewidth of an atom in an optical resonator. *Phys. Rev. Lett.*, 59:2623, 1987.
- [8] M. Brune, F. Schmidt-Kaler, A. Maali, J. Dreyer, E. Hagley, J. M. Raimond, and S. Haroche. Quantum Rabi oscillation: A direct test of field quantization in a cavity. *Phys. Rev. Lett.*, 76:1800, 1996.
- [9] M. Brune, E. Hagley, J. Dreyer, X. Maître, A. Maali, C. Wunderlich, J. M. Raimond, and S. Haroche. Observing the progressive decoherence of the “meter” in a quantum measurement. *Phys. Rev. Lett.*, 77:4887, 1996.
- [10] H. Mabuchi, M. S. Chapman, T. Q. A. Turchette, and H. J. Kimble. Real-time detection of individual atoms falling through a high-finesse optical cavity. *Opt. Lett.*, 21:1393, 1996.

- [11] C. J. Hood, T. W. Lynn, A. C. Doherty, and A. S. Parkins and H. J. Kimble. The atom-cavity microscope: Single-atoms bound in orbit by single photons. *Science*, 287:1447, 2000.
- [12] P. W. H. Pinkse, T. Fischer, P. Maunz, and G. Rempe. Trapping an atom with single photons. *Nature*, 404:365, 2000.
- [13] C. J. Hood, M. S. Chapman, T. W. Lynn, and H. J. Kimble. Real-time cavity QED with single atoms. *Phys. Rev. Lett.*, 80:4157, 1998.
- [14] Claude Cohen-Tannoudji. Atomic motion in laser light. In J. Dalibard, J.-M. Raimond, and J. Zinn-Justin, editors, *Fundamental Systems in Quantum Optics, Proceedings of the Les Houches Summer School, Session LIII*, page 1. North-Holland, Amsterdam, 1992.
- [15] T. W. Hänsch and A. L. Schawlow. Cooling of gases by laser radiation. *Opt. Commun.*, 13:68, 1975.
- [16] D. J. Wineland, R. E. Drullinger, and F. L. Walls. Radiation-pressure cooling of bound resonant absorbers. *Phys. Rev. Lett.*, 40:1639, 1978.
- [17] J. Dalibard and C. Cohen-Tannoudji. Laser cooling below the Doppler limit by polarization gradients: simple theoretical models. *J. Opt. Soc. Am. B*, 6:2023, 1989.
- [18] A. Aspect, E. Arimondo, R. Kaiser, N. Vansteenkiste, and C. Cohen-Tannoudji. Laser cooling below the one-photon recoil energy by velocity-selective coherent population trapping. *Phys. Rev. Lett.*, 61:826, 1988.
- [19] E. A. Cornell and C. E. Wieman. Nobel lecture: Bose-Einstein condensation in a dilute gas, the first 70 years and some recent experiments. *Rev. Mod. Phys.*, 2002.
- [20] W. Ketterle. Nobel lecture: When atoms behave as waves: Bose-Einstein condensation and the atom laser. *Rev. Mod. Phys.*, 74:1131, 2002.
- [21] H. Häffner, W. Hänsel, C. F. Roos, J. Benhelm, D. Chek al kar, M. Chwalla, T. Körber, U. D. Rapol, M. Riebe, P. O. Schmidt, C. Becher, O. Gühne, W. Dür, and R. Blatt. Scalable multiparticle entanglement of trapped ions. *Nature*, 438:643, 2005.
- [22] T. W. Mossberg, M. Lewenstein, and Daniel J. Gauthier. Trapping and cooling of atoms in a vacuum perturbed in a frequency-dependent manner. *Phys. Rev. Lett.*, 67:1723, 1991.

- [23] Maciej Lewenstein and Luis Roso. Cooling of atoms in colored vacua. *Phys. Rev. A*, 47:3385, 1993.
- [24] J. I. Cirac, M. Lewenstein, and P. Zoller. Laser cooling a trapped atom in a cavity: Bad-cavity limit. *Phys. Rev. A*, 51:1650, 1995.
- [25] Vladan Vuletić and Steven Chu. Laser cooling of atoms, ions, or molecules by coherent scattering. *Phys. Rev. Lett.*, 84:3787, 2000.
- [26] Vladan Vuletić, Hilton W. Chan, and Adam T. Black. Three-dimensional cavity Doppler cooling and cavity sideband cooling by coherent scattering. *Phys. Rev. A*, 64:033405, 2001.
- [27] Peter Horak, Gerald Hechenblaikner, Klaus M. Gheri, Herwig Stecher, and Helmut Ritsch. Cavity-induced atom cooling in the strong coupling regime. *Phys. Rev. Lett.*, 79:4974, 1997.
- [28] Gerald Hechenblaikner, Markus Gangl, Peter Horak, and Helmut Ritsch. Cooling an atom in a weakly driven high-Q cavity. *Phys. Rev. A*, 58:3030, 1998.
- [29] Peter Domokos, Peter Horak, and Helmut Ritsch. Semiclassical theory of cavity-assisted atom cooling. *J. Phys. B: At. Mol. Opt. Phys.*, 34:187, 2001.
- [30] P. Domokos and H. Ritsch. Mechanical effects of light in optical resonators. *J. Opt. Soc. Am. B*, 20:1098, 2003.
- [31] P. Maunz, T. Puppe, I. Schuster, N. Syassen, P. W. H. Pinkse, and G. Rempe. Cavity cooling of a single atom. *Nature*, 428:50, 2004.
- [32] J. K. Asbóth, P. Domokos, and H. Ritsch. Correlated motion of two atoms trapped in a single-mode cavity field. *Phys. Rev. A*, 70:013414, 2004.
- [33] András Vukics. Three-dimensional dissipative motion of an atom in an optical cavity. Master's thesis, Roland Eotvos University, Budapest, 2003.
- [34] A. Vukics, P. Domokos, and H. Ritsch. Multidimensional and interference effects in atom trapping by a cavity field. *J. Opt. B: Quant. Semiclass. Opt.*, 6:143, 2004.
- [35] P. Domokos and H. Ritsch. Collective cooling and self-organization of atoms in a cavity. *Phys. Rev. Lett.*, 89:253003, 2002.
- [36] A. Vukics, J. Janszky, and P. Domokos. Cavity cooling of atoms: a quantum statistical treatment. *J. Phys. B: At. Mol. Opt. Phys.*, 38:1453, 2005.

- [37] H. J. Carmichael. Spectrum of squeezing and photocurrent shot noise: a normally ordered treatment. *J. Opt. Soc. Am. B*, 4:1588, 1987.
- [38] J. Dalibard, Y. Castin, and K. Molmer. Wave-function approach to dissipative processes in quantum optics. *Phys. Rev. Lett.*, 68:580, 1992.
- [39] K. Molmer, Y. Castin, and J. Dalibard. Monte Carlo wave-function method in quantum optics. *J. Opt. Soc. Am. B*, 10:524, 1993.
- [40] H. J. Carmichael. Quantum trajectory theory for cascaded open systems. *Phys. Rev. Lett.*, 70:2273, 1993.
- [41] Anton Öttl, Stephan Ritter, Michael Köhl, and Tilman Esslinger. Correlations and counting statistics of an atom laser. *Phys. Rev. Lett.*, 95:090404, 2005.
- [42] Axel Kuhn, Markus Hennrich, and Gerhard Rempe. Deterministic single-photon source for distributed quantum networking. *Phys. Rev. Lett.*, 89:067901, 2002.
- [43] J. McKeever, A. Boca, A. D. Boozer, R. Miller, J. R. Buck, A. Kuzmich, and H. J. Kimble. Deterministic generation of single photons from one atom trapped in a cavity. *Science*, 303:1992, 2004.
- [44] P. Zoller, Th. Beth, D. Binosi, R. Blatt, H. Briegel, D. Bruss, T. Calarco, J. I. Cirac, D. Deutsch, J. Eisert, A. Ekert, C. Fabre, N. Gisin, P. Grangiere, M. Grassl, S. Haroche, A. Imamoglu, A. Karlson, J. Kempe, L. Kouwenhoven, S. Kröll, G. Leuchs, M. Lewenstein, D. Loss, N. Lütkenhaus, S. Massar, J. E. Mooij, M. B. Plenio, E. Polzik, S. Popescu, G. Rempe, A. Sergienko, D. Suter, J. Twamley, G. Wendin, R. Werner, A. Winter, J. Wrachtrup, and A. Zeilinger. Quantum information processing and communication — strategic report on current status, visions and goals for research in Europe. *Eur. Phys. J. D*, 36:203, 2005.
- [45] A. C. Doherty, A. S. Parkins, S. M. Tan, and D. F. Walls. Motion of a two-level atom in an optical cavity. *Phys. Rev. A*, 56:833, 1997.
- [46] J. Leach and P. R. Rice. Cavity QED with quantized center of mass motion. *Phys. Rev. Lett.*, 93:103601, 2004.
- [47] Almut Beige, Peter L. Knight, and Giuseppe Vitiello. Cooling many particles at once. *New J. of Phys.*, 7:96, 2005.
- [48] A. C. Doherty, A. S. Parkins, S. M. Tan, and D. F. Walls. Motional states of atoms in cavity QED. *Phys. Rev. A*, 57:4804, 1998.

- [49] Stefano Zippilli and Giovanna Morigi. Cooling trapped atoms in optical resonators. *Phys. Rev. Lett.*, 95:143001, 2005.
- [50] Stefano Zippilli and Giovanna Morigi. Mechanical effects of optical resonators on driven trapped atoms: Ground-state cooling in a high-finesse cavity. *Phys. Rev. A*, 72:053408, 2005.
- [51] A. Vukics and P. Domokos. Simultaneous cooling and trapping of atoms by a single cavity-field mode. *Phys. Rev. A*, 72:031401, 2005.
- [52] P. Domokos, A. Vukics, and H. Ritsch. Anomalous Doppler effect and polariton-mediated cooling of two-level atoms. *Phys. Rev. Lett.*, 92:103601, 2004.
- [53] C. Doppler. Ueber das farbige licht der doppelsterne und einiger anderer gestirne des himmels. *Abhandlungen der königliche böhmischen Gessellschaft der Wissenschaften*, 2:465, 1842.
- [54] Giovanna Morigi, Jürgen Eschner, and Christoph H. Keitel. Ground state laser cooling using electromagnetically induced transparency. *Phys. Rev. Lett.*, 85:4458, 2000.
- [55] Stefan Nussmann, Karim Murr, Markus Hijlkema, Bernhard Weber, Axel Kuhn, and Gerhard Rempe. Vacuum-stimulated cooling of single atoms in three dimensions. *Nature Physics*, 1:122, 2005.
- [56] C. Maschler, H. Ritsch, A. Vukics, and P. Domokos. Entanglement driven self-organization via a quantum seesaw mechanism. quant-ph/0512101, 2005.
- [57] Mark A. Kasevich. Coherence with atoms. *Science*, 298:1363, 2002.
- [58] D. Jaksch, C. Bruder, J. I. Cirac, C. W. Gardiner, and P. Zoller. Cold bosonic atoms in optical lattices. *Phys. Rev. Lett.*, 81:3108, 1998.
- [59] Markus Greiner, Olaf Mandel, Tilman Esslinger, Theodor W. Hänsch, and Immanuel Bloch. Quantum phase transition from a superfluid to a Mott insulator in a gas of ultracold atoms. *Nature*, 415:39, 2002.
- [60] A. Boca, R. Miller, K. M. Birnbaum, A. D. Boozer, J. McKeever, and H. J. Kimble. Observation of the vacuum Rabi spectrum for one trapped atom. *Phys. Rev. Lett.*, 93:233603, 2004.
- [61] C. Maschler and H. Ritsch. Cold atom dynamics in a quantum optical lattice potential. *Phys. Rev. Lett.*, 95:260401, 2005.

- [62] J. K. Asbóth, P. Domokos, H. Ritsch, and A. Vukics. Self-organization of atoms in a cavity field: Threshold, bistability, and scaling laws. *Phys. Rev. A*, 72:053417, 2005.
- [63] A. T. Black, H. W. Chan, and V. Vuletić. Observation of collective friction forces due to spatial self-organization of atoms: From Rayleigh to Bragg scattering. *Phys. Rev. Lett.*, 91:203001, 2003.
- [64] Seth Lloyd. Coherent quantum feedback. *Phys. Rev. A*, 62:022108, 2000.
- [65] Claude Cohen Tannoudji. *Atoms in electromagnetic fields*. World Scientific Singapore, 1994.
- [66] A. V. Rau, J. A. Dunningham, and K. Burnett. Measurement-induced relative-position localization through entanglement. *Science*, 301:1081, 2003.
- [67] C. Maschler and H. Ritsch. Quantum motion of laser-driven atoms in a cavity field. *Opt. Commun.*, 243:145, 2005.
- [68] D. Jaksch and P. Zoller. The cold atom Hubbard toolbox. *Annals of Physics*, 315: 52, 2005.
- [69] U. Schollwöck. The density-matrix renormalization group. *Rev. Mod. Phys.*, 77: 259, 2005.
- [70] Reinhard M. Noack and Salvatore R. Manmana. Diagonalization- and numerical renormalization-group-based methods for interacting quantum systems. *cond-mat/0510321*, 2005.
- [71] A. C. Doherty, T. W. Lynn, C. J. Hood, and H. J. Kimble. Trapping of single atoms with single photons in cavity QED. *Phys. Rev. A*, 63:013401, 2000.
- [72] I. Protsenko, P. Domokos, V. Lefèvre, J. Hare, J. M. Raimond, and L. Davidovich. Quantum theory of a thresholdless laser. *Phys. Rev. A*, 59:1667, 1999.
- [73] L. Mandel and E. Wolf. *Optical coherence and quantum optics*. Cambridge, 1995.
- [74] L. Collot, V. Lefevre-Seguin, M. Brune, J. M. Raimond, and S. Haroche. Very high-Q whispering-gallery mode resonances observed on fused silica microspheres. *Europhys. Lett.*, 23:327, 1993.
- [75] D. W. Vernooy, A. Furusawa, N. Ph. Georgiades, V. S. Ilchenko, and H. J. Kimble. Cavity QED with high-Q whispering gallery modes. *Phys. Rev. A*, 57:R2293, 1998.

- [76] Wolfgang Singer, Manfred Frick, Stefan Bernet, and Monika Ritsch-Marte. Self-organized array of regularly spaced microbeads in a fiber-optical trap. *J. Opt. Soc. Am. B*, 20:1568, 2003.
- [77] J. T. Bahns, W. C. Stwalley, and P. L. Gould. Laser cooling of molecules: A sequential scheme for rotation, translation, and vibration. *J. Chem. Phys.*, 104:9689, 1996.
- [78] J. Doyle, B. Friedrich, R. V. Krems, and F. Masnou-Seeuws. Quo vadis, cold molecules? *Eur. Phys. J. D*, 31:149, 2004.
- [79] I. S. Vogelius, L. B. Madsen, and M. Drewsen. Rotational cooling of molecules using lamps. *J. Phys. B: At. Mol. Opt. Phys.*, 37:4571, 2004.
- [80] William H. Press, Saul A. Teukolsky, William T. Vetterling, and Brian P. Flannery. *Numerical Recipes in C*. Cambridge, 1992. URL <http://www.nr.com/>.
- [81] R. J. Ballagh. Computational methods for nonlinear partial differential equations. Lectures given at the Institute for Theoretical Physics Innsbruck University, 2000.
- [82] A. Peres. Separability criterion for density matrices. *Phys. Rev. Lett.*, 77:1413, 1996.
- [83] G. Vidal and R. F. Werner. Computable measure of entanglement. *Phys. Rev. A*, 65:032314, 2002.
- [84] E. Anderson, Z. Bai, C. Bischof, S. Blackford, J. Demmel, J. Dongarra, J. Du Croz, A. Greenbaum, S. Hammarling, A. McKenney, and D. Sorensen. *LAPACK Users' Guide, Third Edition*. SIAM, 1999. URL www.netlib.org/lapack/lug/.
- [85] R. Grimm, M. Weidemüller, and Yu.B. Ovchinnikov. Optical dipole traps for neutral atoms. *Adv. At. Mol. Opt. Phys.*, 42:95, 2000.
- [86] M. D. Barrett, J. A. Sauer, and M. S. Chapman. All-optical formation of an atomic Bose-Einstein condensate. *Phys. Rev. Lett.*, 87:010404, 2001.
- [87] Tino Weber, Jens Herbig, Michael Mark, Hans-Christoph Nägerl, and Rudi Grimm. Bose-Einstein condensation of Cesium. *Science*, 299:232, 2003.
- [88] K. Honda, Y. Takasu, T. Kuwamoto, M. Kumakura, Y. Takahashi, and T. Yabuzaki. Optical dipole force trapping of a fermion-boson mixture of Ytterbium isotopes. *Phys. Rev. A*, 66:021401(R), 2002.
- [89] T. A. Savard, K. M. O'Hara, and J. E. Thomas. Laser-noise-induced heating in far-off resonance optical traps. *Phys. Rev. A*, 56:R1095–R1098, 1997.

- [90] V. G. Minogin and Yu. V. Rozhdestvenskii. Stable localization of atoms in a standing light wave field. *Opt. Commun.*, 64:172, 1987.
- [91] P. Maunz, T. Puppe, I. Schuster, N. Syassen, P. W. H. Pinkse, and G. Rempe. Normal-mode spectroscopy of a single bound atom-cavity system. *Phys. Rev. Lett.*, 94:033002, 2005.
- [92] S. J. van Enk, J. McKeever, H. J. Kimble, and J. Ye. Cooling of a single atom in an optical trap inside a resonator. *Phys. Rev. A*, 64:013407, 2001.
- [93] J. McKeever, J. R. Buck, A. D. Boozer, A. Kuzmich, H.-C. Nägerl, D. M. Stamper-Kurn, and H. J. Kimble. State-insensitive cooling and trapping of single atoms in an optical cavity. *Phys. Rev. Lett.*, 90:133602, 2003.
- [94] Peter Horak and Helmut Ritsch. Scaling properties of cavity-enhanced atom cooling. *Phys. Rev. A*, 64:033422, 2001.
- [95] Karim Murr. On the suppression of the diffusion and the quantum nature of a cavity mode. Optical bistability: forces and friction in driven cavities. *J. Phys. B: At. Mol. Opt. Phys.*, 36:2515, 2003.
- [96] T. Fischer, P. Maunz, P. W. H. Pinkse, T. Puppe, and G. Rempe. Feedback on the motion of a single atom in an optical cavity. *Phys. Rev. Lett.*, 88:163002, 2002.
- [97] B. Nagorny, Th. Elsässer, and A. Hemmerich. Collective atomic motion in an optical lattice formed inside a high finesse cavity. *Phys. Rev. Lett.*, 91:153003, 2003.
- [98] W. Ren, J. D. Cresser, and H. J. Carmichael. Spontaneous emission in a standing-wave cavity: Classical center-of-mass motion. *Phys. Rev. A*, 46:7162, 1992.
- [99] M. Wilkens and P. Meystre. Spectrum of spontaneous emission in a fabry-pérot cavity: the effects of atomic motion. *Opt. Commun.*, 94:66, 1992.
- [100] P. M. Alsing, D. A. Cardimona, and H. J. Carmichael. Suppression of fluorescence in a lossless cavity. *Phys. Rev. A*, 45:1793, 1992.
- [101] G. Zaránd, 2006. Private communication.
- [102] Steven R. White. Density matrix formulation for quantum renormalization groups. *Phys. Rev. Lett.*, 69:2863, 1992.
- [103] Ö. Legeza and J. Sólyom. Entropic signature of quantum phase transitions in low-dimensional models. [quant-ph/0511081](https://arxiv.org/abs/quant-ph/0511081), 2005.
- [104] R. Dum, P. Zoller, and H. Ritsch. Monte Carlo simulation of the atomic master equation for spontaneous emission. *Phys. Rev. A*, 45:4879, 1992.

List of publications

- Former publications

1. Z. Farkas, P. Tegzes, A. Vukics, and T. Vicsek. Transitions in the horizontal transport of vertically vibrated granular layers. *Phys. Rev. E*, 60:7022, 1999.
2. A. Vukics, J. Janszky, and T. Kobayashi. Nonideal teleportation in coherent-state basis. *Phys. Rev. A*, 66:023809, 2002.
3. A. Vukics, J. K. Asbóth, and G. Meszéna. Speciation in multidimensional evolutionary space. *Phys. Rev. E*, 68:041903, 2003.

- Publications related to the dissertation

1. A. Vukics, P. Domokos, and H. Ritsch. Multidimensional and interference effects in atom trapping by a cavity field. *J. Opt. B: Quant. Semiclass. Opt.*, 6:143, 2004.
2. P. Domokos, A. Vukics, and H. Ritsch. Anomalous Doppler effect and polariton-mediated cooling of two-level atoms. *Phys. Rev. Lett.*, 92:103601, 2004.
3. A. Vukics, J. Janszky, and P. Domokos. Cavity cooling of atoms: a quantum statistical treatment. *J. Phys. B: At. Mol. Opt. Phys.*, 38:1453, 2005.
4. A. Vukics and P. Domokos. Simultaneous cooling and trapping of atoms by a single cavity-field mode. *Phys. Rev. A*, 72:031401, 2005.
5. J. K. Asbóth, P. Domokos, H. Ritsch, and A. Vukics. Self-organization of atoms in a cavity field: Threshold, bistability, and scaling laws. *Phys. Rev. A*, 72:053417, 2005.
6. C. Maschler, H. Ritsch, A. Vukics, and P. Domokos. Entanglement driven self-organization via a quantum seesaw mechanism. *quant-ph/0512101*, 2005.